P515288.PDF [Page: 4 of 116]

Copy No. 7

DEFENCE R&D DÉFENSE

Incorporation of UK NS94 Ultimate Strength Analysis in MGDSA

Part I: Engineering Considerations

L. Jiang

M.W. Chernuka

MARTEC Ltd.,
Suite 400, 1888 Brunswick Street,
Halifax, NS B3J 3J8

DEFENCE RESEARCH ESTABLISHMENT ATLANTIC

Contractor Report

DREA CR 2000-112

March 2000

National Defence / Défense nationale

Canada

P515288.PDF [Page: 3 of 116]

REPRODUCTION QUALITY NOTICE

This document is the best quality available. The copy furnished to DRDCIM contained pages that may have the following quality problems:

: Pages smaller or Larger than normal

: Pages with background colour or light coloured printing

: Pages with small type or poor printing; and or

: Pages with continuous tone material or colour photographs

Due to various output media available these conditions may or may not cause poor legibility in the hardcopy output you receive.

☒ **If this block is checked, the copy furnished to DRDCIM contained pages with colour printing, that when reproduced in Black and White, may change detail of the original copy.**

THIS IS AN UNEDITED REPORT ON SCIENTIFIC OR TECHNICAL WORK CONTRACTED BY THE DEFENCE RESEARCH ESTABLISHMENT ATLANTIC OF DEFENCE R&D CANADA.

THE CONTENTS OF THE REPORT ARE THE RESPONSIBILITY OF THE CONTRACTOR, AND DO NOT NECESSARILY REFLECT THE OFFICIAL POLICIES OF THE DEPARTMENT OF NATIONAL DEFENCE.

PLEASE DIRECT ENQUIRIES TO:

THE DIRECTOR GENERAL
DEFENCE RESEARCH ESTABLISHMENT ATLANTIC
P.O. BOX 1012
DARTMOUTH, NOVA SCOTIA, CANADA
B2Y 3Z7

102-02803/

Incorporation of UK NS94 Ultimate Strength Analysis in MGDSA

Part I: Engineering Considerations

L. Jiang

M.W. Chernuka

MARTEC Ltd.,
Suite 400, 1888 Brunswick Street,
Halifax, NS B3J 3J8

Defence Research Establishment Atlantic

Contractor Report

DREA CR 2000-112

March 2000

Authors

L. Jiang and M. W. Chernuka

Approved by

Malcolm Smith

Contract Scientific Authority

Approved for release by

Walter E. Ellis

Chair, DREA Document Review Panel

© Her Majesty the Queen as represented by the Minister of National Defence, 2000

INCORPORATION OF UK NS94 ULTIMATE STRENGTH ANALYSIS IN MGDSA

PART I: ENGINEERING CONSIDERATIONS

Martec Report No.: TR-00-15

By:

L. Jiang
M.W. Chernuka

Prepared for:

Defence Research Establishment of Atlantic
9 Grove Street
Dartmouth, NS

Contract No.: W8477-8-0004/001/SV
PWGSC File No.: 005sv.W8477-8-0004

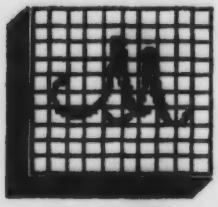

Martec Limited
Advanced Engineering and Research Consultants

400-1888 Brunswick Street
Halifax, NS B3J 3J8
Tel: (902) 425-5101
Fax: (902) 421-1923

101-717 boul St. Joseph
Hull, PQ J8Y 4B6
Tel: (819) 595-3526
Fax: (819) 595-1739

March 2000

ABSTRACT

This report presents all the engineering work related to the incorporation of an ultimate strength analysis capability in MGDSA. The various ultimate strength analysis programs developed by DREA and DERA using the ISUM method were first verified on the PC platform. The ULTMAT program was modified to accept input data at the structural component level, and the accuracy and reliability of the NS94 suite of programs were improved. In order to generate load-shortening curves for damaged stiffened panel structures through nonlinear finite element analyses, the previously developed automatic mesh generator, LSPANEL, was enhanced to include the 8-noded shell element, a corrosion modeling capability, a more realistic residual stress pattern and higher sine functions for imperfection definition. The effects of damage and other important factors on load-shortening behavior of stiffened panels were investigated using the VAST program. Input data translators between VAST and the other nonlinear FE programs, including FABSTRAN and ASAS-NL, were also developed and verified. The detailed mathematical formulations required for evaluating the SSCP23 limit states are presented and the method for calculating component stresses for given extreme bending moments is also included. The input data format for the updated LSPANEL program is summarized in Appendix A. The software development issues related to the present contract are dealt with in the second part of the final report.

RÉSUMÉ

Ce rapport présente tous les travaux techniques relatifs à l'incorporation d'un outil d'analyse de la contrainte de rupture dans MGDSA. Les divers programmes d'analyse de la contrainte de rupture établis par le CRDA et le DERA à l'aide de la méthode ISUM ont d'abord été vérifiés sur plate-forme PC. Le programme ULTMAT a été modifié afin de pouvoir admettre les données d'entrée au niveau des éléments structurels, et la précision ainsi que la fiabilité de l'ensemble de programmes NS94 ont été améliorées. Afin que les analyses non linéaires à éléments finis permettent de générer des courbes de raccourcissement de charge pour les structures de panneaux renforcés endommagés, le générateur automatique de maille LSPANEL développé antérieurement a été amélioré de façon à inclure l'élément de coquille à 8 noeuds, une fonction de modélisation de la corrosion, un modèle de contrainte résiduelle plus réaliste et des fonctions sinusoïdales plus évoluées de définition des imperfections. Les effets des dommages et d'autres facteurs importants sur le raccourcissement de charge des panneaux renforcés ont été étudiés à l'aide du programme VAST. Des traducteurs de données d'entrée entre VAST et les autres programmes FE non linéaires, notamment FABSTRAN et ASAS-NL, ont également été développée et vérifiés. Les formules mathématiques détaillées nécessaires à l'évaluation des états limites SSCP23 sont présentés et la méthode de calcul des contraintes des éléments pour des moments donnés de recourbement extrême est également incluse. L'annexe A résume le format des données d'entrée pour le programme LSPANEL mis à jour. La seconde partie du rapport final aborde les questions de développement de logiciel qui ont trait au présent contrat.

INCORPORATION OF UK NS94 ULTIMATE STRENGTH ANALYSIS IN MGDSA PART I: ENGINEERING CONSIDERATIONS

DREA CR 2000-112

L. Jiang and M.W. Chernuka
Martec Limited

EXECUTIVE SUMMARY

Introduction

Ultimate strength analysis is undertaken to find the bending load that will cause the collapse of a ship hull. Accurate knowledge of this is essential to determine a ship's weight limit and allowable operating conditions. Over the years, specialised analysis codes for evaluating ultimate strength have been developed by defence agencies in several countries. In Canada, the computer code ULTMAT was developed at DREA; in the UK, the NS94 suite of codes was developed at DERA Rosyth. Martec Limited of Halifax Nova Scotia, under contract to DERA Rosyth and DREA, was tasked with bringing together the UK and Canadian ultimate strength analysis codes in a single software application with a common user interface and a common database. A further goal was to provide a link between ultimate strength analysis and the finite-element based ship structural analysis program MGDSA (MAESTRO Graphics – Detail Stress Analysis). The overall objectives were to provide easier access to the analysis tools and to automate the ultimate strength modelling and evaluation process.

Principal Results

This report describes the engineering aspects involved in developing the unified ultimate strength application. As a result of the developments undertaken in this work, cross-sectional models can be generated automatically from existing finite element ship models. Once this has occurred, an ultimate strength analysis can be carried out immediately through the application interface. Customisation of the model, data and analysis options is also permitted. Graphical tools are provided for reviewing of results. The net result is a very significant reduction in the time required to carry out ultimate strength modelling and analysis. With the unified application, an ultimate strength assessment can now be carried out in a matter of minutes if a finite element model of the ship already exists. This is a considerable increase in efficiency over previous efforts requiring several hours.

Significance of Results

Automated evaluation of ultimate strength is an essential component of the ongoing Improved Ship Structural Maintenance Management (ISSMM) project. The results of this study directly pertain to how ultimate strength analysis is to be implemented in the ISSMM Software Tool (IST). The automation and improved efficiency that has resulted from this work will mean that ultimate strength analysis will now be accessible to a wider group of users in the CF community. Furthermore, the Navy will be provided with answers to its ultimate strength queries more quickly, and hence a reduced cost.

INCORPORATION DANS MGDSA DE L'ANALYSE DE LA CONTRAINTE DE RUPTURE NS94 DU ROYAUME-UNI
PARTIE I : CONSIDÉRATIONS RELATIVES À L'INGÉNIERIE

DREA-CR-2000-112

L. Jiang et M.W. Chernuka
Martec Limited

SOMMAIRE

Introduction

Une analyse de la contrainte de rupture est entreprise dans le but de déterminer la charge de flexion qui provoquera la rupture d'une coque de navire. La connaissance précise de cette charge est essentielle pour établir le poids limite et les conditions d'exploitation admissibles d'un navire. Avec les années, des organisations de défense de plusieurs pays ont constitué des codes d'analyse spécialisés permettant d'évaluer la contrainte de rupture. Au Canada, le code informatique ULTMAT a été développé au CRDA; au Royaume-Uni, l'ensemble de codes NS94 a été établi au DERA Rosyth. Dans le cadre d'un contrat du DERA Rosyth et du CRDA, Martec Limited d'Halifax (Nouvelle-Écosse) a été chargée de regrouper les codes d'analyse de la contrainte de rupture du Royaume-Uni et du Canada afin de constituer une seule application logicielle à interface utilisateur commune et à base de données commune. Les travaux visaient également à constituer un lien entre l'analyse de la contrainte de rupture et le programme MGDSA d'analyse structurelle des navires à partir d'éléments finis (MAESTRO Graphics - Analyse détaillée de contrainte). Les objectifs globaux consistaient à faciliter l'accès aux outils d'analyse et à automatiser le processus de modélisation et d'évaluation de la contrainte de rupture.

Principaux résultats

Ce rapport décrit les aspects d'ingénierie que comporte le développement de l'application unifiée d'analyse de la contrainte de rupture. Les résultats des travaux effectués permettent de générer automatiquement des modèles de sections transversales à partir des modèles de navires existants à éléments finis. Cela fait, l'interface de l'application peut servir à exécuter immédiatement une analyse de la contrainte de rupture. Il est également possible de personnaliser le modèle, les données et les options d'analyse. Des outils graphiques sont prévus pour l'examen des résultats. Il est ainsi possible de réduire considérablement le temps nécessaire pour effectuer la modélisation et l'analyse de la contrainte de rupture. L'application unifiée permet maintenant d'effectuer une évaluation de la contrainte de rupture en quelques minutes seulement s'il existe déjà un modèle à éléments finis du navire. Cela représente une nette augmentation d'efficacité par rapport aux travaux antérieurs, qui prenaient plusieurs heures.

Importance des résultats

L'évaluation automatisée de la contrainte de rupture constitue un élément essentiel de l'actuel projet de gestion améliorée de la maintenance de la structure des navires (GAMSN). Les résultats de cette étude portent directement sur la façon dont l'analyse de la contrainte de rupture doit être intégrée à l'outil logiciel GAMSN (IST). L'automatisation et l'amélioration d'efficacité qui ont résulté de ces travaux signifient que l'analyse de la contrainte de rupture sera dorénavant accessible à un plus large groupe d'utilisateurs au sein des FC. La Marine recevra donc plus rapidement des réponses à ses questions de contrainte de rupture, ce qui entraînera une réduction des coûts.

TABLE OF CONTENTS

ABSTRACT ii
RÉSUMÉ ii
EXECUTIVE SUMMARY iii
SOMMAIRE iv
TABLE OF CONTENTS v
LIST OF TABLES vi
LIST OF FIGURES vii

1. INTRODUCTION 1.1

2. MODIFICATION AND VERIFICATION OF THE ULTIMATE STRENGTH ANALYSIS PROGRAMS, ULTMAT AND THE NS94 SUITE 2.1
   2.1 ULTMAT 2.1
   2.2 NS94 Suite 2.3
   2.3 Ultimate Strength Analysis of the 1/3 Scale Welded Steel Frigate Model 2.6

3. MODIFICATION OF THE LSPANEL PROGRAM FOR GENERATING INPUT DATA FILES FOR LOAD-SHORTENING CURVE COMPUTATIONS USING VAST, FABSTRAN AND ASAS-NL 3.1
   3.1 VAST 3.1
   3.2 FABSTRAN 3.8
   3.3 ASAS-NL 3.12

4. STRUCTURAL COMPONENT STRENGTH ASSESSMENT BASED ON THE SSCP23 LIMIT STATES 4.1
   4.1 Calculation of SSCP23 Limit States of Structural Components 4.1
      4.1.1 Buckling of Plating Between Stiffeners 4.1
      4.1.2 Buckling of Longitudinally Stiffened Panel 4.3
      4.1.3 Lateral Buckling of Stiffener (Tripping) 4.4
      4.1.4 Overall Yielding of Structural Components 4.5
   4.2 Calculation of Average Stresses in Structural Components Under Given Bending Moments in Horizontal and Vertical Planes 4.6

5. CONCLUSIONS AND RECOMMENDATION FOR FURTHER WORK 5.1

6. REFERENCES 6.1

APPENDIX A: LIST OF INPUT PARAMETERS FOR THE LSPANEL PROGRAM

LIST OF TABLES

Table 3.1: Percentage Reductions Used in Corroded Stiffened Panel Models 3.16
Table 3.2: Detailed Dimensions of Cross-section of the Stiffened Panel 3.16
Table 3.3: Input Data for Nonlinear of a Typical Stiffened Panel Using FABSTRAN.. 3.17
Table 3.4: A Typical Input Data File for Nonlinear Analysis Using ASAS-NL..... 3.19

LIST OF FIGURES

Figure 2.1: Cross-Section of the 1/3 Welded Steel Frigate Model 2.9
Figure 2.2: Comparison of Sagging and Hogging Moment-Curvature Curves Predicted by the Original and Modified ULTMAT Program Using a Set of Normalized Load-Shortening Curves Generated by VAST 2.10
Figure 2.3: Comparison of Sagging and Hogging Moment-Curvature Curves Predicted by ULTMAT and NS94C Using a Set of Bilinear Load-Shortening Curves Incorporated into the NS94C Program 2.11
Figure 2.4: Comparison of Sagging and Hogging Moment-Curvature Curves Predicted by ULTMAT Using the VAST-Generated and Bilinear Load-Shortening Curves 2.12
Figure 2.5: Comparison of the Bi-Axial Bending Interaction Curves Predicted by the Original and Modified Versions of the NS94D Program. 2.13

Figure 3.1: Finite Element Meshes for Elastic-Plastic, Post-Buckling Analysis of a Typical Stiffened Panel. (a) 4-Noded Shell Element Mesh 3.22
Figure 3.1: (Continued) Finite Element Meshes for Elastic-Plastic, Post-Buckling Analysis of a Typical Stiffened Panel. (b) 8-Noded Shell Element Mesh 3.23
Figure 3.2: Comparison of Load-Shortening Curves Predicted by the 4-Noded and 8-Noded Shell Elements With and Without the Residual Stress Effect 3.24
Figure 3.3: Final Deformed Configurations of the Typical Stiffened Panel. (a) 4-Noded Shell Element 3.25
Figure 3.3: (Continued) Final Deformed Configurations of the Typical Stiffened Panel. (b) 8-Noded Shell Element 3.26
Figure 3.4: Comparison of Load-Shortening Curves for Non-Corroded and Corroded Stiffened Panels with Symmetric and Non-Symmetric Corrosion Patterns 3.27
Figure 3.5: Plate Thickness Variation in Corroded Stiffened Panels. (a) Symmetric Corrosion 3.28
Figure 3.5: (Continued) Plate Thickness Variation in Corroded Stiffened Panels. (b) Non-Symmetric Corrosion 3.29
Figure 3.6: Final Deformed Configuration of the Corroded Stiffened Panel with Symmetric Corrosion Pattern 3.30
Figure 3.7: Stiffened Panel with Magnified Symmetric Geometric Imperfection 3.31
Figure 3.8: Stiffened Panel with Magnified Anti-Symmetric Geometric Imperfection ... 3.32
Figure 3.9: Finite Element Mesh of a Typical Stiffened Panel with Different Form of Geometric Imperfection. (a) Symmetric Imperfection 3.33
Figure 3.9: (Continued) Finite Element Mesh of a Typical Stiffened Panel with Different Form of Geometric Imperfection. (b) Non-Symmetric Imperfection 3.34
Figure 3.10: Comparison of Load-Shortening Curves Predicted by Using Symmetric and Non-Symmetric Geometric Imperfections 3.35

Figure 3.11: Final Deformed Configurations of the Stiffened Panel Predicted Using Different Form of Geometric Imperfections. (a) Symmetric Imperfection 3.36
Figure 3.11: (Continued) Final Deformed Configurations of the Stiffened Panel Predicted Using Different Form of Geometric Imperfections. (b) Non-Symmetric Imperfection 3.37
Figure 3.12: Improved Block Form Residual Stress Distribution in Plate and Web 3.38
Figure 3.13: Comparison of Load-Shortening Curves of the Typical Stiffened Panel Obtained Using the Original and Improved Block Form Residual Stress Distribution 3.39
Figure 3.14: Final Deformed Configuration of the Typical Stiffened Panel Predicted Using the Improved Block Form Residual Stress Distribution 3.40
Figure 3.15: Comparison of the Load-Shortening Curves Obtained Using Coarse Mesh of 4-Noded Shell Element with Block Form and Thermal Residual Stress Distributions 3.41
Figure 3.16: Comparison of the Load-Shortening Curves Obtained Using Coarse Mesh of 8-Noded Shell Element with Block Form and Thermal Residual Stress Distributions 3.42
Figure 3.17: Refined Finite Element Mesh of the Typical Stiffened Panel 3.43
Figure 3.18: Comparison of the Load-Shortening Curves Obtained Using Fine Mesh of 4-Noded Shell Element with Block Form and Thermal Residual Stress Distributions 3.44
Figure 3.19: Final Deformed Configuration of the Typical Stiffened Panel Predicted Using the Refined Mesh and Thermal Residual Stresses 3.45
Figure 3.20: The Center Loaded Clamped-Clamped Truss System Utilized for Testing the FABSTRAN Program 3.46
Figure 3.21: Comparison of Load-Center Deflection Curves of the Truss System Predicted by VAST and FASBTRAN with Different Cross-Section Representations 3.47
Figure 3.22: Comparison of Load-Center Deflection Curves of the Truss System Predicted by VAST and FASBTRAN with Constant Displacement Increment 3.48
Figure 3.23: Comparison of Load-Center Deflection Curves of the Truss System Predicted by VAST and FASBTRAN with Automatic Solution Step Adjustment 3.49
Figure 3.24: Comparison of Load-Center Deflection Curves of the Truss System Predicted by VAST and FASBTRAN with Small Solution Steps 3.50
Figure 3.25: Finite Element Mesh of a Stiffened Panel Utilized to Compare Load-Shortening Curves Predicted by the VAST and FABSTRAN Programs 3.51
Figure 3.26: Comparison of Load-Shortening Curves Predicted by FABSTRAN and VAST with Different Boundary Conditions 3.52
Figure 3.27: Final Deformed Configurations Predicted by VAST Using Different Boundary Conditions. (a) End-to-End Model 3.53
Figure 3.27: (Continued) Final Deformed Configurations Predicted by VAST Using Different Boundary Conditions. (b) Center-to-Center Model 3.54

Figure 3.28: Comparison of Load-Shortening Curves Predicted by FABSTRAN and VAST for a Typical Stiffened Panel 3.55
Figure 3.29: Problem Geometry and Material Properties for Geometrically Nonlinear Analysis of a Hinged Shallow Spherical Shell Subjected to a Center Point Load 3.56
Figure 3.30 Initial Finite Element Mesh and Final Deformed Configuration of the Hinged Shallow Spherical Shell 3.57
Figure 3.31: Load-Center Deflection Curves of the Hinged Shallow Spherical Shell Predicted by the VAST and ASAS-NL Programs 3.58
Figure 3.32: Problem Geometry and Material Properties for Geometrically Nonlinear Analysis of a Hinged Cylindrical Shell Subjected to a Center Point Load 3.59
Figure 3.33: Initial Finite Element Mesh and Final Deformed Configuration of the Hinged Cylindrical Shell 3.60
Figure 3.34: Load-Deflection Curves at Center and Edge Nodes of the Hinged Cylindrical Shell Predicted by the VAST and ASAS-NL Programs 3.61
Figure 3.35: Problem Geometry and Material Properties for Geometrically Nonlinear, Elastic-Plastic Analysis of a Hinged Spherical Shell Subjected to a Center Point Load 3.62
Figure 3.36: Initial Finite Element Mesh and Final Deformed Configuration of the Hinged Spherical Shell 3.63
Figure 3.37: Load-Center Deflection Curves of the Hinged Spherical Shell Predicted by the VAST and ASAS-NL Programs 3.64
Figure 3.38: 8-Noded Shell Element Mesh of a Typical Stiffened Panel 3.65
Figure 3.39: Comparison of Load-Shortening Curves Predicted by the VAST and ASAS-NL Program 3.66
Figure 3.40: Final Deformed Configuration of the Stiffened Panel Predicted by VAST 3.67

Figure 4.1: Digitized Load Shortening Curves for Buckling of Plate Between Stiffeners with Average Initial Imperfections 4.8
Figure 4.2: Comparison of Plate Collapse Stresses Predicted by the Analytical Formulations of Von Karman and Faulkner and the Nonlinear Finite Element Solutions 4.9
Figure 4.3: Digitized Column Strength Curves Obtained by Nonlinear Finite Element Analyses of Stiffened Panels with Average Initial Imperfection 4.10

1. INTRODUCTION

Ultimate strength analysis is a very important part of the ship integrity assessment procedure required in the Improved Ship Structural Maintenance Management (ISSMM) project. The ultimate bending strength is defined as the maximum nonlinear elastic-plastic bending capacity of the hull under different loading conditions. Because the complete collapse of a ship cross-section is normally very complicated and may involve a series of highly nonlinear large displacement elastic-plastic deformations, the most accurate method for predicting the ultimate strength of a ship cross-section involves performing full-scale nonlinear finite element analyses, in which structural details, such as residual stresses and initial imperfections, can be included. However, this analysis procedure is unpractical even on modern computers due to its enormous demand on computing power. For design purposes, a simplified approximate method for predicting ultimate strength of ship structures has been developed. In this method, the ship cross-sections are first divided into structural components, such as longitudinally stiffened panels, transversely stiffened panels and hard corners, and the nonlinear behavior of each component is then utilized to predict the behavior of the entire cross-section. This method is commonly known as the Integrated Structural Unit Method or ISUM. Using this method, a number of ultimate strength analysis programs have been developed including the ULTMAT program of DREA and the NS94 suite of programs of DERA. In the present contract, these ultimate strength analysis programs are incorporated into the MAESTRO Graphics Detail Stress Analysis (MGDSA) program through the development of a stand alone GUI system for ultimate strength applications.

As the first step in the present development, all the ultimate strength programs incorporated in the ultimate application shell program were verified through extensive numerical testing. In order to be more consistent with the NS94 programs, the ULTMAT program was modified to accept input data at the structural component level, rather than the plate-stiffener level. Various modifications were also made in the NS94 programs for ensuring their accuracy and reliability on the PC platform. The results of numerical verification and details on source code modification are presented in Chapter 2.

As mentioned earlier, the core of all the ultimate strength analysis programs is the load-shortening curve database generated by using the nonlinear finite element method. In Chapter 3, the issues of computing load-shortening curves using three different nonlinear FE programs, namely VAST, FABSTRAN and ASAS-NL, were considered. The previously developed finite element model generator for stiffened panels, LSPANEL, were reviewed and several useful new features were implemented, including an option for using 8-noded shell element, a corrosion damage modeling capability, a more realistic residual stress pattern, an option for using self-equilibrium residual stress distributions generated by the newly developed thermal stress capability in VAST and various higher order sine functions for improved representation of initial imperfections. The effects of various factors on the plastic collapse behavior of a typical stiffened panel were investigated using the VAST finite element program. In order to become familiar with the input data format of FABSTRAN and ASAS-NL, a large number of nonlinear problems were solved using these programs. The solutions to these test problems indicated that small solution steps were required in FABSTRAN analysis to ensure accuracy of solutions, and on the other hand, fine tuning of solution control parameters of ASAS-NL were still required to obtain complete load-shortening curve of stiffened panel. Based on the experience gained during these numerical studies, input data translators were developed which transformed input data for VAST into the FABSTRAN and ASAS-NL format. The input data format for the updated LSPANEL program is given in Appendix A.

The issue of structural component strength assessment was dealt with in Chapter 4. In that chapter, the limit states from the SSCP23 were first discussed and the four limit states considered in the present contract were presented in detail. Mathematical formulations for the calculation of component forces under extreme bending moment are also described.

Finally, conclusions and recommendations for further work are presented in Chapter 5.

2. MODIFICATION AND VERIFICATION OF THE ULTIMATE STRENGTH ANALYSIS PROGRAMS, ULTMAT AND THE NS94 SUITE

As mentioned in the proceeding chapter, the ultimate bending strength of a ship hull girder needs to be evaluated to assess the structural integrity of ship hull structures when various types of damage and degradation occur. Over the years, a number of computer programs for ultimate strength analysis have been developed based on the Integrated Structural Unit Method (ISUM) by DREA of Canada and DERA of UK. These programs were extensively verified on the PC platform and the results are discussed in this chapter. Some difficulties with these programs were revealed during this testing and modifications to the source codes were required to resolve these difficulties. These required modifications are also presented in this chapter.

2.1 ULTMAT

ULTMAT is a computer program developed by DREA for predicting ultimate load-carrying capacity of ship cross-sections subjected to vertical bending moments [2.1]. This program was developed based on the classical beam theory, namely planar cross-sections perpendicular to the neutral axis in original undeformed configuration remain planar and perpendicular to the neutral axis after deformation. The nonlinear bending moment-curvature curves of given ship sections were obtained through an incremental application of curvature. In each curvature increment, the axial strain increment in each structural component was computed by the product of the incremental curvature and the distance between the center of gravity of the component and the instantaneous neutral axis of the ship cross-section. An iteration algorithm was utilized to continuously update the instantaneous neutral axis to satisfy the equilibrium condition in the axial direction over the entire cross-section. After the total axial strains were obtained, the corresponding axial stresses in stiffened panels were evaluated by interpolating a group of pre-determined normalized load-shortening or effective stress-strain curves based on the plate and column slenderness ratios of the stiffened panel, whereas the stresses in hard corners, as well as other non-stiffened panel components, were estimated using an elastic-perfect-plastic stress-strain relation.

The input files for the original ULTMAT program were in the DIGFEM files format. In these files, geometry of ship cross-sections were defined at the stiffener-plate level. Key points were supplied at plate-stiffener or plate-plate junctions, including coordinates of these key points and cross-sectional geometric properties of the associated stiffeners. Each plate segment, which connects two key points, were completely defined by the numbers of these key points and the thickness of the plate. Structural components, including stiffened panels and hard corners, were automatically generated by ULTMAT. This input data format provided a convenient interface between the ultimate strength program and the DIGFEM data for ship cross-sections. However, as will be discussed later, this format, in which the stiffeners and plates were specified separately, is inconsistent with that of the UK NS94 suite of programs where ship cross-sections are defined by geometric parameters of structural components, such as stiffened panels and hard corners. This inconsistency in the input data format would significantly increase difficulties associated with the development of the ultimate strength analysis shell program. As a result, it has been decided at a meeting with the Scientific Authority to modify the input data format of the ULTMAT program from the stiffener-plate level (DIGFEM format) to the structural component level (NS94 format).

To achieve this goal, the ULTMAT program was divided into two sub-programs. The first sub-program was responsible for reading the DIGFEM files, generating structural components, calculating geometric properties of each structural component and creating input data file in a format similar to that of the NS94 programs. The second program, which was still named ULTMAT, reads the input data file created by the first program along with the normalized load-shortening curve database to predict moment-curvature curves of the ship cross-section.

During the present modification of the ULTMAT program, a number of enhancements of the original code were also accomplished. A capability for calculating the moment-curvature curves for hogging load conditions was first restored, so the sagging and hogging moment-curvature curves can now be obtained in a single execution of the ULTMAT program. The second enhancement was to expand the size of the load-shortening curve database from 16 curves to 100 curves, and to allow arbitrary spacing of the plate slenderness

ratio, β, and the column slenderness ratio, λ, corresponding to these curves. The maximum number of data points permitted in each curve was also increased. The third improvement to ULTMAT was associated with the identification and correction of bugs in the interpolation algorithm utilized in the program for calculating effective stress values for given strains in an arbitrary stiffened panel.

As will be demonstrated later in this chapter, the moment-curvature curves predicted by the modified ULTMAT program were in excellent agreement with the NS94 solutions. However, it should be pointed out that similar to the NS94C/D programs, ULTMAT only uses the pre-defined load-shortening curve database for ultimate strength calculations. As a result, special load-shortening curves associated with the damaged structural components are not permitted. Such a capability should be developed in the ULTMAT program.

2.2 NS94 Suite

The NS94 suite of programs was developed at DERA for ultimate strength analyses of ship structures. This suite contain four independent programs named NS94A, NS94B, NS94C and NS94D [2.2, 2.3], respectively. All of these programs were developed based on the ISUM method mentioned at the beginning of this chapter. Among these programs, NS94A and C can be used to generate single moment-curvature curves for vertical bending, whereas NS94B and D are able to create bi-axial interaction curves for both symmetric and unsymmetric ship cross-sections. The load-shortening curves are also utilized in different ways in these programs. NS94A and B require load-shortening curves for each structural component type and these curves must be included in the input data. On the other hand, NS94C and D utilize a set of generic bi-linear load-shortening curves embedded into the programs. Unlike the DIGFEM file format, the input data for all the NS94 programs contain information on geometric and material properties at the structural component level.

Similar to the ULTMAT program, the NS94 programs also compute the moment-curvature curves through an incremental application of curvature changes about the instantaneous neutral axis of the ship cross-section. However, the NS94 codes adopt a

numerical algorithm similar to the forward Euler method for numerical integration, in which the geometric and material properties of each structural component at the beginning of a curvature increment are utilized in the computations involved in the present solution step. Although this treatment of the curvature increment is straightforward and avoided iterations, it can cause numerical instability problems which are commonly seen in almost any explicit integration algorithms. For this reason, the accuracy of solutions can be very sensitive to the size of the solution step used in the analyses, and obviously, the proper selection of the curvature increment becomes extremely important.

Except for NS94D, the solution step size must be provided by the user in the input data file. In the present implementation of the NS94 programs in the ultimate strength shell, the solution step size was automatically calculated based on the curvature change corresponding to the first yield in the ship cross-section. Assuming that the global Y and Z axis are in the horizontal and vertical directions, respectively, the Z-coordinate of the initial neutral axis, Z_N, can be calculated as:

$$Z_N = \frac{\sum E_i A_i Z_i}{\sum E_i A_i} \tag{2.1}$$

where E_i, A_i and Z_i denote the Young's modulus, area and Z-coordinate of the i^{th} structural component, respectively. Using Z_N, the largest distance between structural members and the neutral axis, Z_{max} can then be evaluated as:

$$Z_{max} = \max\left(|Z_i - Z_N|\right). \tag{2.2}$$

Assuming the averaged yield stress for the cross-section is σ_Y, and it follows from simple beam theory that the curvature change corresponding to the first yield, κ_Y, can be expressed as:

$$\kappa_Y = \frac{\sigma_Y}{E Z_{max}} . \tag{2.3}$$

The curvature increment for ultimate strength analysis using the NS94 programs was selected as $\kappa_Y/200$. The total number of curvature increments was specified as 1000, which should be sufficient for producing the moment-curvature curves of interest.

As mentioned in the preceding paragraph, in the NS94D program, which predicts bi-axial interaction curves of ship cross-sections, the solution step size is determined automatically by the program. As a result, there is no need for the user to supply the curvature increment through the input data file. Because the bi-axial interaction curve of a ship cross-section contains ultimate bending capacities under arbitrary combinations of vertical and horizontal bending moments, its computation requires multiple ultimate strength analyses with different ratios of vertical and horizontal moments. In NS94D, either 13 or 24 ultimate strength analyses are performed, depending on whether the ship cross-section is symmetric about the vertical axis. For these analyses, the increments of the vertical and horizontal bending moments are adjusted through two arrays defined by:

```
DIMENSION ymom(24), zmom(24)
DATA zmom/1. , 1. , 1. , 1. , 1. , 1. , 1E-08 , -1. , -1. , -1. ,
#     -1. , -1. , -1. , -1. , -1. , -1. , -1. , -1. , -1E-08 , 1. ,
#     1. , 1. , 1. , 1./
DATA ymom/0. , 0.3333 , 0.6667 , 1. , 1.5 , 3. , 1E+08 , -3. ,
#     -1.5 , -1. , -0.6667 , -0.3333 , 0. , 0.3333 , 0.6667 , 1. ,
#     1.5 , 3. , 1E+08 , -3.0 , -1.5 , -1. , -0.6667 , -0.3333/
```

For the ic^{th} analysis, the moment increments were calculated as:

```
dmz = bmincr*zmom(ic)
dmy = dmz*ymom(ic)
```

where `bmincr` is also evaluated based on the first yield under vertical bending situation using a similar approach as described in Equations (2.1)-(2.3). Although this algorithm has been verified by DERA on various workstations, it contains a serious drawback: the total increment of the combined vertical and horizontal bending moment, which can be expressed as:

```
dm = sqrt(dmz**2+dmy**2) = bmincr*zmom(ic)*sqrt(1.0+ymom(ic)**2),
```

vary considerably using the execution of the program, due to the variation of the ratio of the

horizontal and vertical bending moments. For instance, when `ic=6`, `ymom(6)=3.0`, `zmom(6)=1.0`, the actual combined bending moment increment, dm, is increased to 3.16 times of the original vertical bending increment, `bmincr`. As mentioned above, because the NS94 programs adopt an explicit integration scheme, the accuracy of the predicted moment-curvature curves can be sensitive to the size of the solution step. This increase of the solution step size can cause significant errors in the predicted bi-axial interaction curve. To ensure the accuracy of computation, the combined bending moment increment should be kept constant for all ultimate strength analyses involved in the calculation of the bi-axial interaction curve. In the present work, this is achieved by modifying the original program to:

```
dmz = bmincr*zmom(ic)/sqrt(ymom(ic)**2+zmom(ic)**2)
dmy = dmz*ymom(ic)/abs(zmom(ic))
```

In addition to the reduction of the combined incremental bending moment, the maximum number of solution steps specified in the original version of NS94D is also increased. This increase is required to ensure that the peak bending moments are predicted within the maximum number of solution steps.

In addition to the above modifications in NS94D, several other modifications were also made in the NS94 programs during the present incorporation of these programs into the ultimate strength shell. The purpose of these modifications was to be able to analyze the CPF model. Among these modifications, the sizes of the arrays for storing geometric and material properties of structural components and load-shortening curves were increased, so these programs could now handle larger and more complicated ship cross-sections. All real arrays had been changed from single precision to double precision to achieve improved accuracy of computation. In order to run these programs through the ultimate strength analysis shell, a capability was added to enter the file name and its path through the command line.

2.3 Ultimate Strength Analysis of the 1/3 Scale Welded Steel Frigate Model

In order to test the newly improved ULTMAT and NS94 programs, ultimate strength analysis of the UK 1/3-scale welded steel frame frigate model is considered [2.4]. This model was selected because of the availability of the experimental data. The geometry of the cross-section was provided by DREA in the DIGFEM format and is shown in Figure 2.1. Because the ultimate strength shell program had not been developed at the time when this testing took place, the input data files for the new ULTMAT program and the NS94C/D programs were generated using the data pre-processing program developed based on the first part of the original ULTMAT code.

First, the sagging and hogging moment-curvature curves predicted by the original and modified versions of the ULTMAT program are compared in Figure 2.2. These computations were carried out using a set of normalized effective stress-strain curves created by the VAST program. Following the correction of the errors in the interpolation algorithm for load-shortening curves, the predicted ultimate bending moment capacity was significantly reduced for both sagging and hogging loading conditions. The corrected solutions are more conservative.

The results obtained by ULTMAT and NS94C were then compared. In these analyses, the 24 bilinear load-shortening curves embedded in NS94C were extracted and used for the ULTMAT run. The moment-curvature curves obtained by ULTMAT and NS94C are compared in Figure 2.3 for both sagging and hogging conditions and these curves are in excellent agreement. However, to obtain the same accuracy, smaller solution step sizes need to be used in the NS94C analysis, due to the explicit nature of the solution algorithm.

The ULTMAT results obtained using the VAST-generated load-shortening curves and the NS94C bilinear curves are compared in Figure 2.4. The pre-buckling solutions from these two ULTMAT analyses are in close agreement. But, in the post-buckling range, the moment-curvature curves predicted using the bilinear load-shortening curves decline too fast, as shown in Figure 2.4, and the solutions based on the load-shortening curves generated by

nonlinear finite element analyses are in much closer agreement with the experimental data presented by Dow [2.4].

The bi-axial bending interaction curve for the 1/3 welded steel frigate model was also obtained using both the original and modified versions of the NS94D program. The result is displayed in Figure 2.5. It is obvious that the original version of NS94D generated unreasonable numerical results. These errors were found to be associated with the improper definitions of the solution step size and the maximum number of solution steps. Using the modified version of NS94D, excellent bi-axial interactive curves were obtained.

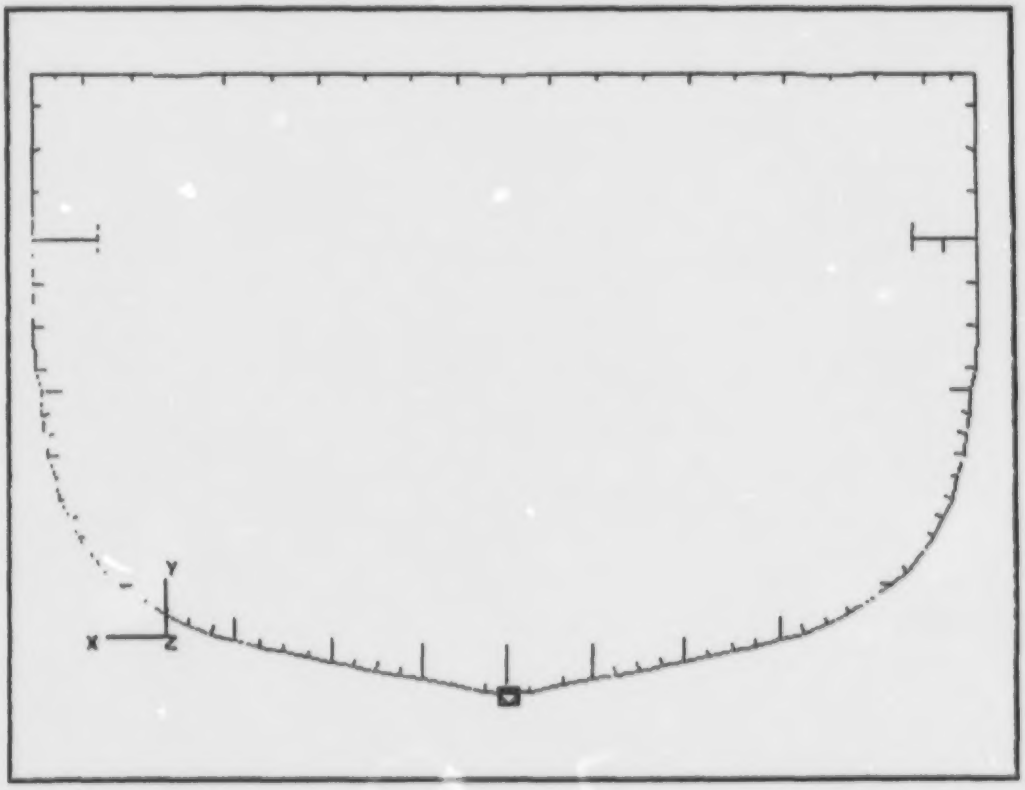

Figure 2.1: Cross-Section of the 1/3 Welded Steel Frigate Model

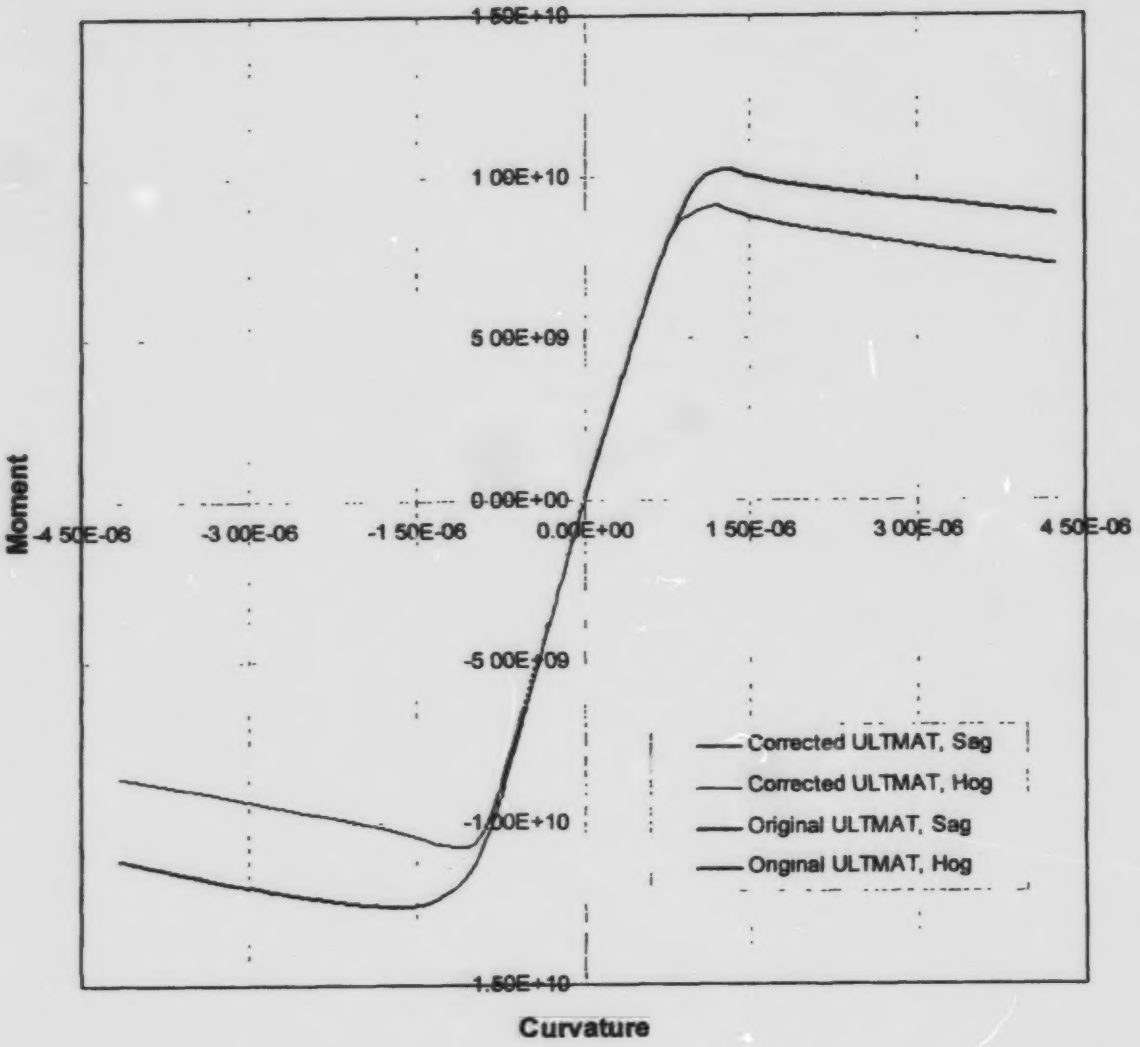

Figure 2.2: Comparison of Sagging and Hogging Moment-Curvature Curves Predicted by the Original and Modified ULTMAT Program Using a Set of Normalized Load-Shortening Curves Generated by VAST

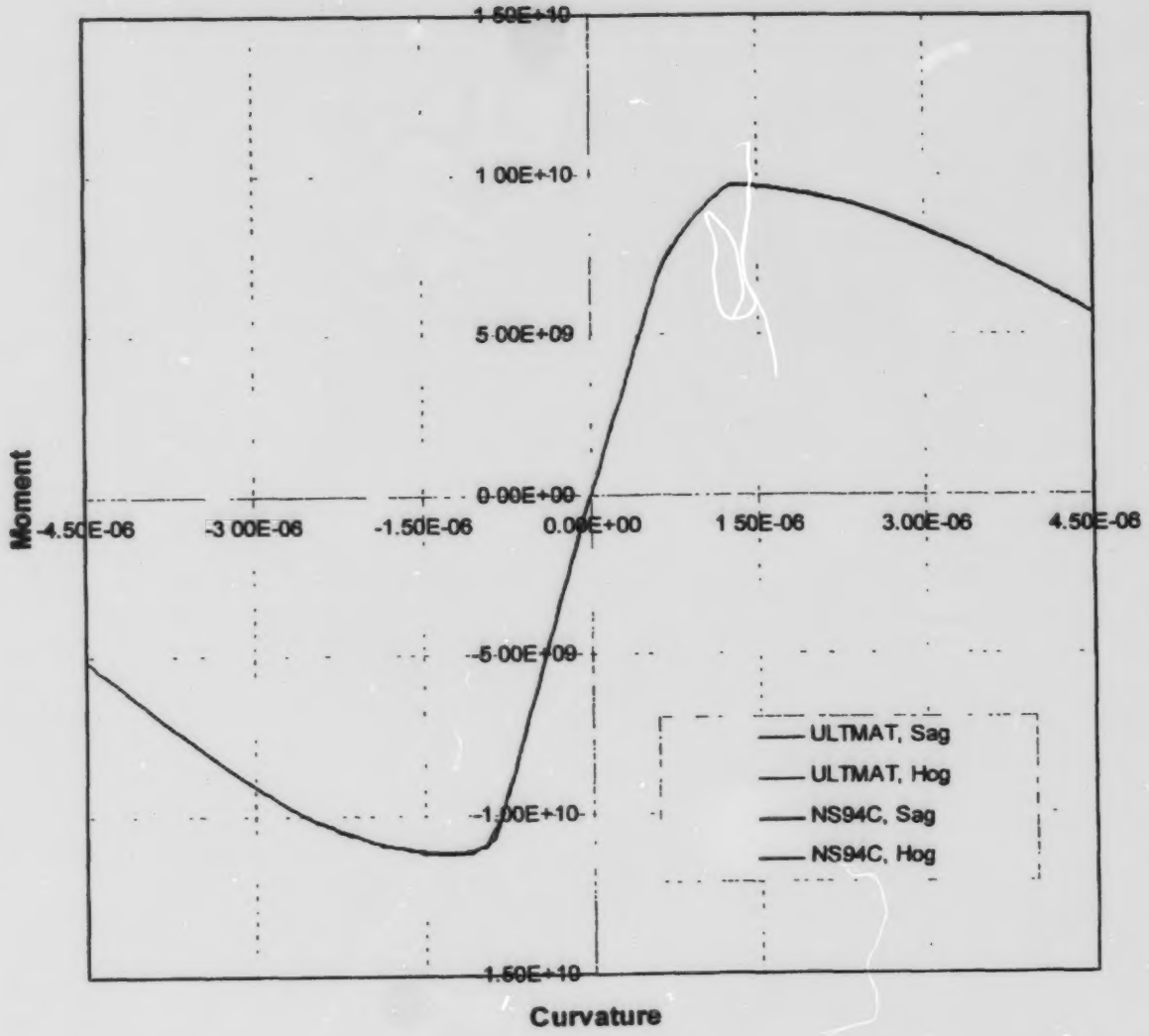

Figure 2.3: Comparison of Sagging and Hogging Moment-Curvature Curves Predicted by ULTMAT and NS94C Using a Set of Bilinear Load-Shortening Curves into the Incorporated NS94C Program

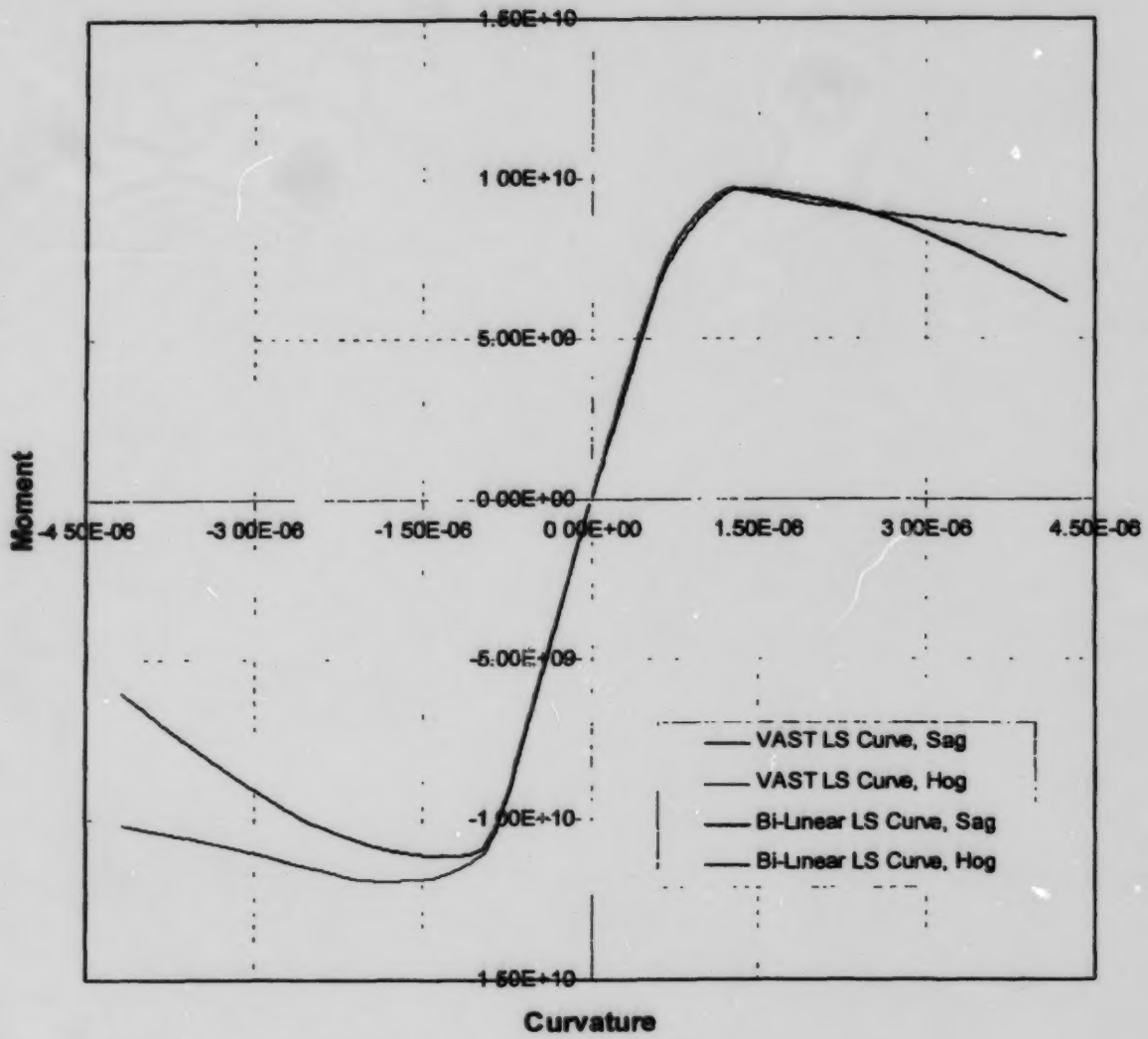

Figure 2.4: Comparison of Sagging and Hogging Moment-Curvature Curves Predicted by ULTMAT Using the VAST-Generated and Bilinear Load-Shortening Curves

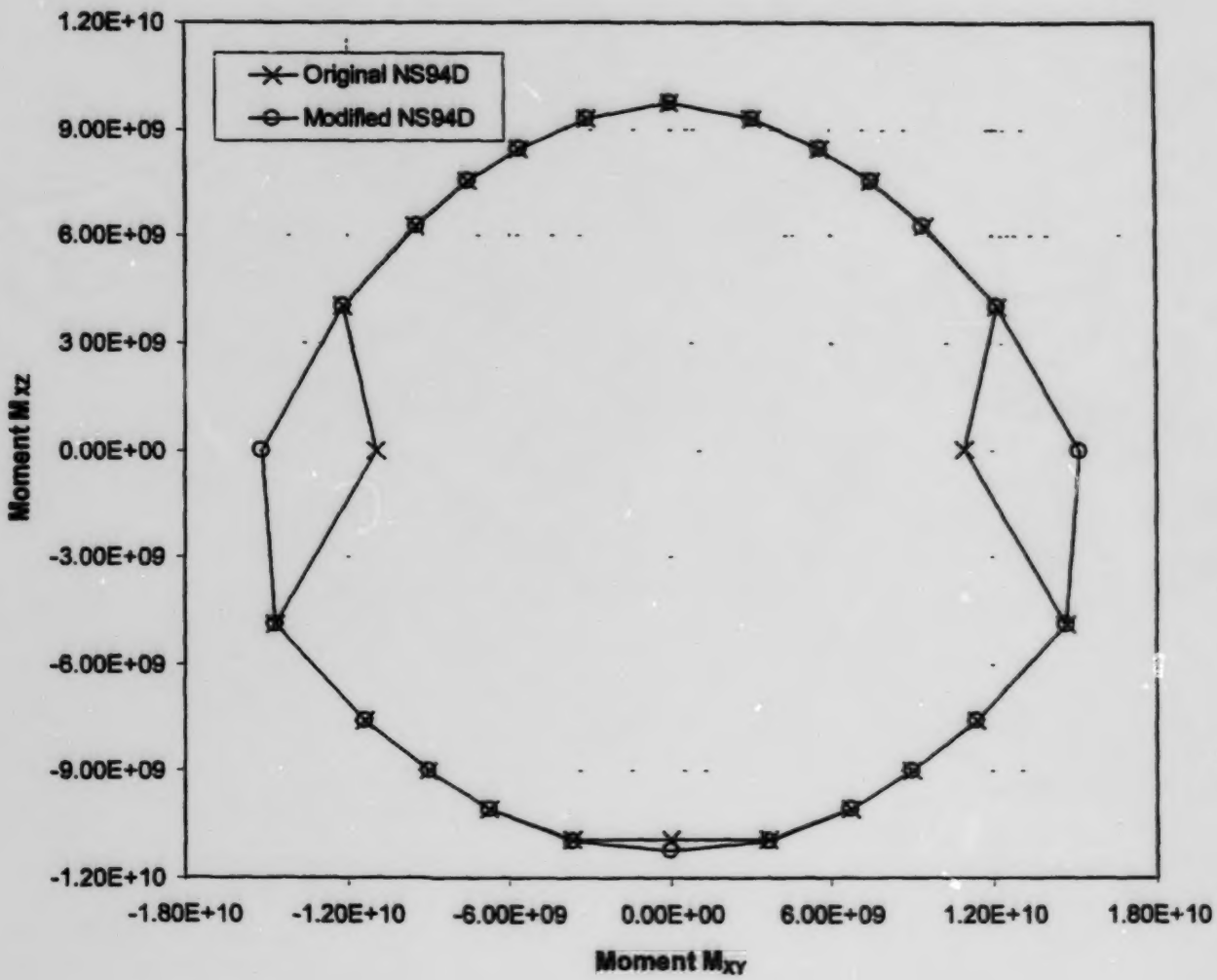

Figure 2.5: Comparison of the Bi-Axial Bending Interaction Curves Predicted by the Original and Modified Versions of the NS94D Program.

3. MODIFICATION OF THE LSPANEL PROGRAM FOR GENERATING INPUT DATA FILES FOR LOAD-SHORTENING CURVE COMPUTATIONS USING VAST, FABSTRAN AND ASAS-NL

LSPANEL is an automatic model generator for nonlinear plastic collapse analysis of stiffened panels. This program was originally developed under a previous contract for generating load-shortening curve database for the Halifax class frigate [3.1]. The original LSPANEL program could only generate the 4-noded quadrilateral shell element models for the VAST program. The detailed dimensions of the stiffener cross-sections were provided by the user, and the plate dimensions could either be directly specified or automatically computed based on the user supplied column and slenderness ratios and the ratio of the stiffener cross-section area to the total cross-section area of the stiffened panel. The initial geometric imperfection was defined by combining the components of stiffener and plate imperfections. Variations of the magnitude of imperfections in both the axial and transverse directions were expressed by half-sine functions. A block form residual stress distribution was assumed in plate and the stiffener was assumed residual stress free. Two boundary conditions, namely the end-to-end and center-to-center boundary conditions, were considered. For both boundary conditions, multi-point constraint equations were utilized to enforce the end sections to remain planer after nonlinear deformations.

In the present contract, the LSPANEL program was significantly improved by implementing the 8-noded shell element, various corrosion patterns, improved residual stress patterns, higher-order geometric imperfection terms, and options for generating input data files for the FABSTRAN and ASAS-NL programs. The input parameters required by the modified LSPANEL program are provided in Appendix A at the end of this report.

3.1 VAST

As mentioned above, the first major enhancement to the LSPANEL program was to provide an option for creating finite element models of stiffened panels using the 8-noded shell element. This was one of the additional request made by Bob Dow during his visit to Martec in 1999. Bob Dow pointed out that he preferred the 8-noded element because based on

experience at DERA, the 8-noded shell element normally produced more accurate nonlinear results than the 4-noded one. In order to incorporate this higher-order shell element into LSPANEL, two additional subroutines had been developed to calculate the coordinates of the mid-side nodes both over cross-section and along the axial direction, and to form the nodal connectivity arrays. This new modeling option had been fully tested for various meshing parameters which led to both uniform and locally refined finite element meshes. To compare the accuracy of the 4-noded and 8-noded shell elements, a typical stiffened panel with plate slenderness ratio β=2.0, column slenderness ratio λ=0.6 and stiffener-to-total area ratio As/A=0.2 was considered. The finite element meshes of both shell elements are displayed in Figure 3.1. It should be noted that these two meshes possessed approximately the same number of degrees-of-freedom and as a result, led to comparable levels of computational efforts. The load-shortening curves and final deformed shapes predicted by both elements are compared in Figures 3.2 and 3.3, respectively. Very close agreement between these solutions was observed.

The next improvement of the LSPANEL program in this contract was the incorporation of a corrosion modeling capability based on the corrosion patterns specified by DREA [3.2]. These corrosion patterns included uniform, sinusoidal and edge reductions of thicknesses of plate, web and flange. Assuming the X, Y and Z axis were along the lateral, axial and vertical directions, respectively, the percentage of thickness reduction at an arbitrary point in plate segments at both sides of the stiffener can be expressed as:

$$P(X,Y) = P_{01} + P_{S1}\sin\left(\frac{\pi|X|}{b}\right)\cos\left(\frac{\pi Y}{a}\right) + \left(P_{C1}\frac{|X|}{b} + P_{A1}\frac{b-|X|}{b}\right)\cos\left(\frac{\pi Y}{a}\right) + \left(P_{B1}\frac{a+2Y}{2a} + P_{D1}\frac{a-2Y}{2a}\right)\sin\left(\frac{\pi|X|}{b}\right), \qquad for\ X<0 \tag{3.1a}$$

and

$$P(X,Y) = P_{02} + P_{S2}\sin\left(\frac{\pi X}{b}\right)\cos\left(\frac{\pi Y}{a}\right) + \left(P_{A2}\frac{X}{b} + P_{C2}\frac{b-X}{b}\right)\cos\left(\frac{\pi Y}{a}\right) + \left(P_{B2}\frac{a+2Y}{2a} + P_{D2}\frac{a-2Y}{2a}\right)\sin\left(\frac{\pi X}{b}\right), \qquad for\ X \geq 0 \tag{3.1b}$$

where P_0 and P_s denote the amplitudes of the uniform and sinusoidal thickness reductions, whereas P_A, P_B, P_C and P_D indicate percentage thickness reductions on the four edges of the left and right plate segments, respectively. "a" and "b" indicate the panel length and the plate width. In order to model unsymmetric corrosion patterns, the coefficients for plates left and right to the stiffener were specified independently in the LSPANEL program.

By taking a similar approach for the web, the percentage thickness reduction in the web can be expressed as:

$$P(Y,Z) = P_0 + P_S\sin\left(\frac{\pi Z}{D_W}\right)\cos\left(\frac{\pi Y}{a}\right) + \left(P_P\frac{D_W - Z}{D_W} + P_F\frac{Z}{D_W}\right)\cos\left(\frac{\pi Y}{a}\right) \tag{3.2}$$

where P_0 and P_s again denote the amplitudes of the uniform and sinusoidal components of the percentage thickness reductions, whereas P_P and P_F indicate percentage thickness reductions along the plate-web and flange-web junctions. D_W denotes the height of the web.

As for the plate segments on different sides of the web, the thickness variations in flange segments on either side of the web can also be expressed by separate mathematical formulas as:

$$P(X,Y) = P_0 + P_S\sin\left(\frac{\pi|X|}{D_F}\right)\cos\left(\frac{\pi Y}{a}\right) + \left(P_W\frac{D_F - 2|X|}{D_F} + P_{E1}\frac{2|X|}{D_F}\right)\cos\left(\frac{\pi Y}{a}\right), \qquad for\ X < 0 \tag{3.3b}$$

and

3.4

$$P(X,Y) = P_0 + P_s \sin\left(\frac{\pi X}{D_F}\right)\cos\left(\frac{\pi Y}{a}\right) + \left(P_W \frac{D_F - 2X}{D_F} + P_{E2}\frac{2X}{D_F}\right)\cos\left(\frac{\pi Y}{a}\right), \quad for\ X \geq 0 \tag{3.3a}$$

where P_0 and P_s denote the amplitudes of the uniform and sinusoidal thickness reductions over the whole flange, and P_W and P_{E2} indicate thickness reductions at the flange-web junction and left and right outer edges of the flange, respectively. D_F denotes the width of the flange. The coefficient P_E at both edges can be specified independently.

Using this capability, a number of finite element meshes of corroded stiffened panels were generated and the effect of corrosion on the load-shortening behavior of these panels was studied. Nonlinear finite element solution was first obtained for a non-corroded stiffened panel which had the same geometric properties as considered earlier in this section, namely β=2.0, λ=0.6, As/A=0.2. The load-shortening curves obtained with and without residual stresses are shown in Figure 3.4. Two corroded panels, which had symmetric and non-symmetric plate corrosions about the stiffener, were then considered. The percentage thickness reductions used in these corroded models are summarized in Table 3.1 and the plate thickness distributions are displayed in Figure 3.5. Load-shortening curves were computed for both symmetrically and non-symmetrically corroded panels and the results are compared with those from the non-corroded stiffened panel in Figure 3.4. Significant reductions in the load-carrying capacity of stiffened panels caused by corrosion are indicated in these load-shortening curves. The final failure configurations predicted for corroded and non-corroded panels are almost identical, so only the one obtained for the symmetrically corroded model is given in Figure 3.6. Stiffened panels with symmetric and non-symmetric flange corrosions were also considered, however, for this particular panel, flange corrosions had no significant impact on the predicted overall nonlinear behavior. This was probably because for the present combination of geometric parameters, the plate was considerably weaker than the stiffener and would buckle earlier than the stiffener even when the stiffener was corroded.

In the previous contract for load-shortening curve generation using the VAST

program, the pattern of plate imperfection specified by DREA was symmetric about the stiffener and contained two imperfection components, a stiffener imperfection and a plate imperfection [3.1]. A typical geometrically imperfect panel is shown in Figure 3.7. This pattern was similar to imperfections caused by welding. However, it could be argued that it would be more appropriate to use an anti-symmetric imperfection pattern in the load-shortening curve computation because such pattern was more consistent with the lowest buckling mode of plate. For testing purposes, an anti-symmetric plate imperfection pattern was implemented into the LSPANEL program, in which initial distortions in plate can be expressed as:

$$\Delta Z = \delta \cos\left(\frac{\pi Y}{a}\right) + \omega_0 \cos\left(\frac{\pi Y}{a}\right) \sin\left(\frac{\pi X}{b}\right) \tag{3.4}$$

where δ and ω_0 denote the amplitudes of the stiffener and plate imperfections, respectively, and the initial distortions in the stiffener were computed as:

$$\begin{aligned} \Delta Z &= X \sin(\theta) + Z \cos(\theta) + \delta \cos\left(\frac{\pi Y}{a}\right) \\ \Delta X &= X \cos(\theta) - Z \sin(\theta) \end{aligned} \tag{3.5}$$

where

$$\theta = \tan^{-1}\left(\frac{\omega_0 \pi}{b} \cos\left(\frac{\pi Y}{a}\right)\right). \tag{3.6}$$

This distortion pattern for stiffener ensures that the web remains perpendicular to the distorted plate along the length of the stiffened panel. A typical stiffened panel with the anti-symmetric imperfection defined in Equations (3.4)-(3.6) is shown in Figure 3.8.

In order to compare the load-shortening curves predicted by using these two forms of imperfections, the stiffened panel discussed in the preceding paragraphs was reconsidered using both the symmetric and anti-symmetric geometric imperfections. The finite element meshes are presented in Figure 3.9. Because the initial distortions were comparable to the magnitude of the plate thickness, they could hardly be seen in the finite element meshes. By

including a linear buckling mode as additional geometric imperfections, nonlinear post-buckling analyses were performed successfully for both symmetric and anti-symmetric imperfections and the predicted load-shortening curves are presented in Figure 3.10. Contrary to the initial expectations, the use of the anti-symmetric imperfection pattern on this stiffened panel model resulted in a higher peak load and higher post-buckling stiffness than those for the symmetric imperfection. The final deformed configurations obtained using these two imperfections were almost identical, as shown in Figure 3.11. Although the above numerical results indicated that the anti-symmetric imperfections corresponding to a single half-sine wave in the longitudinal direction might be inappropriate for load-shortening curve calculations, the use of higher-order anti-symmetric imperfections defined as:

$$\Delta Z_{add} = \cos\left(\frac{\pi Y}{a}\right)\sin\left(\frac{\pi X}{b}\right)\left[\sum_{n=1,3,5,} p_n \cos\left(\frac{n\pi Y}{a}\right)\right] \tag{3.7}$$

as additional imperfections has been proved to be very successful [3.3]. These imperfections have also been incorporated in the present version of the LSPANEL program.

The final improvement of LSPANEL accomplished in the present contract was related to the enhancement in residual stress representation. In the previous contract for generating load-shortening curves using VAST [3.1], residual stresses were only specified in the plate using a block approximation as shown in Figure 3.12(a). However, experimental data confirmed that significant residual stresses also existed in the web [3.4]. Based on the measured residual stress distribution, a bi-linear approximation was developed in the present work to model residual stresses in the web, as shown in Figure 3.12(b), and has been implemented in the LSPANEL program. Load-shortening curves were obtained using the original and improved residual stress patterns and the results are compared in Figure 3.13. For the present stiffened panel (β=2.0, λ=0.6, As/A=0.2), the addition of residual stresses in the web had no significant effect on the overall nonlinear behavior. This is probably because the residual stresses prescribed in the web are in self-equilibrium in the axial direction and the buckling stiffness of the plate is relatively weaker. The final deformed configuration of the stiffened panel obtained by using the improved residual stress distribution is displayed in

Figure 3.14, which is in close agreement with that obtained using the original residual stress pattern.

It had been discovered earlier [3.5] that for stiffened panel with large plat slenderness value and large plate imperfections, the application of the block-form residual stresses in the plate resulted in a significant lack of self-equilibrium associated with the initial stress distribution and the automatic redistribution of the stresses might cause a negative load at the beginning of the predicted load-shortening curve. In order to obtain a more accurate residual stress pattern, thermal stress analyses have been suggested [3.4]. In this analysis, fictitious temperature variations are specified at the plate-web and/or the web-flange junctions to simulate the cool-down process after the welding and thereby self-equilibrium of the resulting thermal stress field is guaranteed. For the purpose of generating residual stresses to be used in nonlinear post-buckling analysis of stiffened panels, a fully automated linear thermal stress analysis capability has recently been developed in the VAST program [3.3].

A comparison of the load-shortening curves obtained using the block form residual stresses and those generated by using thermal stress analyses was carried out for both 4-noded and 8-noded shell elements. The results are presented in Figures 3.15 and 3.16. From these results, it was readily recognized that for the 4-noded shell element, the load-shortening curve predicted using residual stresses generated by the thermal stress analysis was quite sensitive to the finite element mesh. This is probably because in the thermal stress solutions with very coarse meshes, the tensile stress region could become wider than that prescribed in the block form distribution. In the fully automatic thermal analysis procedure in VAST, the maximum tensile stress at the plate-web junction was scaled to the initial yield stress of the material. Due to self-equilibrium residual stress distribution, the increase of the tensile stress zone resulted in an increase of the maximum compressive stresses in the plate, which caused the initial yielding of the plate to occur earlier. The eight-noded shell element solution was, however, less sensitive to the mesh, due to the existence of the mid-side nodes. To confirm the above observation, a refined four-noded finite element mesh, as shown in Figure 3.17, was then considered. The load-shortening curves obtained using different residual stress patterns are compared in Figure 3.18 and significantly improved agreement between these solutions

was observed. The final deformed shape predicted using the refined mesh and the thermal residual stresses are given in Figure 3.19, which is in very good agreement with that obtained earlier using the coarser mesh.

It was originally planned to generate load-shortening curves of hard corners using nonlinear finite element analyses, and for this purpose, the LSPANEL program would have to be modified for creating finite element models of hard corners. In addition, because hard corners contained plate segments meeting at a common point in arbitrary angles, boundary conditions must be specified in skewed coordinate systems. In geometrically nonlinear analyses, these skewed systems need to be repeatedly updated based on the most recent deformed configurations. Such a capability was not implemented in the current version of the VAST program. However, during Bob Dow's visit, he pointed out that there was no need to perform nonlinear FE analyses for hard corners, as the nonlinear behavior of such structural components could be satisfactorily approximated by elastic-perfectly-plastic stress strain curves with a reduced cross-sectional area. Bob Dow claimed that a formulae for this reduced area was implemented in all the NS94 programs. However, after a study of the source code, this formulae was not identified. Attempts to obtain this formulae directly from DERA have also been unsuccessful.

3.2 FABSTRAN

FABSTRAN is a computer program for evaluating static and dynamic large-displacement, elastic-plastic behavior of plane-frames and beam-column structures. This program was developed by DERA based on an incremental finite element formulation and both initial geometric imperfection and arbitrary residual stress distributions were permitted. FABSTRAN is one of the nonlinear finite element programs to be incorporated into the ultimate strength analysis program for generating load-shortening curves of stiffened panels.

For testing purposes, the elastic post-buckling response of a clamped-clamped simple truss structure subjected to a center point load was first considered using both the VAST and FABSTRAN programs. This problem has been widely used to test the performance of

geometrically nonlinear beam formulations, and is often referred as the Williams toggle problem [3.6]. The geometric and material properties, boundary conditions and external load are shown in Figure 3.20. This example problem was previously solved by using FABSTRAN and the resulting load-deflection curve was compared with the analytical solution of Williams [3.6] in the FABSTRAN manual [3.7] with excellent agreement. In this previous FABSTRAN analysis, half of the truss system was modeled using five beam elements.

In order to make direct comparisons with the FABSTRAN results published in reference [3.7], an identical finite element mesh was utilized in the present analysis. The VAST program was first used to obtain the complete load-center deflection curve using 15 solution steps. The VAST result, which is shown in Figure 3.21, was in excellent agreement with the analytical solution of Williams [3.6]. After a careful study of the FABSTRAN user's manual, input data files for FABSTRAN were generated from the VAST input data format. In the FABSTRAN program, geometric information about the beam cross section could be defined using two methods, depending on whether material nonlinearity was involved in the analysis. If only geometric nonlinearities were expected, the beam cross-sectional properties were defined using area and moment of inertia (NC=3). However, if material nonlinearity was also going to be considered, the layered beam approach must be utilized (NC=2), in which the elastic-plastic material properties could be defined independently for each layer. It is obvious that for elastic-plastic post-collapse analysis of stiffened panels, the layered beam option must be employed.

In the present nonlinear analyses of the truss system using FABSTRAN, the elastic material option (NC=3) was first considered, in which the beam cross-sectional properties were defined using area and moment of inertia. In this case, FABSTRAN also produced a complete load-center deflection curve in 15 solution steps. This curve is also shown in Figure 3.21, which is in close agreement with the analytical solution published by Williams [3.6]. The same geometrically nonlinear problem was then solved using the layered beam option (NC=2). The rectangular beam cross-section was divided into 10 layers. In order to ensure elastic deformations throughout the nonlinear analysis, fictitiously high values of initial yield stresses were specified for all layers. However, with this beam cross-section definition,

significant discrepancies between the FABSTRAN prediction and the analytical solution were observed in both pre- and post-buckling regions as indicated in Figure 3.21. Various solution techniques and convergence tolerances were attempted at this point. The results are presented in Figures 3.22 and 3.23. It was obvious that the use of advanced solution algorithms did not improve the accuracy of FABSTRAN solutions.

By examining the FABSTRAN results shown in Figure 3.23, it was finally recognized that the errors in the nonlinear solution increased with the increase of the solution step size. Motivated by this finding, additional FABSTRAN analyses were performed using a significantly reduced step size (1/100 of the original). As expected, with this extremely small solution step size, FABSTRAN did produce more accurate load-deflection curve as shown in Figure 3.24. This observation indicates that FABSTRAN should be used with caution. In particular, small solution steps must always be utilized when it is employed to generate load-shortening curves of stiffened panels.

In order to test further the accuracy of load-shortening curves predicted by the FABSTRAN program, nonlinear plastic collapse analyses of a typical stiffened panel were performed using both the FABSTRAN and VAST programs. The FABSTRAN input file for this stiffened panel was provided by DERA as a test case with the executable file of FABSTRAN. The geometric properties of the stiffened panel cross-section were extracted from the FABSTRAN data file and are summarized in Table 3.2, and the material properties utilized in these analyses were E=207000 MPa, ν=0.3 and σ_Y=275 MPa. These geometric and material properties led to a plate slenderness ratio of β=3.264 and a column slenderness ratio of λ=0.3448. The finite element mesh employed in the VAST analyses was generated using the LSPANEL program and is displayed in Figure 3.25.

Two boundary conditions were considered in the VAST analyses, including an end-to-end model and a center-to-center model. The load-shortening curves predicted by using different boundary conditions are compared with the FABSTRAN prediction in Figure 3.26 with reasonably good agreement. For this particular stiffened panel, the center-to-center model produced a highest peak load, but FABSTRAN predicted the greatest post-buckling

strength. The final deformed configurations of the stiffened panel obtained by using VAST for both boundary conditions are shown in Figure 3.27. It should be pointed out that since FABSTRAN uses planer beam elements, it requires significantly less execution time than the VAST program for computing load-shortening curve of a given stiffened panel. However, FABSTRAN is unable to handle stiffened panels with local damage, such as corrosion, and stiffened panels involving more complicated collapse modes, such as those dominated by stiffener buckling.

After we became familiar with the FABSTRAN input data format, an automatic model generator was developed in the LSPANEL program for automatic generation of FABSTRAN input data for load-shortening curve computations of a user defined stiffened panels. This model generator required information on elastic-plastic material properties and detailed geometrical descriptions of the stiffened panel structure to be considered, including cross-sectional dimensions and panel length along the axial direction. All this information was available in the input data for the LSPANEL program.

The procedure for idealizing the stiffened panel into beam elements and representing the cross-section using material layers were developed following the sample input file provided by DERA. For "Tee" stiffener cross-section, the flange and web were each divided into 10 equal layers. In order to avoid potential singularity of global stiffness matrix caused by complete yielding of a cross-section, 20 pseudo layers, which had widths of one percent of the physical layers and extremely high yield stresses, were added to the cross-section to provide a strain hardening modulus of 0.01E, where E is the Young's modulus. A uniform compressive residual stress, which was equal to 10 percent of the yield stress, was assumed in both the flange and web. For plate, load-shortening curves obtained using moderate residual stresses and imperfections were utilized.

In the axial direction, the stiffened panel was discretized into 20 equally-spaced planar beam elements. Unlike the input data for standard finite element programs, element geometry in FABSTRAN was not directly defined using nodal coordinates, but rather through the beam lengths and local coordinate systems defined at each end of the beam element. This

definition requires evaluation of beam orientations in the X-Z plane. If the center-to-center boundary condition was adopted and the amplitude of geometric imperfection at the left end was assumed to equal half of the one at the right end, as suggested by Bob Dow, the vertical imperfection was readily to be expressed as:

$$\Delta Z(X) = \begin{cases} -\delta_0 \sin\left(\frac{\pi}{a}\left(X - \frac{a}{2}\right)\right) & for\ X < \frac{a}{2} \\ -2\delta_0 \sin\left(\frac{\pi}{a}\left(X - \frac{a}{2}\right)\right) & for\ X > \frac{a}{2} \end{cases} \tag{3.8}$$

where "a" again denotes the length of the stiffened panel and δ_0 equals to 2/3 of the maximum stiffener imperfection used for generating the equivalent shell element model. The beam orientations could be readily obtained by differentiating the above imperfection expression with respect to the axial coordinate, X. To obtain nonlinear solutions in the post-buckling range, the displacement control method had been utilized through application of displacement increments at the left end of the stiffened panel. The constant displacement increment was selected such that the average axial strain reached yield strain in 33 solution steps. A total of 200 solutions steps were specified, which should be sufficient to provide load-shortening curves required in most of the ultimate strength analyses.

A typical FABSTRAN input data file generated by the LSPANEL program is listed in Table 3 3. This data set was prepared for the stiffened panel, which had been extensively studied in this chapter. The load-shortening curves obtained by using FABSTRAN and VAST are compared in Figure 3.28. Very good agreement was found between these two solutions. However, it should be noticed that the FABSTRAN solution became unstable in the post-buckling range and the execution terminated due to conditioning problem at an end-shortening around 10 mm.

3.3 ASAS-NL

A special purpose model translator was developed in the LSPANEL program for translating finite element models of stiffened panels from the VAST format to the ASAS-NL format [3.8]. The current version of the translator was capable of handling solution control parameters required by the highly nonlinear post-buckling analysis, elastic-plastic material properties, concentrated nodal loads and multi-point constraint equations. However, only one element type, namely the 8-noded shell, has been implemented in the present contract to satisfy the requirement of DERA. Distributed element loads have not yet been incorporated, as they are not required in load-shortening curve calculations. The proper procedures for modeling residual stresses and corrosion-induced thickness reductions in ASAS-NL analyses have not yet been identified and request for technical support has been forwarded to DERA.

The overall structure of the input data file for ASAS-NL was quite straightforward and similar to that for the VAST program. This input file included data sections of global solution control parameters, nodal coordinates and element connectivities, material and geometric properties, boundary conditions and external loads. Each data section was terminated with the keyword END, and the whole file must be terminated by the keyword STOP. A typical input data file prepared for a geometrically nonlinear analysis of a shallow spherical shell using ASAS-NL is given in Table 3.4.

The data specifying control parameters were referred as Preliminary Data in ASAS-NL user manual [3.8]. These data indicate the type of current analysis (static or transient) and the type of anticipated nonlinearities (large displacements, plasticity, creep, follower force effect et al). Parameters for the advanced nonlinear algebraic equation solution algorithms, i.e. the displacement control method and the constant arc-length method, were defined through the SOLU command. These parameters included total number of solution steps, displacement increment for the first step, as well as the maximum displacement and load parameter for the purpose of termination of the nonlinear runs. To use the automatic solution step adjustment capability, the desired number of iterations for each solution step must also be provided in the same command. The UPDA command controlled the frequency for updating nodal

coordinates and tangent stiffness matrix during nonlinear analyses. The FILE command controlled the generation of the restart files. Finally, information to be written into the ASCII result file was specified through the OUTP and BLOC commands.

The preliminary data section was followed by the structural data section which included nodal coordinates, element connectivity, and material/geometric properties. Nodal coordinates could be defined in Cartesian, cylindrical and spherical coordinate systems, and could be provided with respect to either global or local systems. The element connectivity data was led by keywords indicating the element type. Elements were grouped based on material properties. However, element numbers were not required in the input data file and were automatically generated by the program when the element data were processed. The material property definition included Young's modulus, Poisson's ratio and mass density. For elastic-plastic material types, it also included initial yield stress and work hardening modulus. For 8-noded shell element, the only geometry property to be defined was the shell thickness. The boundary conditions data contained information on suppressed degrees-of-freedom, prescribed displacements and multi-point constraint equations. The external loads were provided in the loading data section.

In order to verify the ASAS-NL input data files generated by the newly developed model translator, three well-known test problems for nonlinear finite element programs were considered and the ASAS-NL results were compared with the VAST solutions. The first test case was a geometrically nonlinear analysis of a hinged shallow spherical shell. The problem geometry and material properties are given in Figure 3.29. Making use of the symmetry, only one quarter of the shell was discretized into four 8-noded shell elements. The finite element mesh and the final deformed configuration predicted by VAST are shown in Figure 3.30, and the load-center deflection curves obtained by ASAS-NL and VAST are compared in Figure 3.31. Both programs produced complete solution to this nonlinear problem successfully, and the results are in excellent agreement.

The second test case considered in the present study was a hinged cylindrical shell as shown in Figure 3.32. Compared with the previous problem, this test case was more difficult

due to the snap-back behavior of the loaded node. Again, making use of symmetry, one quarter of the cylindrical shell was represented by nine 8-noded shell element as shown in Figure 3.33. The final deformed configuration predicted by VAST is also shown in Figure 3.33. The load-vertical deflection curves at both center and edge of the shell obtained by ASAS-NL and VAST are compared in Figure 3.34. Excellent agreement between these solutions is again observed.

In the third test problem, we considered an elastic-plastic, post-buckling analysis of a spherical shell subjected to a center point load. Geometric and material properties of the spherical shell are shown in Figure 3.35. Due to symmetry, in the present analysis, one quarter of the shell was discretized into 12 8-noded shell elements. The original and deformed meshes are shown in Figure 3.36. The load-center deflection curves predicted by ASAS-NL and VAST are compared in Figure 3.37. These two solutions are in close agreement at the early stage of nonlinear deformation, however, ASAS-NL predicted a considerably higher peak load than VAST. The reason for this discrepancy is not well understood yet.

Because the results for the above test problems confirmed the correctness of the ASAS-NL input data files generated by the newly developed model translator, a nonlinear plastic post-buckling analysis of a typical stiffened panel was then performed. The geometric parameters for the stiffened panel considered in this analysis were still selected as β=2.0, λ=0.6 and As/A=0.2. The finite element mesh using 8-noded shell elements is shown in Figure 3.38. The VAST program was first utilized to perform nonlinear analyses and load-shortening curves were obtained with and without the residual stresses taken into account. Both curves are displayed in Figure 3.39 and the final deformed shape predicted by VAST is given in Figure 3.40. ASAS-NL was then used to solve this problem. Although ASAS-NL predicted a pre-buckling response which was in good correlation with the VAST results, the analysis stopped right after the peak load was passed and post-buckling solution could not be obtained. During a telephone conversation with Bob Dow, he pointed out that the solution parameters used in the ASAS-NL analysis could be finely tuned to achieve an improved performance. Upon his request, the input data file was sent to him by e-mail for DERA investigation, however, no specific advice on how to proceed has yet been received.

Table 3.1: Percentage Reductions Used in Corroded Stiffened Panel Models

Corrosion Pattern	Plate 1 (x<0)		Plate 2 (x>0)	
	Uniform	Sinusoidal	Uniform	Sinusoidal
Symmetric	10%	40%	10%	40%
Unsymmetric	20%	20%	10%	20%

Table 3.2: Detailed Dimensions of Cross-section of the Stiffened Panel

Component	Width/Depth (mm)	Thickness (mm)
Plate	600	6.7
Web	113.6	6.534
Flange	62.865	13.40

Table 3.3: Input Data for Nonlinear of a Typical Stiffened Panel Using FABSTRAN

```
load shortening stiffened panel model (test1)
    1     0     0     0     0     0     0      0.00
          2          21          20           1           1         200           3     0     1
  207000.0     79615.4       350.0           0           0           1          25     0.0010
          1          41           1
          1     158.790     76.200      1.420    -35.000 0.100E+10 1.00 1.00
          2     157.370     76.200      1.420    -35.000 0.100E+10 1.00 1.00
          3     155.950     76.200      1.420    -35.000 0.100E+10 1.00 1.00
          4     154.530     76.200      1.420    -35.000 0.100E+10 1.00 1.00
          5     153.110     76.200      1.420    -35.000 0.100E+10 1.00 1.00
          6     151.690     76.200      1.420    -35.000 0.100E+10 1.00 1.00
          7     150.270     76.200      1.420    -35.000 0.100E+10 1.00 1.00
          8     148.850     76.200      1.420    -35.000 0.100E+10 1.00 1.00
          9     147.430     76.200      1.420    -35.000 0.100E+10 1.00 1.00
         10     146.010     76.200      1.420    -35.000 0.100E+10 1.00 1.00
         11     158.790      0.762      1.420    -35.000 0.100E+10 .1E9 1.00
         12     157.370      0.762      1.420    -35.000 0.100E+10 .1E9 1.00
         13     155.950      0.762      1.420    -35.000 0.100E+10 .1E9 1.00
         14     154.530      0.762      1.420    -35.000 0.100E+10 .1E9 1.00
         15     153.110      0.762      1.420    -35.000 0.100E+10 .1E9 1.00
         16     151.690      0.762      1.420    -35.000 0.100E+10 .1E9 1.00
         17     150.270      0.762      1.420    -35.000 0.100E+10 .1E9 1.00
         18     148.850      0.762      1.420    -35.000 0.100E+10 .1E9 1.00
         19     147.430      0.762      1.420    -35.000 0.100E+10 .1E9 1.00
         20     146.010      0.762      1.420    -35.000 0.100E+10 .1E9 1.00
         21     138.035      7.200     14.530    -35.000 0.100E+10 1.00 1.00
         22     123.505      7.200     14.530    -35.000 0.100E+10 1.00 1.00
         23     108.975      7.200     14.530    -35.000 0.100E+10 1.00 1.00
         24      94.445      7.200     14.530    -35.000 0.100E+10 1.00 1.00
         25      79.915      7.200     14.530    -35.000 0.100E+10 1.00 1.00
         26      65.385      7.200     14.530    -35.000 0.100E+10 1.00 1.00
         27      50.855      7.200     14.530    -35.000 0.100E+10 1.00 1.00
         28      36.325      7.200     14.530    -35.000 0.100E+10 1.00 1.00
         29      21.795      7.200     14.530    -35.000 0.100E+10 1.00 1.00
         30       7.265      7.200     14.530    -35.000 0.100E+10 1.00 1.00
         31     138.035      0.072     14.530    -35.000 0.100E+10 .1E9 1.00
         32     123.505      0.072     14.530    -35.000 0.100E+10 .1E9 1.00
         33     108.975      0.072     14.530    -35.000 0.100E+10 .1E9 1.00
         34      94.445      0.072     14.530    -35.000 0.100E+10 .1E9 1.00
         35      79.915      0.072     14.530    -35.000 0.100E+10 .1E9 1.00
         36      65.385      0.072     14.530    -35.000 0.100E+10 .1E9 1.00
         37      50.855      0.072     14.530    -35.000 0.100E+10 .1E9 1.00
         38      36.325      0.072     14.530    -35.000 0.100E+10 .1E9 1.00
         39      21.795      0.072     14.530    -35.000 0.100E+10 .1E9 1.00
         40       7.265      0.072     14.530    -35.000 0.100E+10 .1E9 1.00
         41      -6.615    643.468     13.230      0.000 0.100E+10 1.13 1.00    20 48.6
          3
          1       0.0         0.0        -1.0
         11       0.0        -1.0         0.0
         21      -1.0         0.0        -1.0
          0
          1
          1  0.123064   0.000000   0.000000          0           0           0
          1         1    121.306      0.000          0           0
          1  0.00000  -10.73284  -0.02118          2     0.00000  -10.73284  -0.02118
          2         1    121.306      0.000          0           0
          2  0.00000  -10.73284  -0.06303          3     0.00000  -10.73284  -0.06303
```

3	1	121.306	0.000	0	0		
3	0.00000	-10.73284	-0.10332	4	0.00000	-10.73284	-0.10332
4	1	121.306	0.000	0	0		
4	0.00000	-10.73284	-0.14107	5	0.00000	-10.73284	-0.14107
5	1	121.306	0.000	0	0		
5	0.00000	-10.73284	-0.17535	6	0.00000	-10.73284	-0.17535
6	1	121.306	0.000	0	0		
6	0.00000	-10.73284	-0.20531	7	0.00000	-10.73284	-0.20531
7	1	121.306	0.000	0	0		
7	0.00000	-10.73284	-0.23021	8	0.00000	-10.73284	-0.23021
8	1	121.306	0.000	0	0		
8	0.00000	-10.73284	-0.24945	9	0.00000	-10.73284	-0.24945
9	1	121.306	0.000	0	0		
9	0.00000	-10.73284	-0.26254	10	0.00000	-10.73284	-0.26254
10	1	121.306	0.000	0	0		
10	0.00000	-10.73284	-0.26917	11	0.00000	-10.73284	-0.26917
11	1	121.306	0.000	0	0		
11	0.00000	-10.73284	-0.53834	12	0.00000	-10.73284	-0.53834
12	1	121.306	0.000	0	0		
12	0.00000	-10.73284	-0.52508	13	0.00000	-10.73284	-0.52508
13	1	121.306	0.000	0	0		
13	0.00000	-10.73284	-0.49889	14	0.00000	-10.73284	-0.49889
14	1	121.306	0.000	0	0		
14	0.00000	-10.73284	-0.46043	15	0.00000	-10.73284	-0.46043
15	1	121.306	0.000	0	0		
15	0.00000	-10.73284	-0.41062	16	0.00000	-10.73284	-0.41062
16	1	121.306	0.000	0	0		
16	0.00000	-10.73284	-0.35070	17	0.00000	-10.73284	-0.35070
17	1	121.306	0.000	0	0		
17	0.00000	-10.73284	-0.28215	18	0.00000	-10.73284	-0.28215
18	1	121.306	0.000	0	0		
18	0.00000	-10.73284	-0.20665	19	0.00000	-10.73284	-0.20665
19	1	121.306	0.000	0	0		
19	0.00000	-10.73284	-0.12606	20	0.00000	-10.73284	-0.12606
20	1	121.306	0.000	0	0		
20	0.00000	-10.73284	-0.04237	21	0.00000	-10.73284	-0.04237

Table 3.4: A Typical Input Data File for Nonlinear Analysis Using ASAS-NL

```
SYST DATA AREA 1000000
JOB STAT
TITL LARG * SHALLOW SPHERICAL SHELL, 8-NODED SHELL, 3X3 MESH
SOLU ARCL 30 INCDIS     1 Z -0.100E+02 MAXDIS  1 Z 300.0
UPDA GEOM
UPDA STIF ITER ALL
FILE ARCH SAVE1
FILE NSTF SAVE2
SAVE STEP  0
OUTP 1 ALL
BLOC 1 DISP     1
END
COOR
CART
    1  0.000E+00  0.000E+00  0.254E+04
    2  0.131E+03  0.000E+00  0.254E+04
    3  0.262E+03  0.000E+00  0.253E+04
    4  0.392E+03  0.000E+00  0.251E+04
    5  0.523E+03  0.000E+00  0.249E+04
    6  0.654E+03  0.000E+00  0.245E+04
    7  0.785E+03  0.000E+00  0.242E+04
    8  0.000E+00  0.131E+03  0.254E+04
    9  0.262E+03  0.131E+03  0.252E+04
   10  0.523E+03  0.131E+03  0.248E+04
   11  0.785E+03  0.131E+03  0.241E+04
   12  0.000E+00  0.262E+03  0.253E+04
   13  0.131E+03  0.262E+03  0.252E+04
   14  0.262E+03  0.262E+03  0.251E+04
   15  0.392E+03  0.262E+03  0.250E+04
   16  0.523E+03  0.262E+03  0.247E+04
   17  0.654E+03  0.262E+03  0.244E+04
   18  0.785E+03  0.262E+03  0.240E+04
   19  0.000E+00  0.392E+03  0.251E+04
   20  0.262E+03  0.392E+03  0.250E+04
   21  0.523E+03  0.392E+03  0.245E+04
   22  0.785E+03  0.392E+03  0.238E+04
   23  0.000E+00  0.523E+03  0.249E+04
   24  0.131E+03  0.523E+03  0.248E+04
   25  0.262E+03  0.523E+03  0.247E+04
   26  0.392E+03  0.523E+03  0.245E+04
   27  0.523E+03  0.523E+03  0.243E+04
   28  0.654E+03  0.523E+03  0.240E+04
   29  0.785E+03  0.523E+03  0.236E+04
   30  0.000E+00  0.654E+03  0.245E+04
   31  0.262E+03  0.654E+03  0.244E+04
   32  0.523E+03  0.654E+03  0.240E+04
   33  0.785E+03  0.654E+03  0.233E+04
   34  0.000E+00  0.785E+03  0.242E+04
   35  0.131E+03  0.785E+03  0.241E+04
   36  0.262E+03  0.785E+03  0.240E+04
   37  0.392E+03  0.785E+03  0.238E+04
   38  0.523E+03  0.785E+03  0.236E+04
   39  0.654E+03  0.785E+03  0.233E+04
   40  0.785E+03  0.785E+03  0.228E+04
```

```
END
ELEM
MATP 1
TCS8       1      2      3      9     14     13     12      8   1
TCS8       3      4      5     10     16     15     14      9   1
TCS8       5      6      7     11     18     17     16     10   1
TCS8      12     13     14     20     25     24     23     19   1
TCS8      14     15     16     21     27     26     25     20   1
TCS8      16     17     18     22     29     28     27     21   1
TCS8      23     24     25     31     36     35     34     30   1
TCS8      25     26     27     32     38     37     36     31   1
TCS8      27     28     29     33     40     39     38     32   1
END
MATE
1 ISO  0.689E+02  0.300E+00
END
GEOM
1 TCS8 0.994E+02
END
SUPP
X       1
Y       1
RX      1
RY      1
RZ      1
Y       2
RX      2
RZ      2
Y       3
RX      3
RZ      3
Y       4
RX      4
RZ      4
Y       5
RX      5
RZ      5
Y       6
RX      6
RZ      6
X       7
Y       7
Z       7
RX      7
RZ      7
X       8
RY      8
RZ      8
X      12
RY     12
RZ     12
X      19
RY     19
RZ     19
X      23
RY     23
```

```
RZ     23
X      30
RY     30
RZ     30
X      34
Y      34
Z      34
RY     34
RZ     34
X      11
Y      11
Z      11
X      18
Y      18
Z      18
X      22
Y      22
Z      22
X      29
Y      29
Z      29
X      33
Y      33
Z      33
X      35
Y      35
Z      35
X      36
Y      36
Z      36
X      37
Y      37
Z      37
X      38
Y      38
Z      38
X      39
Y      39
Z      39
X      40
Y      40
Z      40
END
CONS
END
LOAD 1
PROP
SET  1
NODAL LO
Z  -0.250E+03      1
END
STOP
```

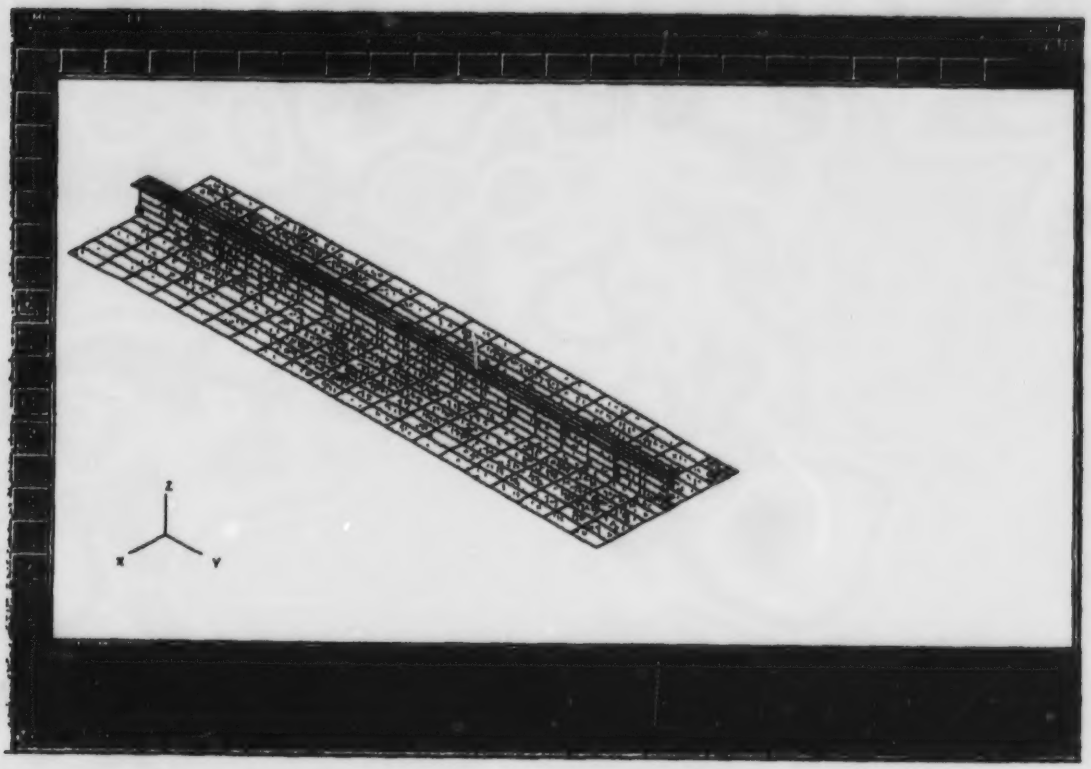

Figure 3.1: Finite Element Meshes for Elastic-Plastic, Post-Buckling Analysis of a Typical Stiffened Panel. (a) 4-Noded Shell Element Mesh

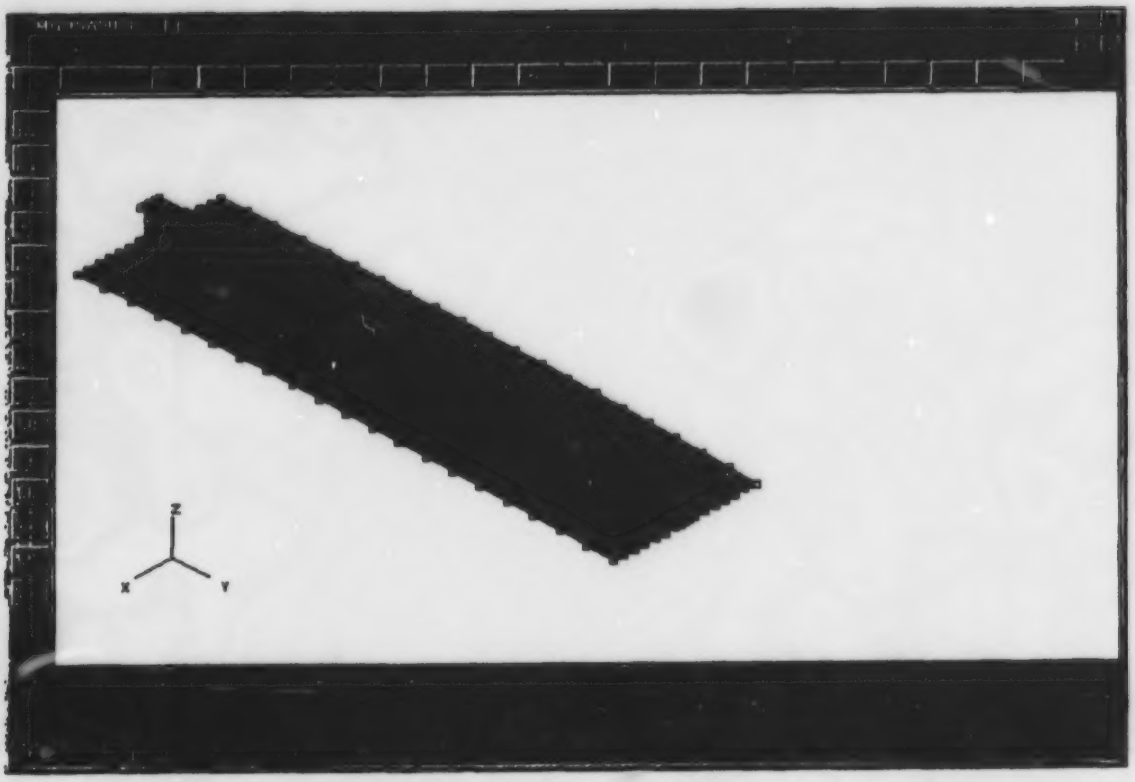

Figure 3.1(Continued): Finite Element Meshes for Elastic-Plastic, Post-Buckling Analysis of a Typical Stiffened Panel. (b) 8-Noded Shell Element Mesh

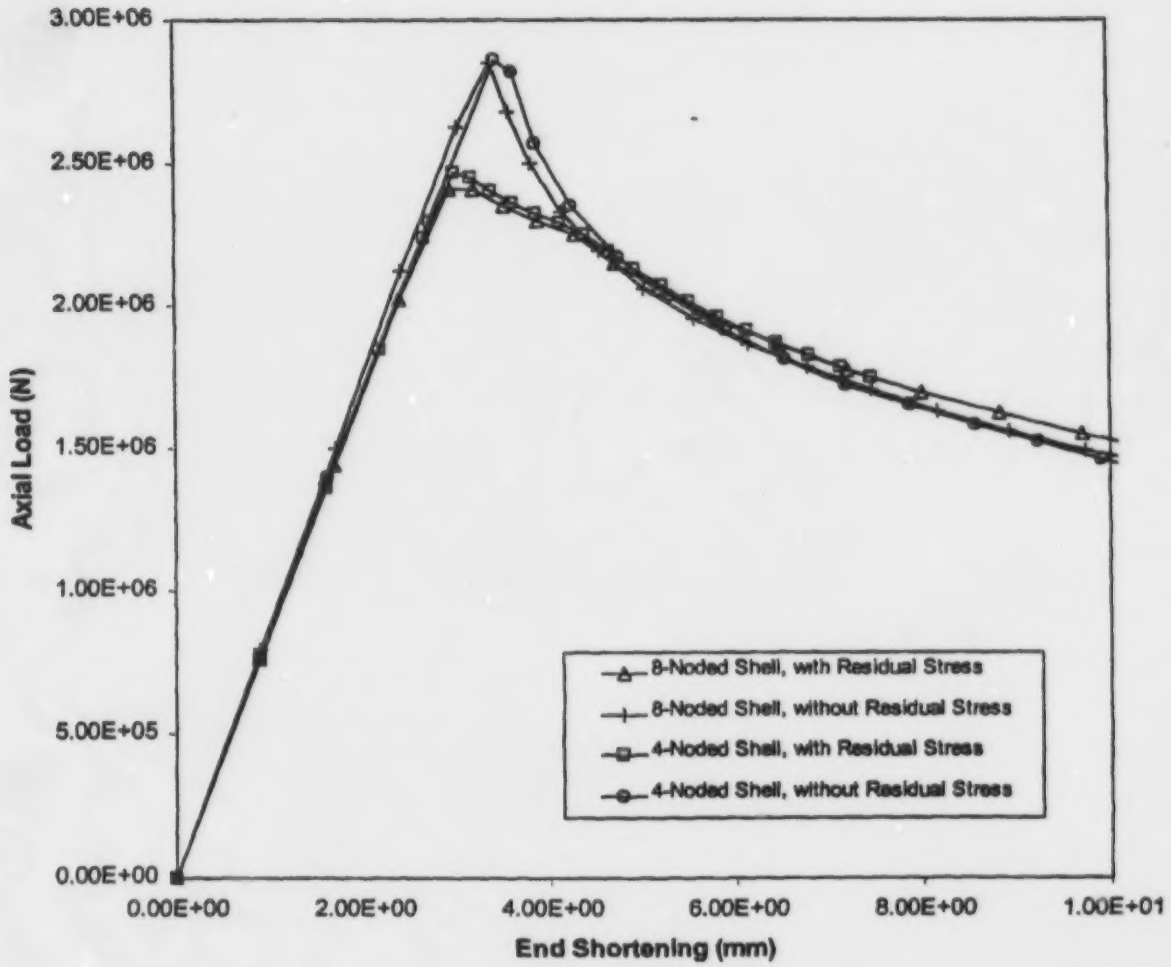

Figure 3.2: Comparison of Load-Shortening Curves Predicted by the 4-Noded and 8-Noded Shell Elements With and Without the Residual Stress Effect

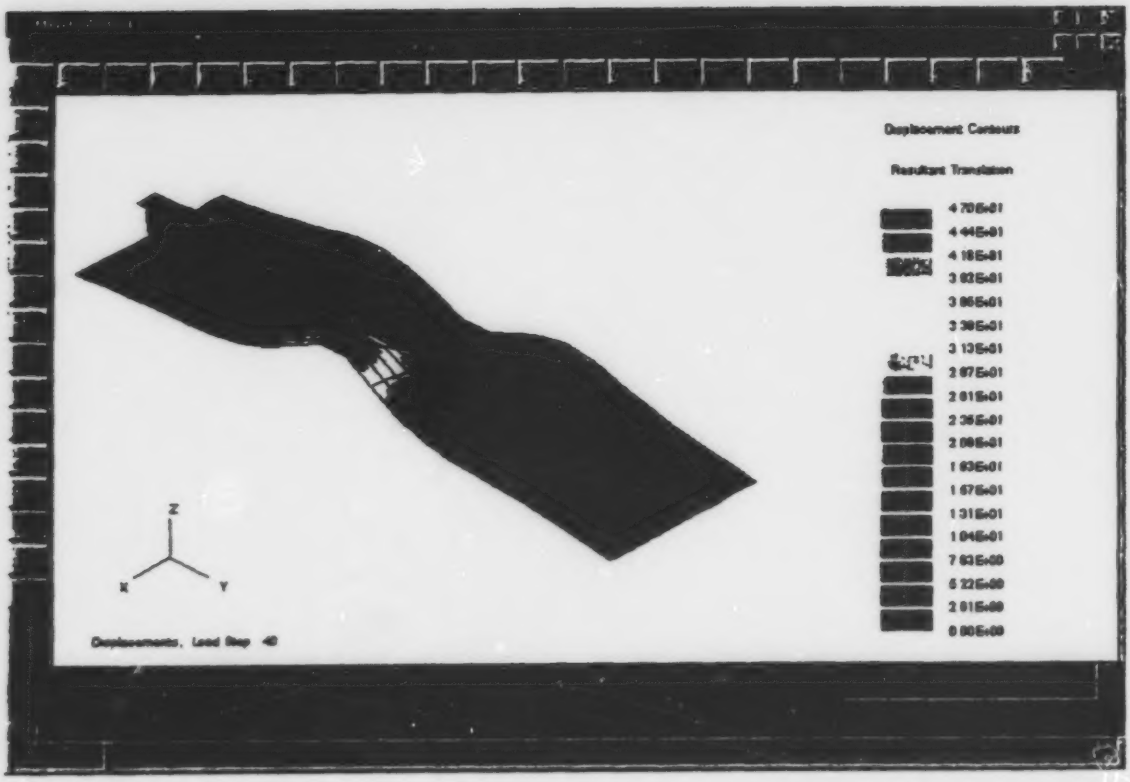

Figure 3.3: Final Deformed Configurations of the Typical Stiffened Panel. (a) 4-Noded Shell Element

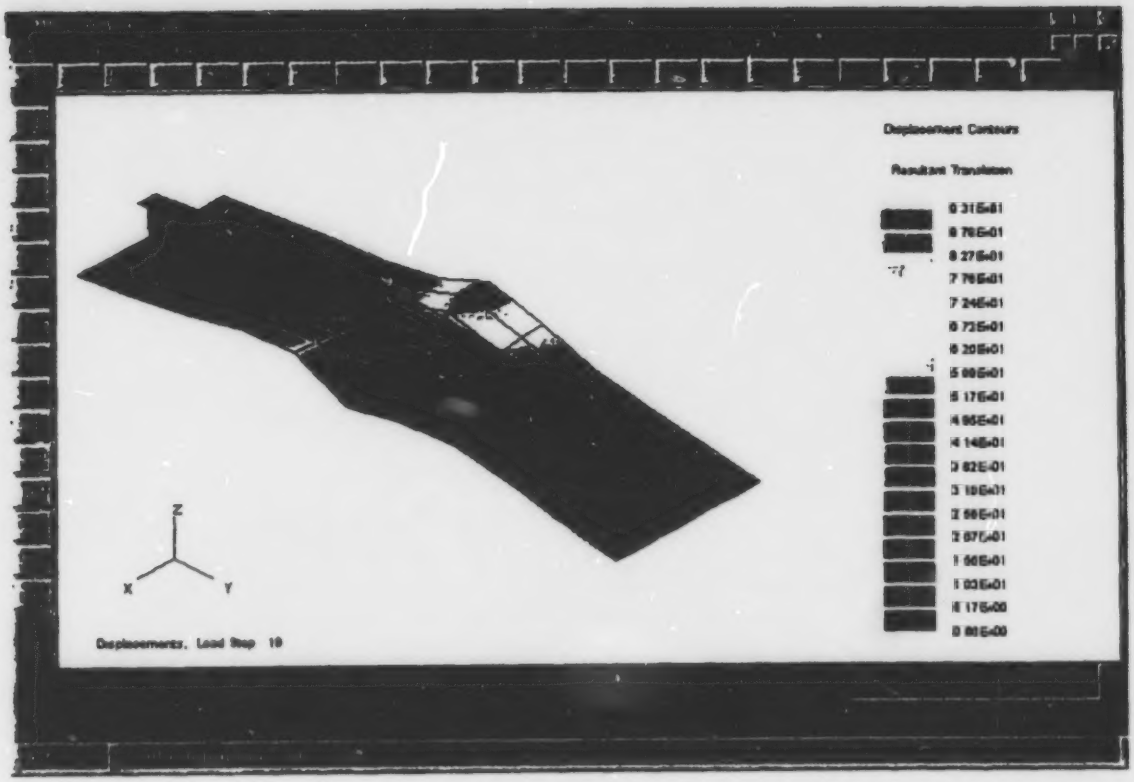

Figure 3.3(Continued): Final Deformed Configurations of the Typical Stiffened Panel. (b) 8-Noded Shell Element.

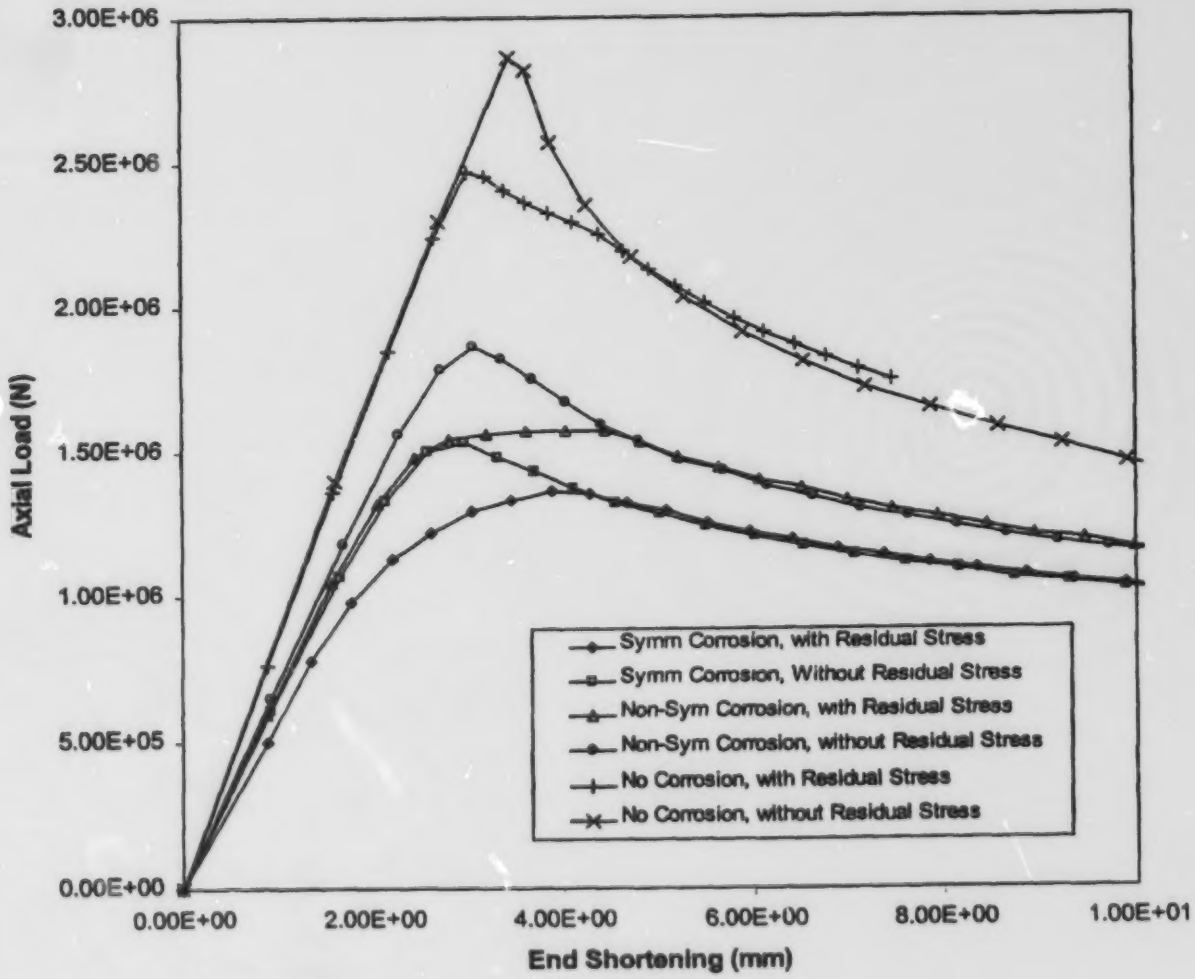

Figure 3.4: *Comparison of* Load-Shortening Curves for Non-Corroded and Corroded Stiffened Panels with Symmetric and Non-Symmetric Corrosion Patterns

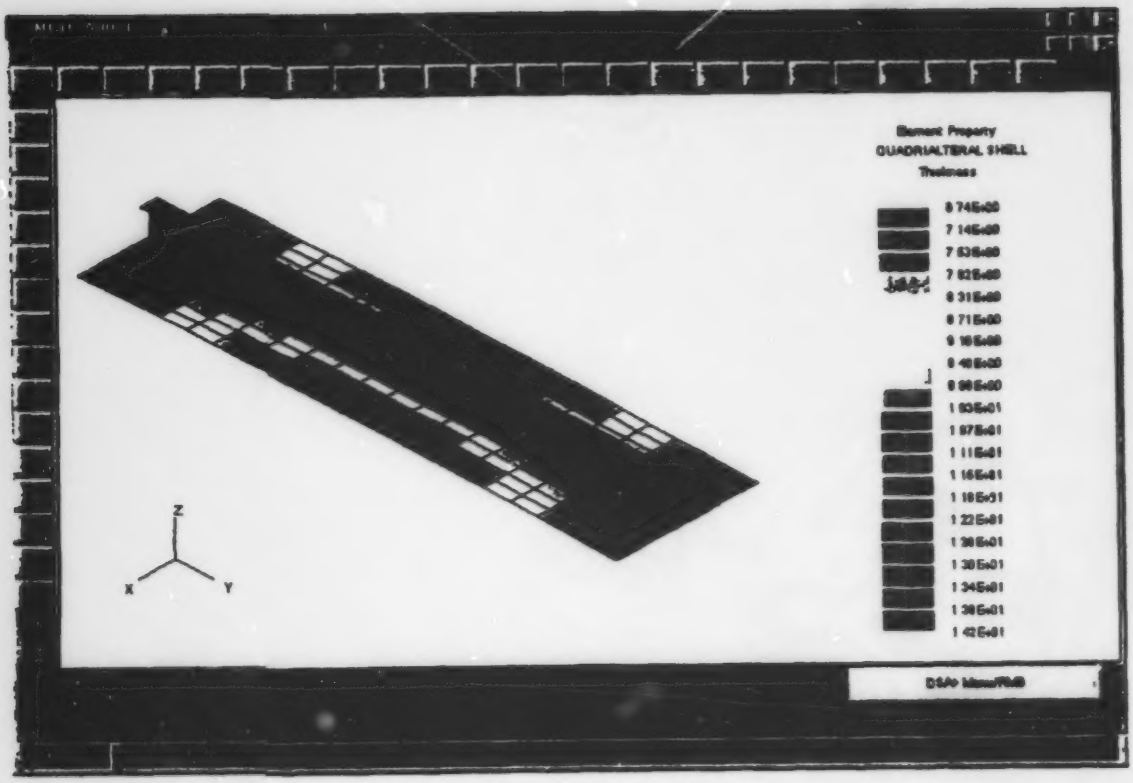

Figure 3.5: Plate Thickness Variation in Corroded Stiffened Panels.(a) Symmetric Corrosion

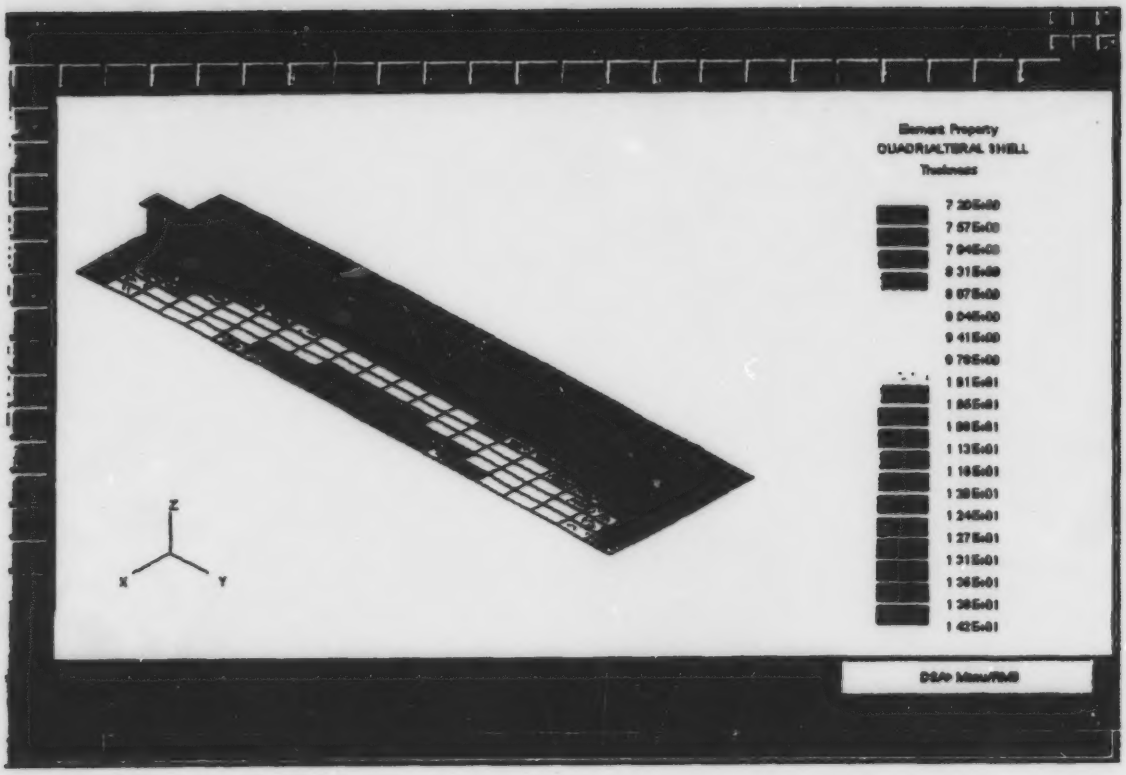

Figure 3.5(Continued): Plate Thickness Variation in Corroded Stiffened Panels. (b) Non-Symmetric Corrosion

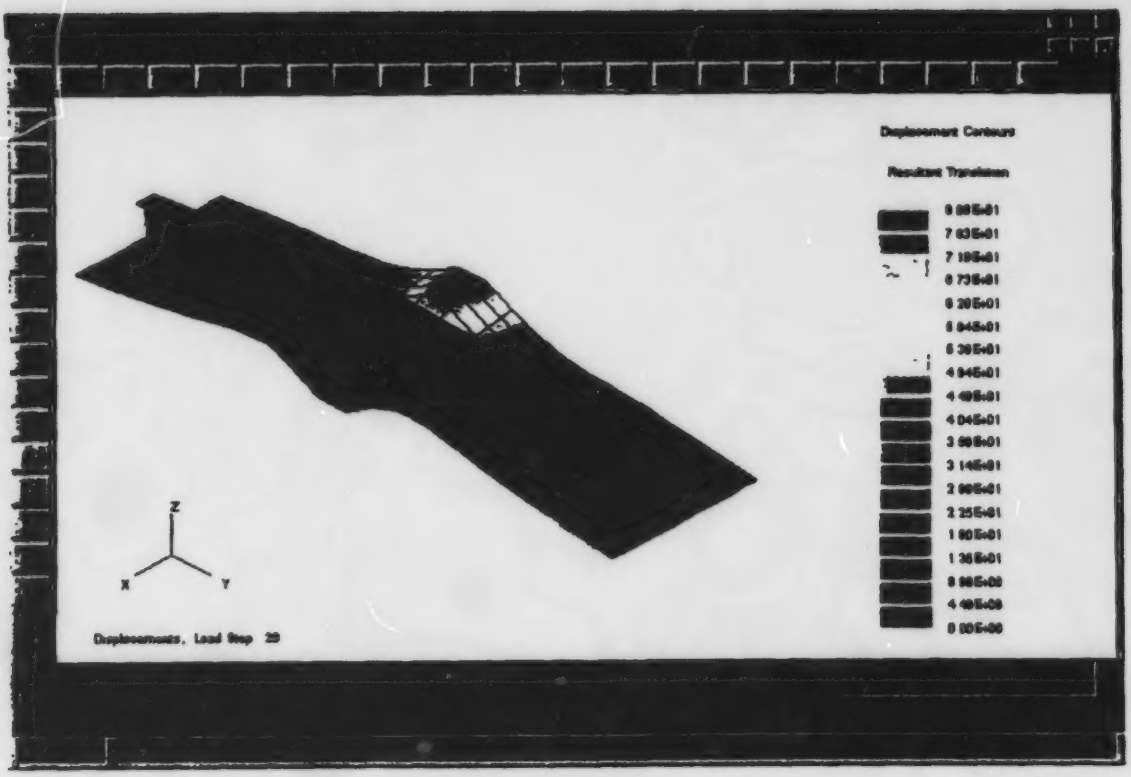

Figure 3.6: Final Deformed Configuration of the Corroded Stiffened Panel with Symmetric Corrosion Pattern

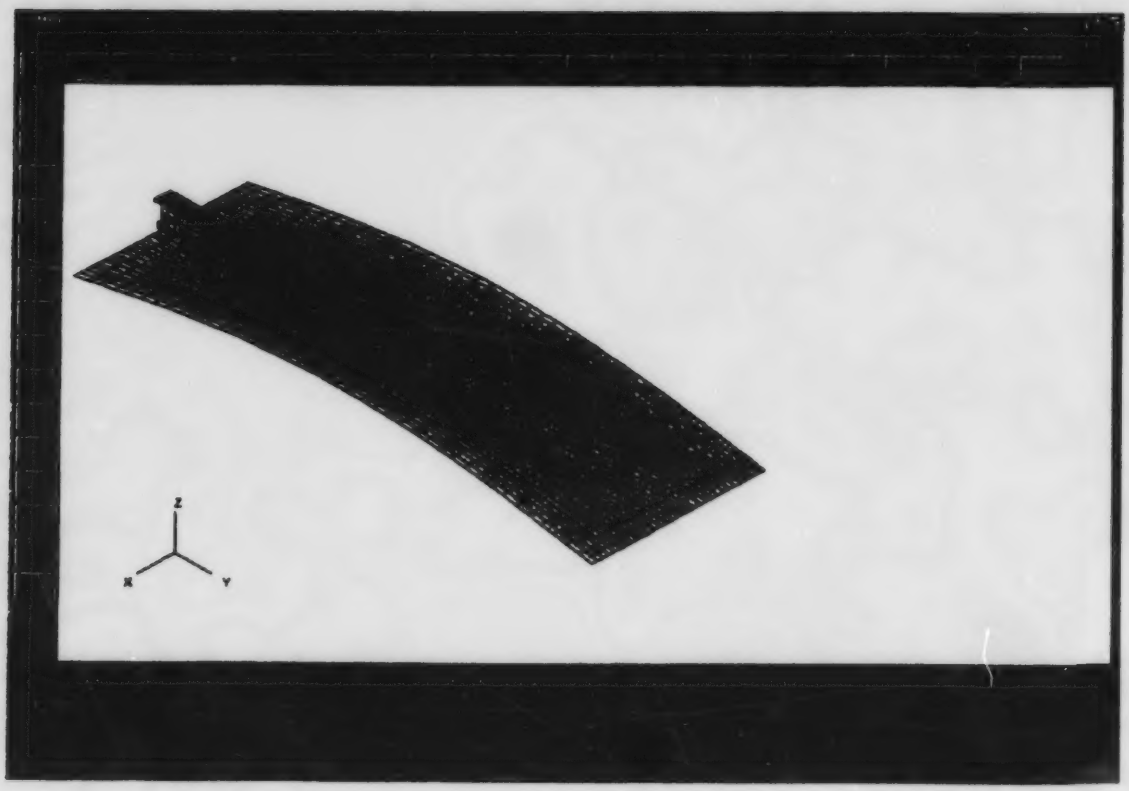

Figure 3.7: Stiffened Panel with Symmetric Geometric Imperfection

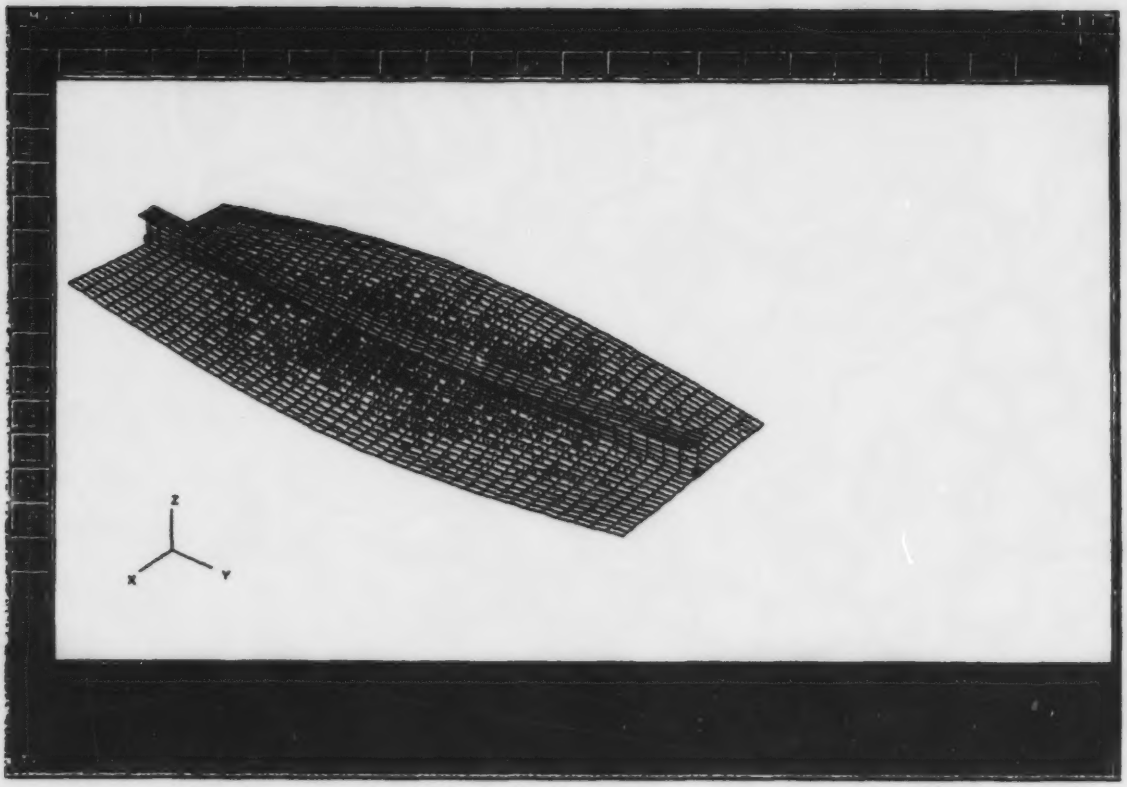

Figure 3.8: Stiffened Panel with Anti-Symmetric Geometric Imperfection

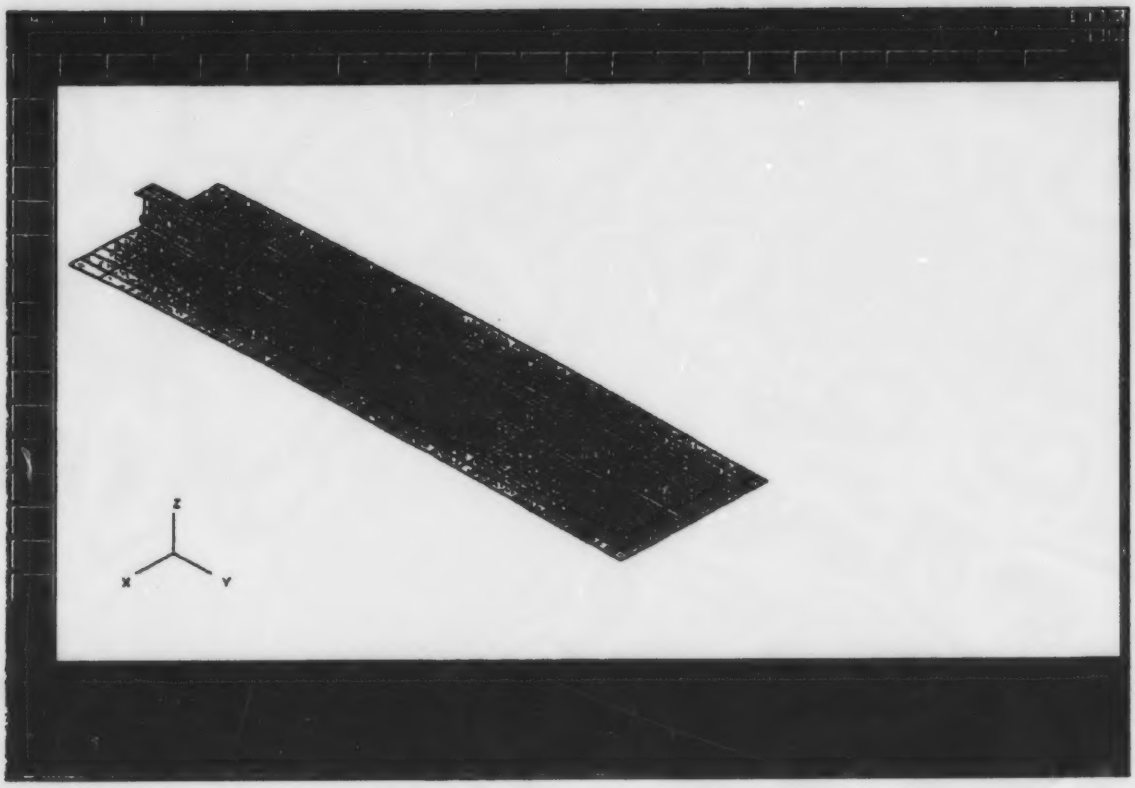

Figure 3.9: Finite Element Mesh of a Typical Stiffened Panel with Different Form of Geometric Imperfection. (a) Symmetric Imperfection

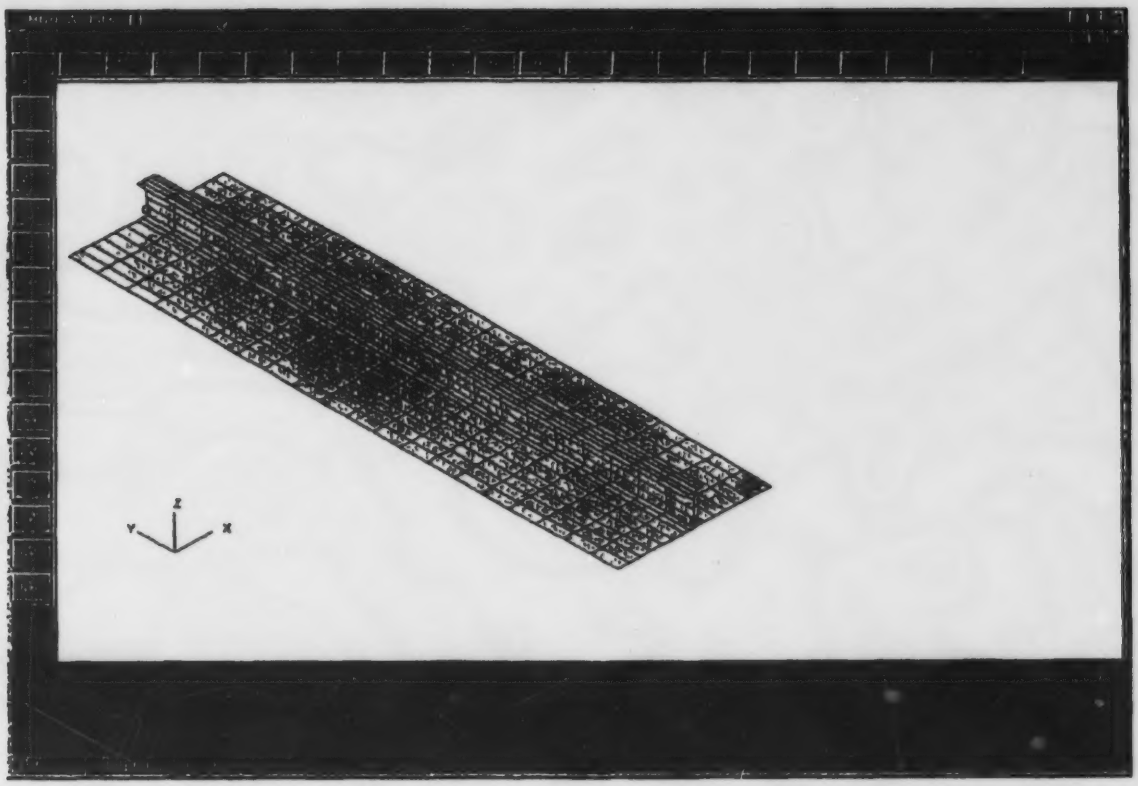

Figure 3.9(Continued): Finite Element Mesh of a Typical Stiffened Panel with Different Form of Geometric Imperfection. (b) Non-Symmetric Imperfection

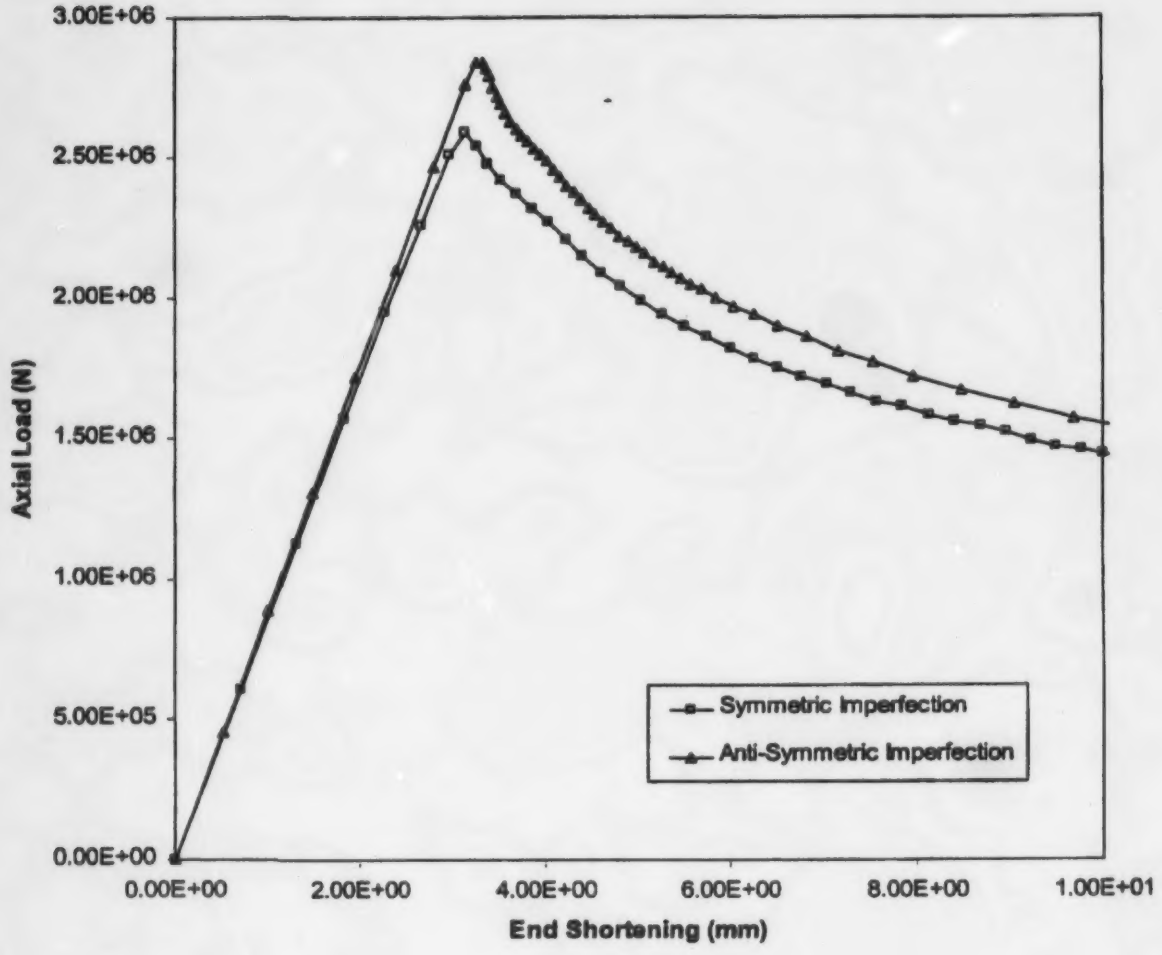

Figure 3.10: Comparison of Load-Shortening Curves Predicted by Using Symmetric and Non-Symmetric Geometric Imperfections

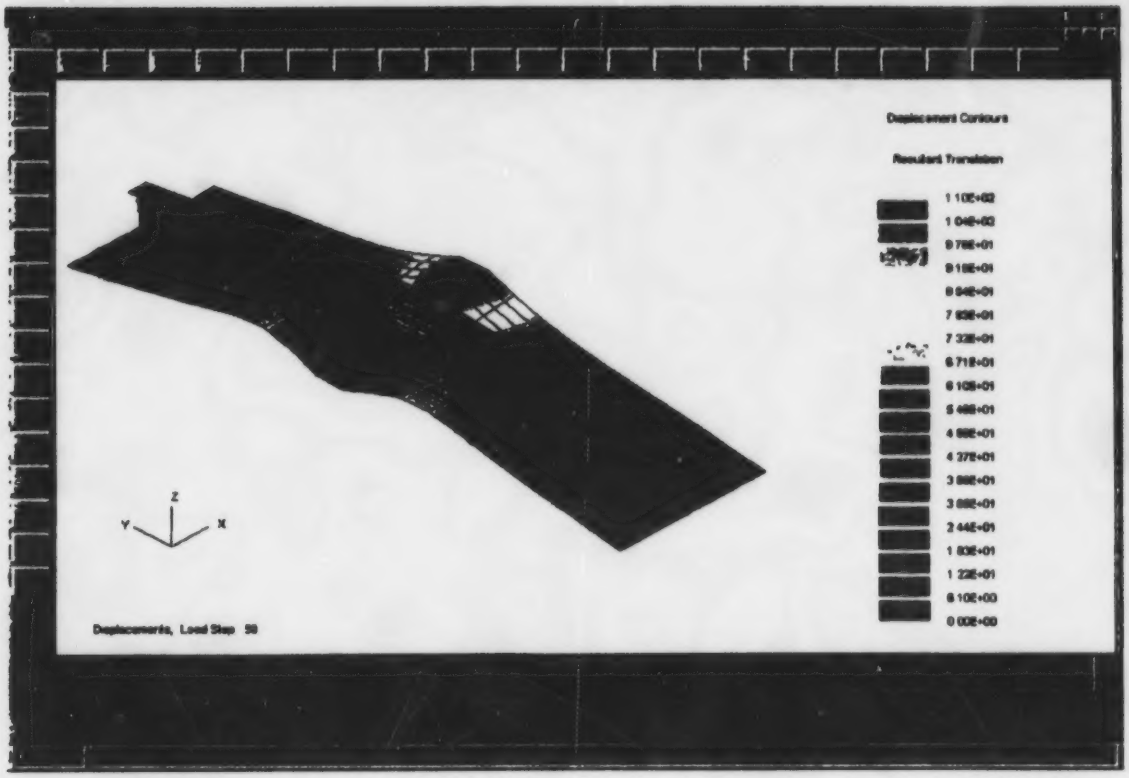

Figure 3.11: Final Deformed Configurations of the Stiffened Panel Predicted Using Different Form of Geometric Imperfections. (a) Symmetric Imperfection

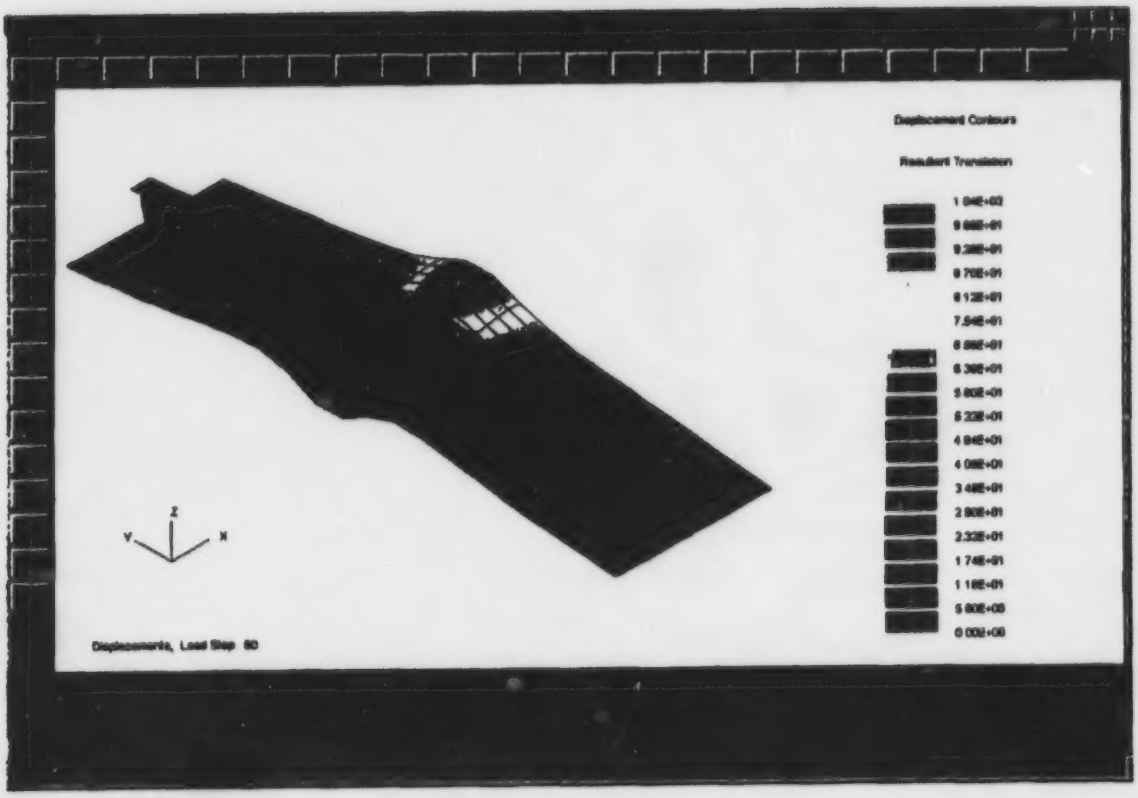

Figure 3.11(Continued): Final Deformed Configurations of the Stiffened Panel Predicted Using Different Form of Geometric Imperfections. (b) Non-Symmetric Imperfection

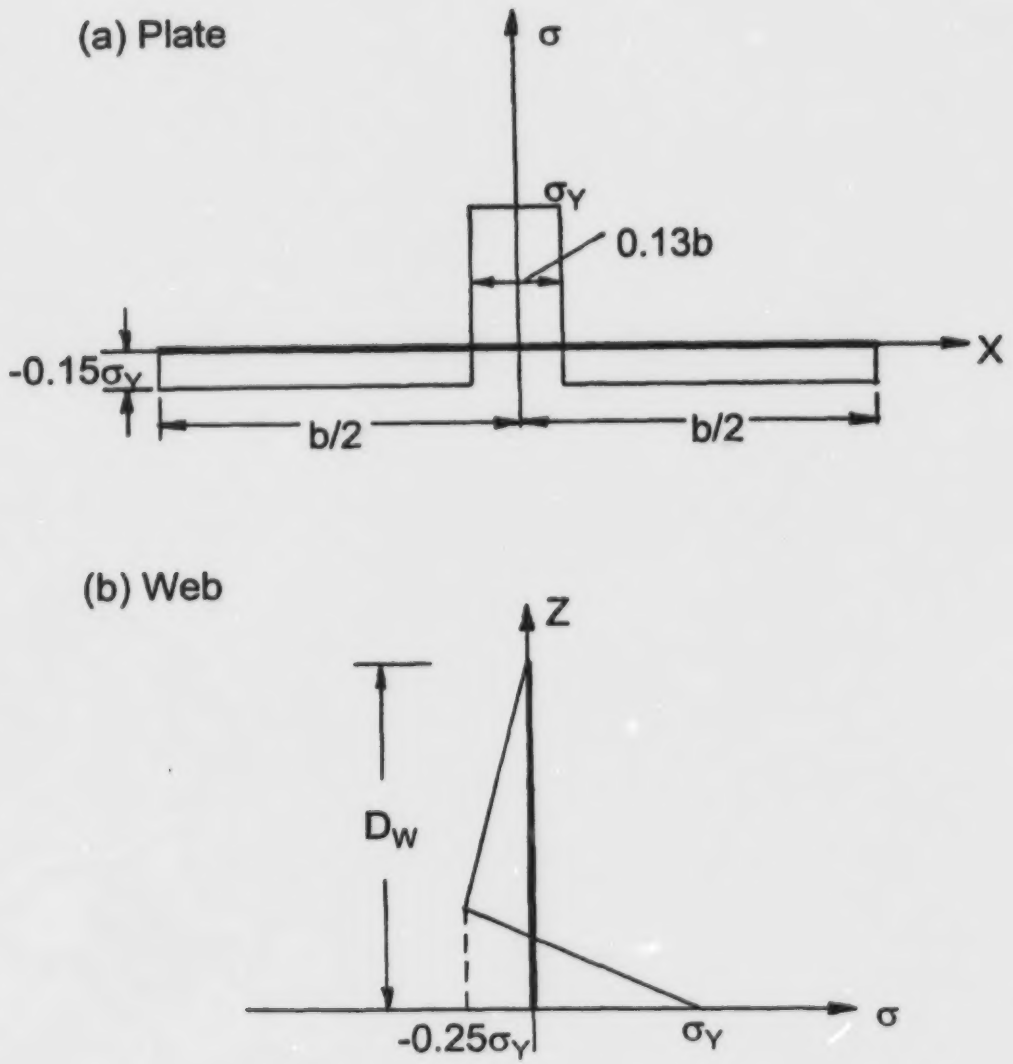

Figure 3.12: Improved Block Form Residual Stress Distribution in Plate and Web

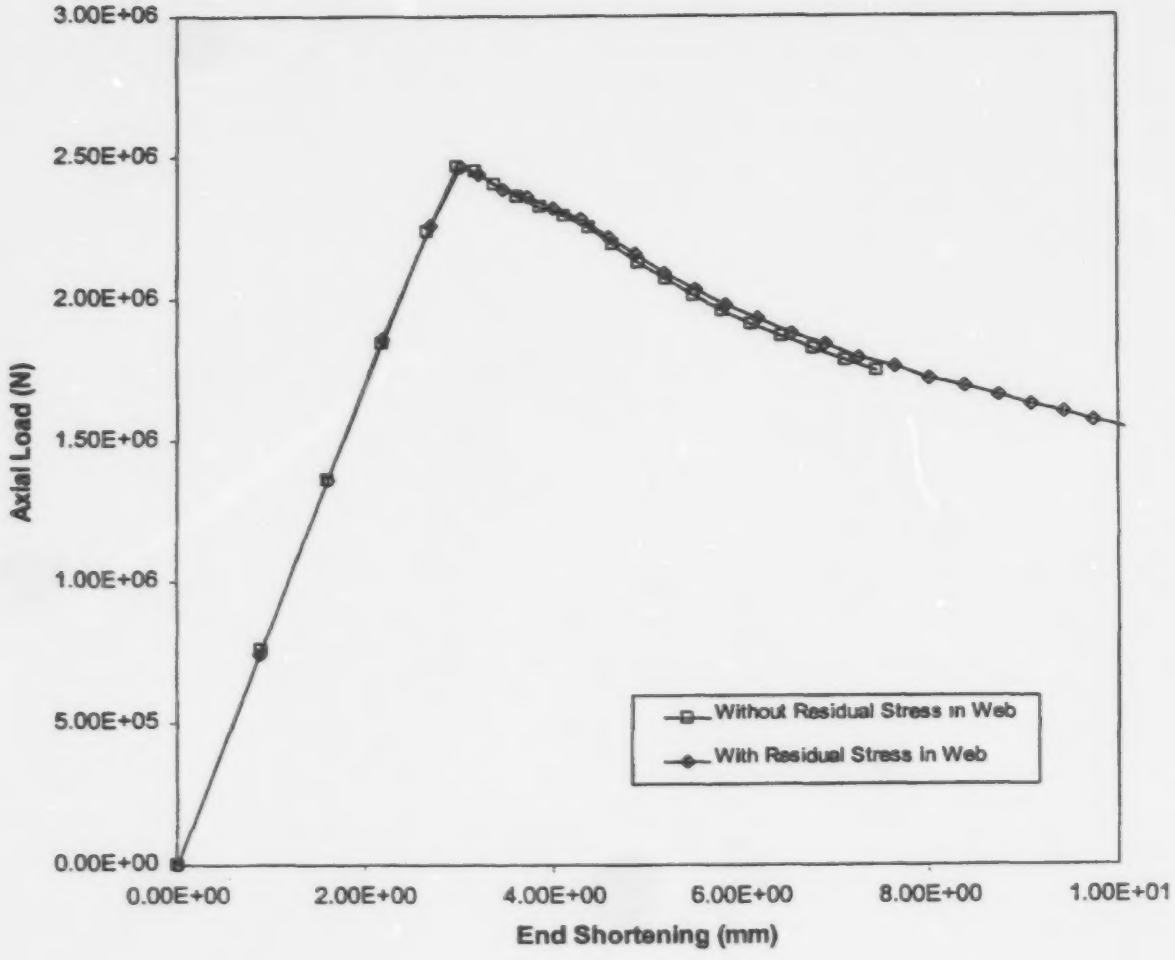

Figure 3.13: Comparison of Load-Shortening Curves of the Typical Stiffened Panel Obtained Using the Original and Improved Block Form Residual Stress Distribution

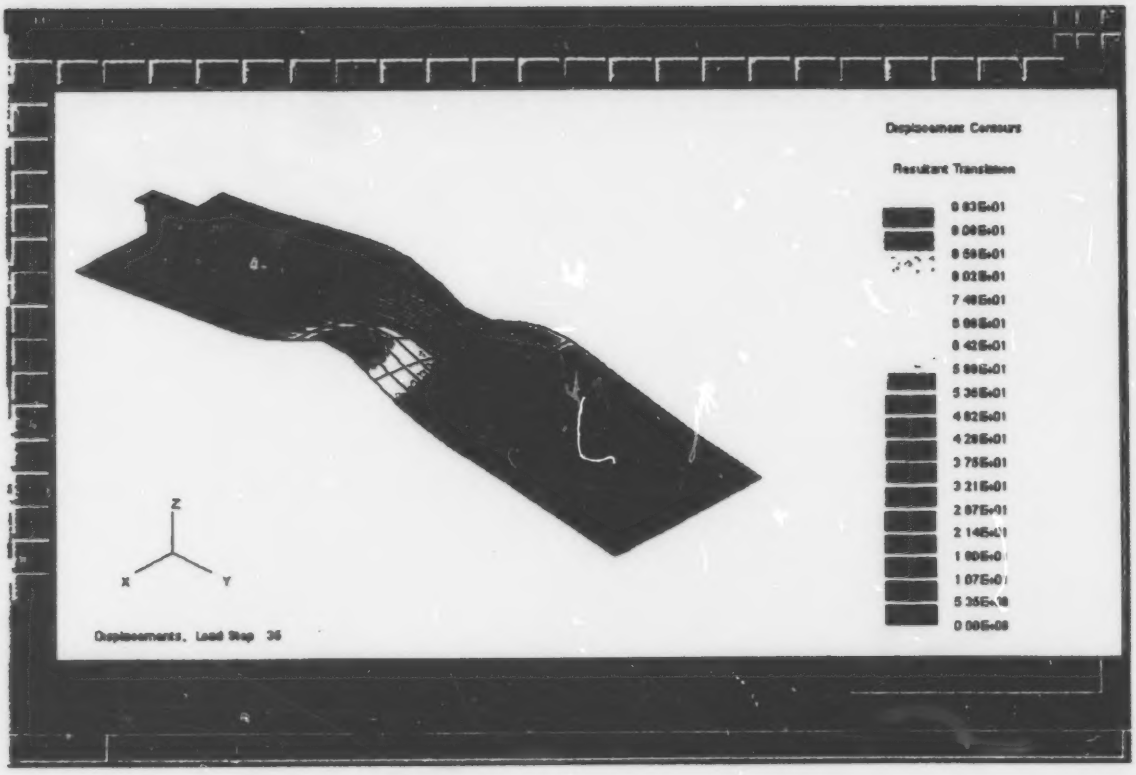

Figure 3.14: Final Deformed Configuration of the Typical Stiffened Panel Predicted Using the Improved Block Form Residual Stress Distribution

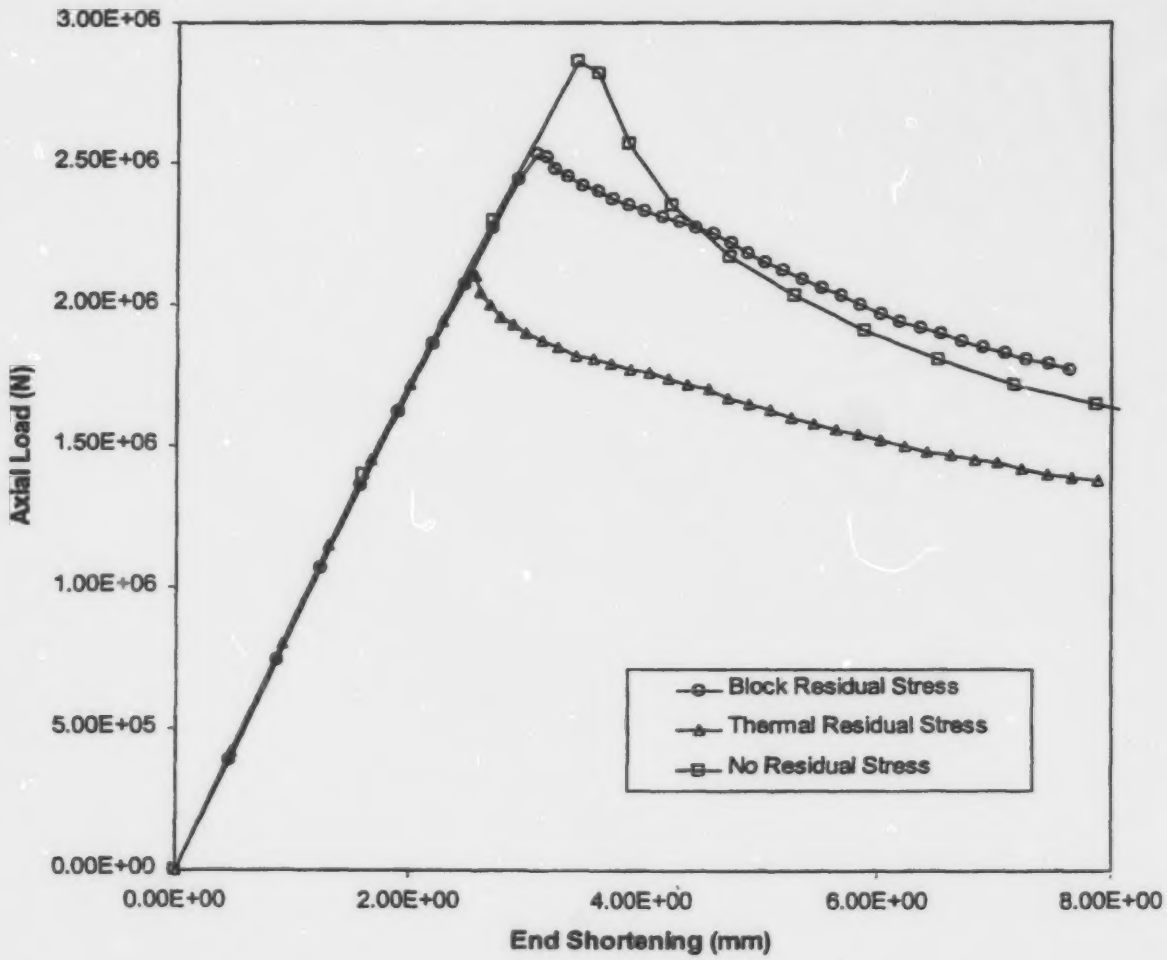

Figure 3.15: Comparison of the Load-Shortening Curves Obtained Using Coarse Mesh of 4-Noded Shell Element with Block Form and Thermal Residual Stress Distributions

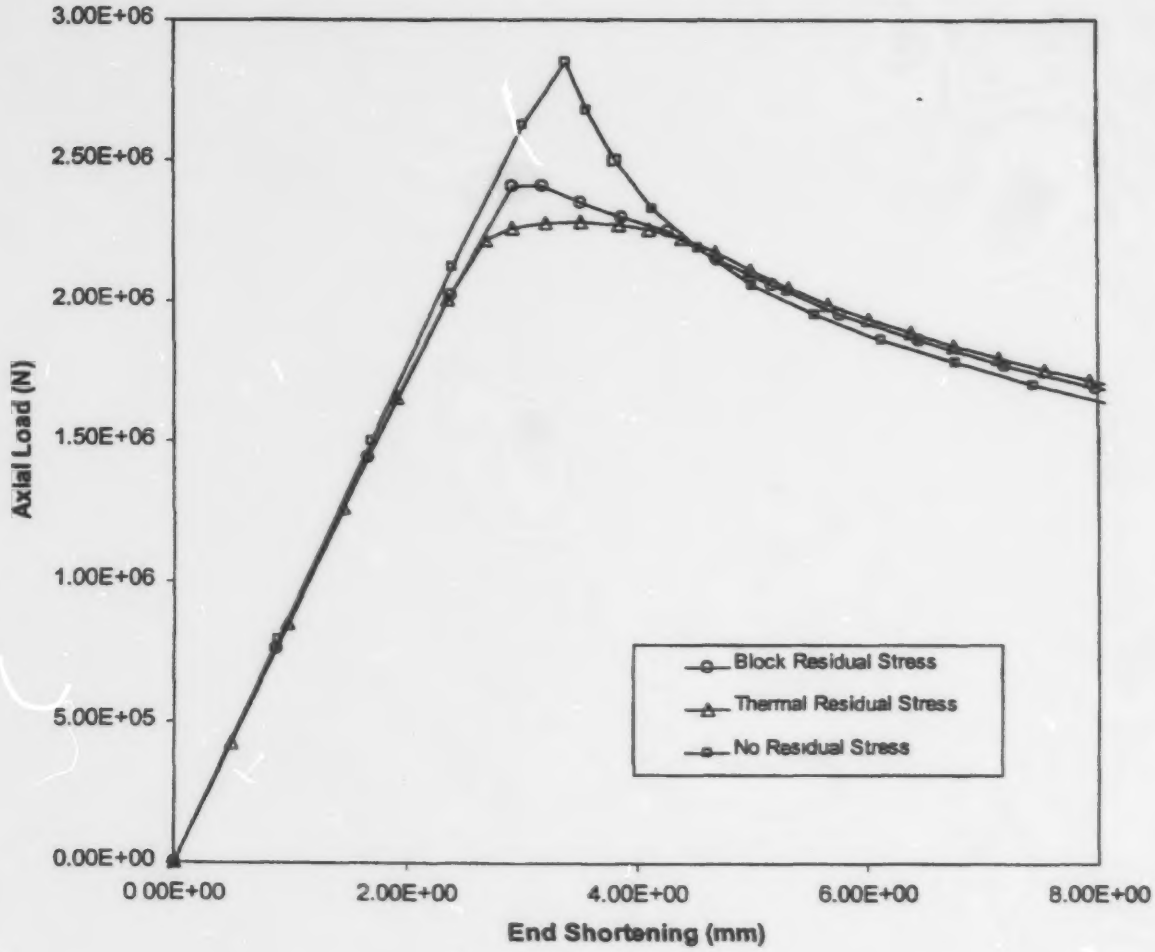

Figure 3.16: Comparison of the Load-Shortening Curves Obtained Using Coarse Mesh of 8-Noded Shell Element with Block Form and Thermal Residual Stress Distributions

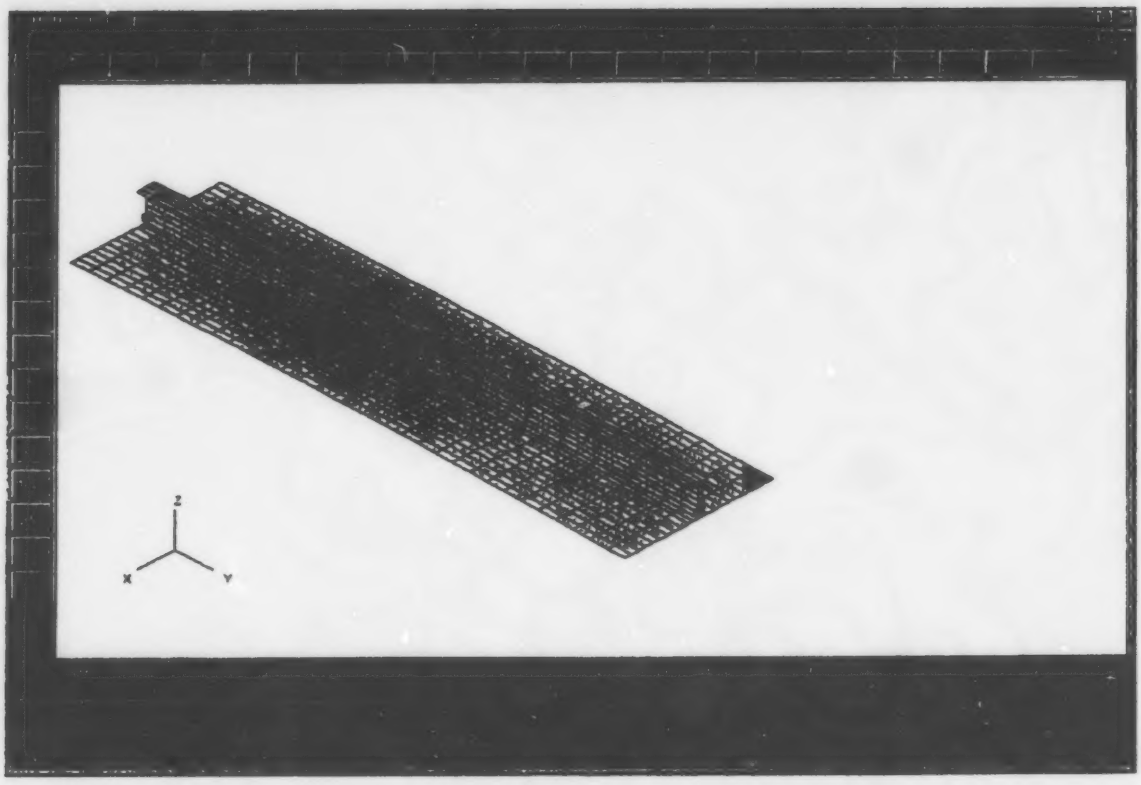

Figure 3.17: Refined Finite Element Mesh of the Typical Stiffened Panel

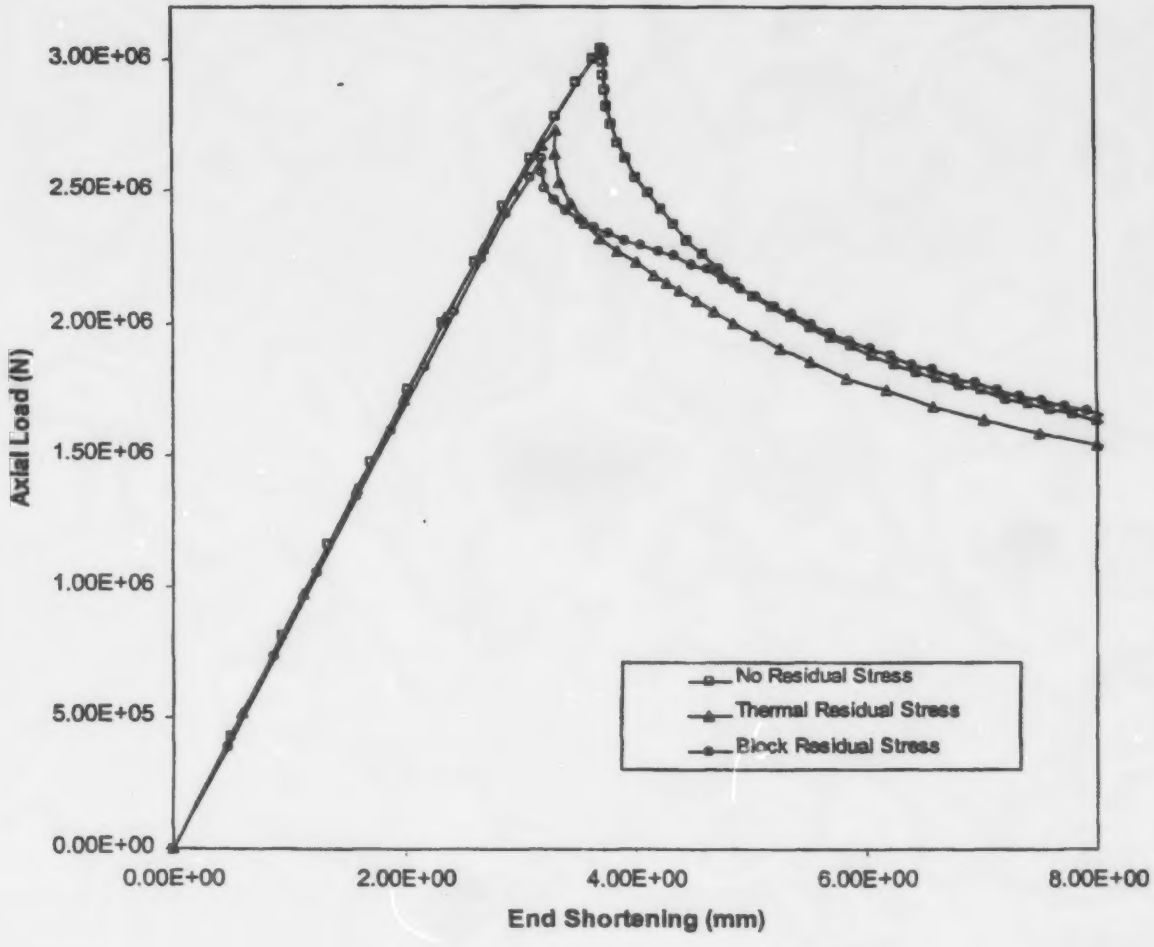

Figure 3.18: Comparison of the Load-Shortening Curves Obtained Using Fine Mesh of 4-Noded Shell Element with Block Form and Thermal Residual Stress Distributions

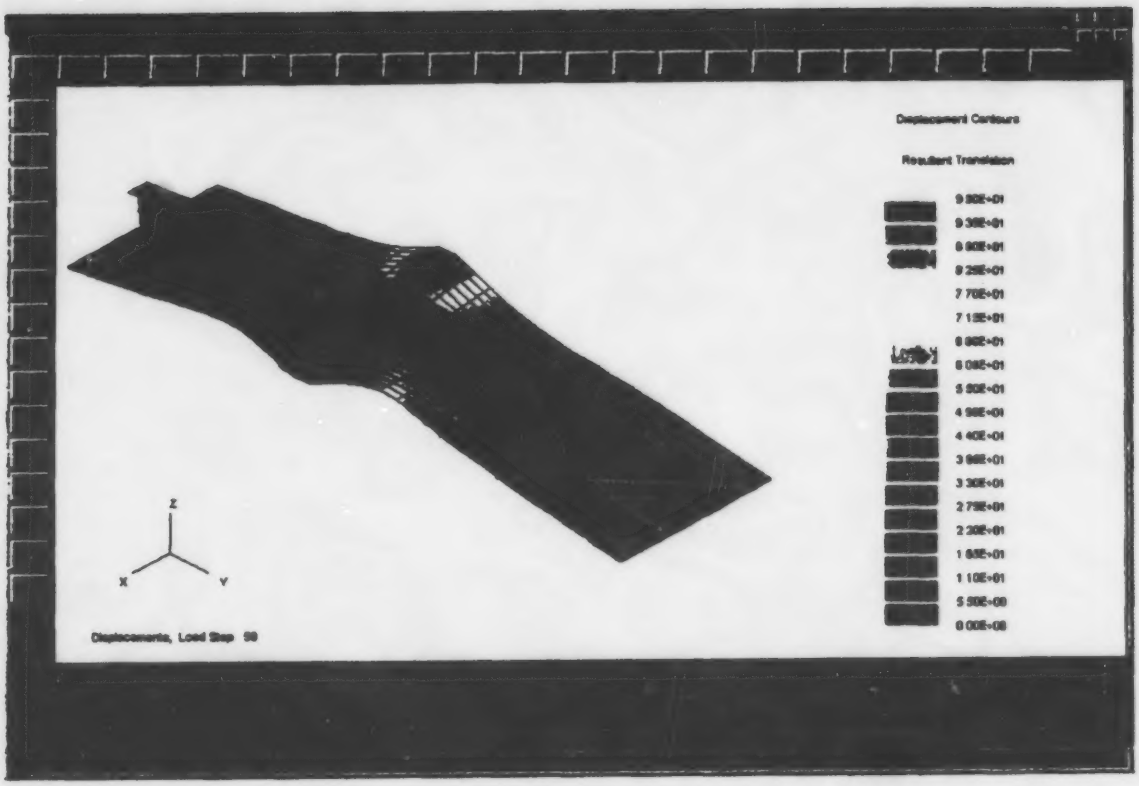

Figure 3.19: Final Deformed Configuration of the Typical Stiffened Panel Predicted Using the Refined Mesh and Thermal Residual Stresses

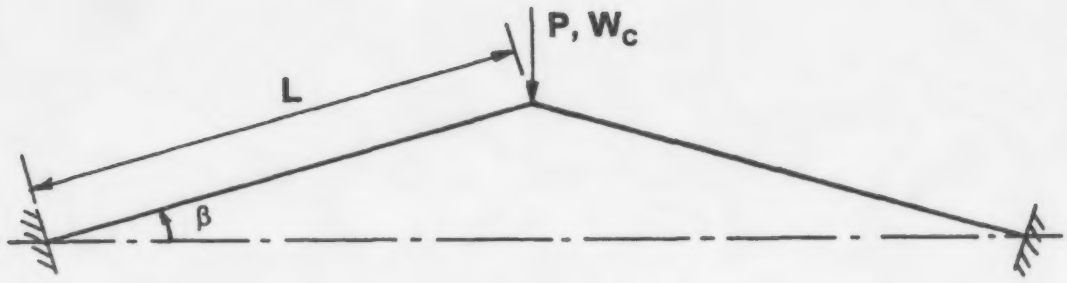

L=12.94 in
EA=1.885x10^6 lb
EI=9.27x10^3 lb in^2
β=$\sin^{-1}$ (0.02985)

Figure 3.20: The Center Loaded Clamped-Clamped Truss System Utilized for Testing the FABSTRAN Program

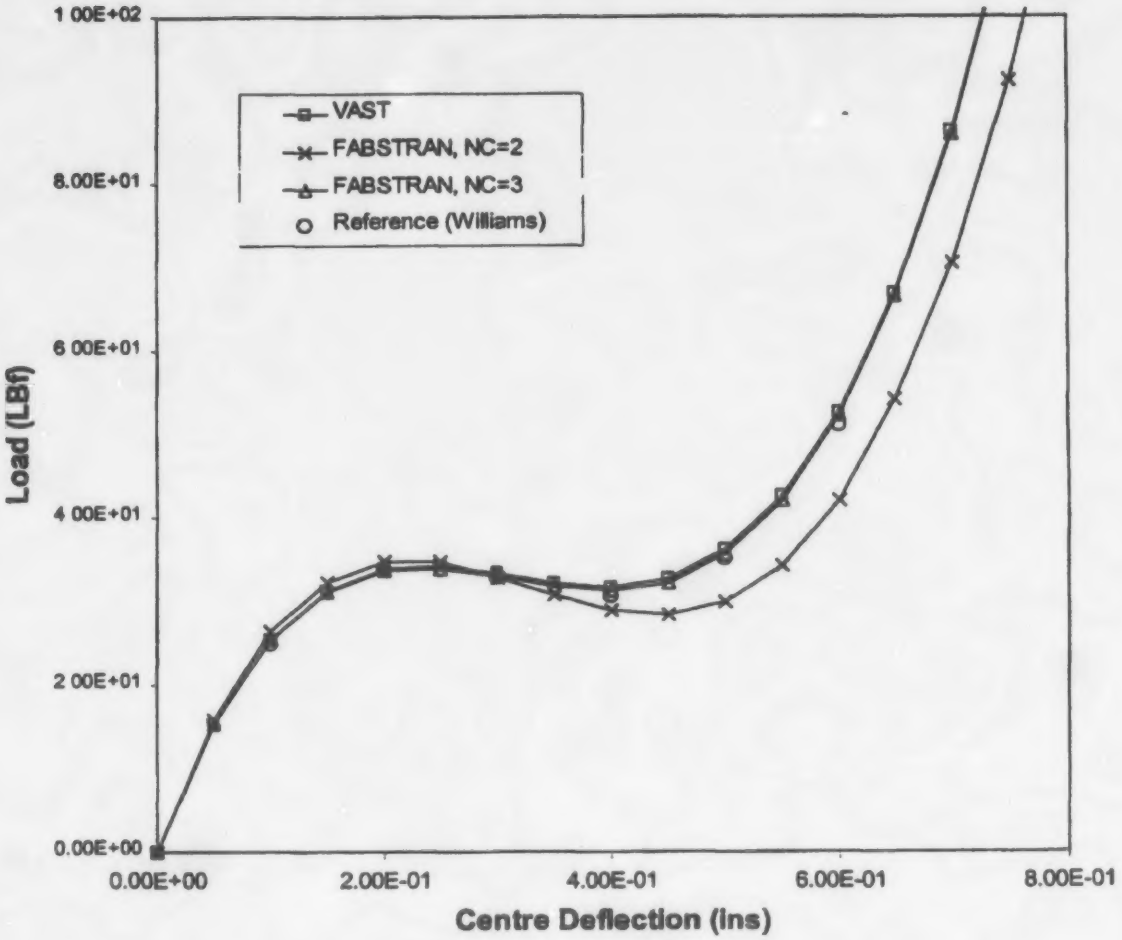

Figure 3.21: Comparison of Load-Center Deflection Curves of the Truss System Predicted by VAST and FASBTRAN with Different Cross-Section Representations

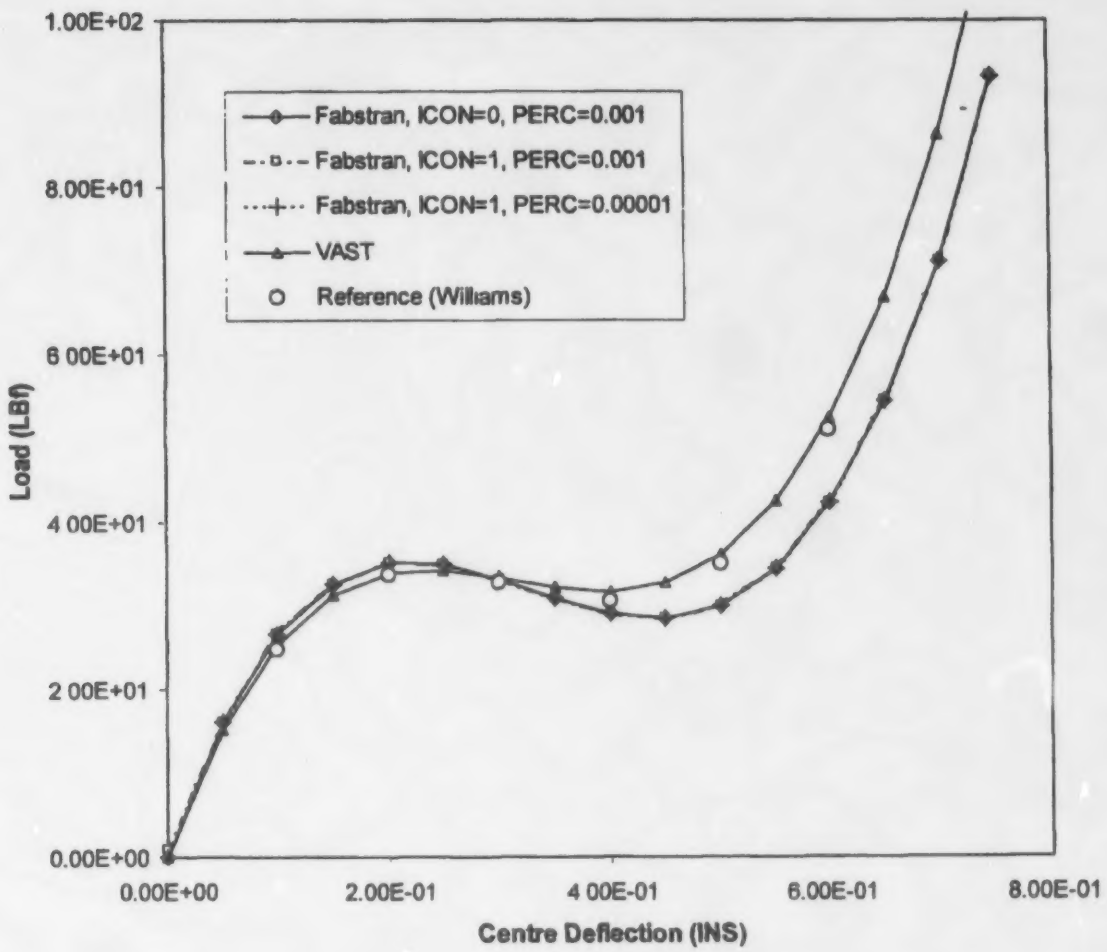

Figure 3.22: Comparison of Load-Center Deflection Curves of the Truss System Predicted by VAST and FASBTRAN with Constant Displacement Increment

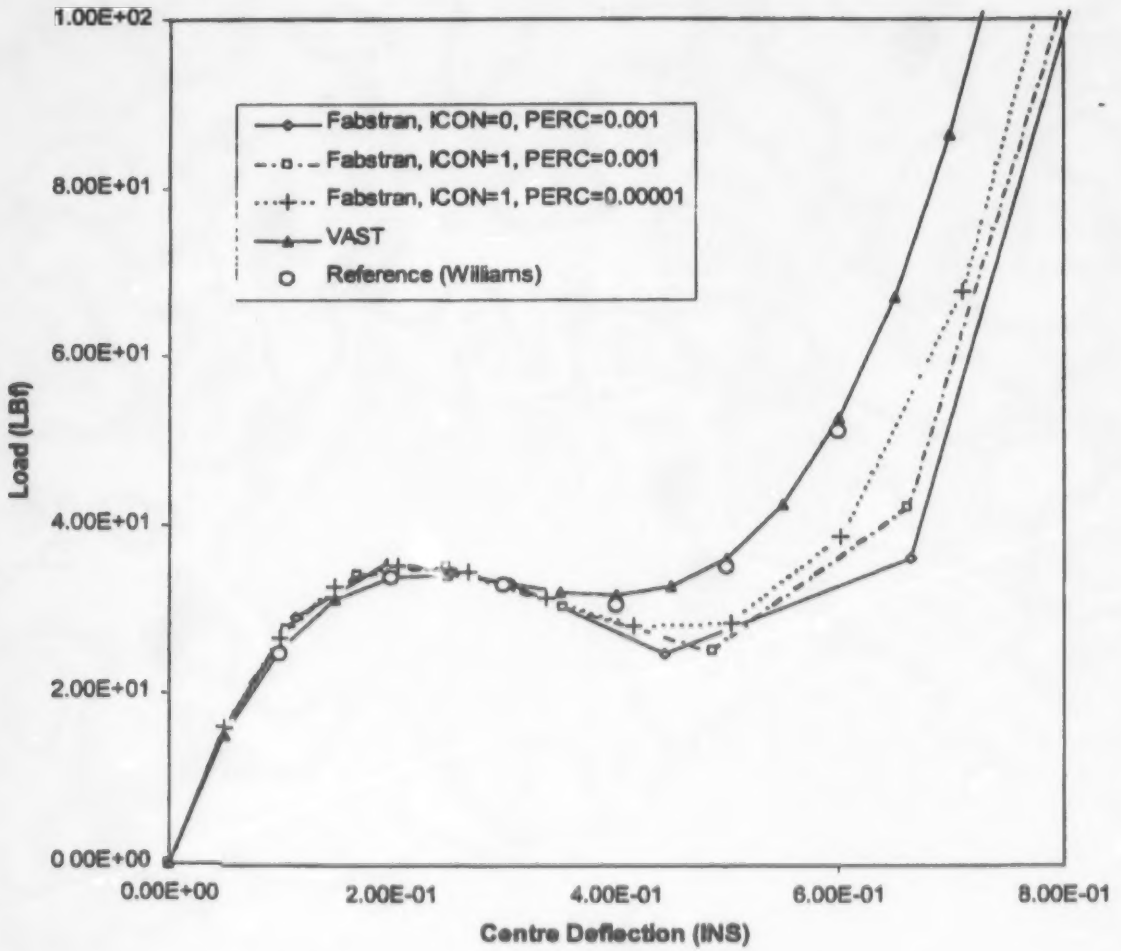

Figure 3.23: Comparison of Load-Center Deflection Curves of the Truss System Predicted by VAST and FASBTRAN with Automatic Solution Step Adjustment

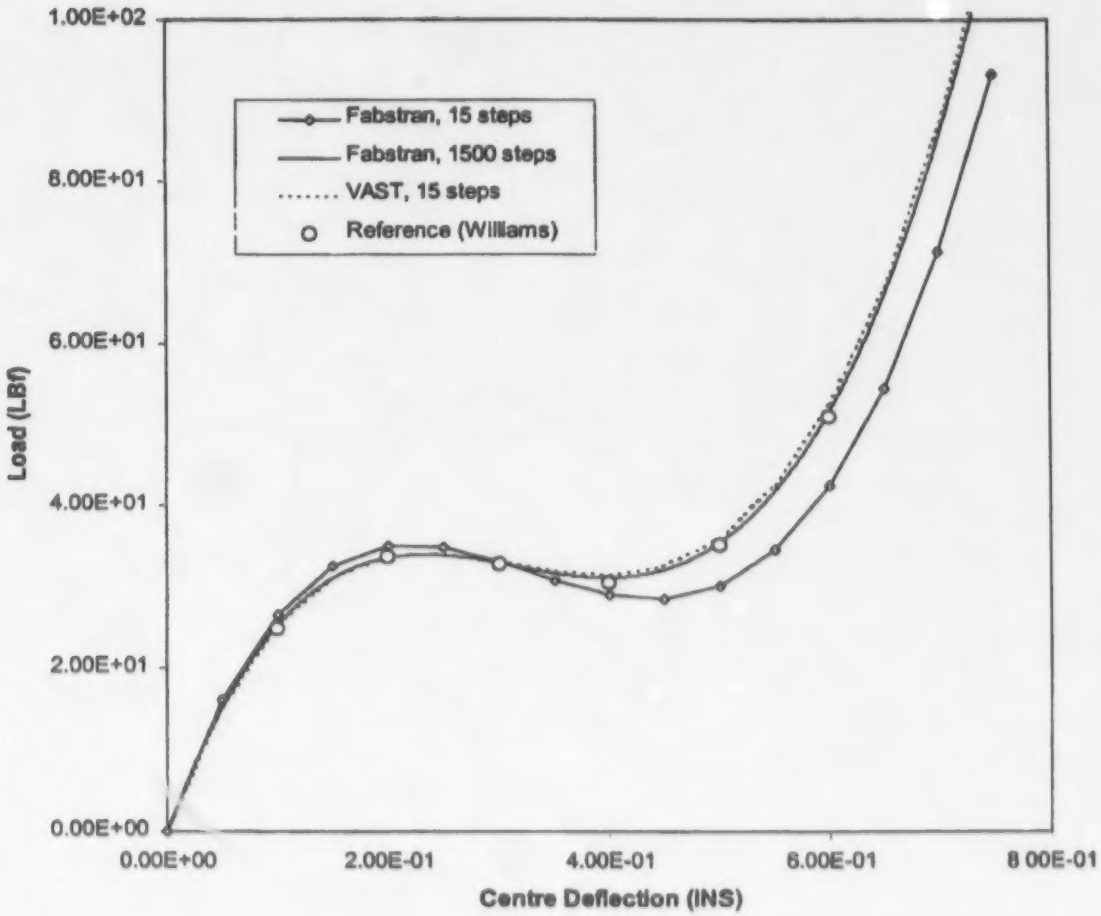

Figure 3.24: Comparison of Load-Center Deflection Curves of the Truss System Predicted by VAST and FASBTRAN with Small Solution Steps

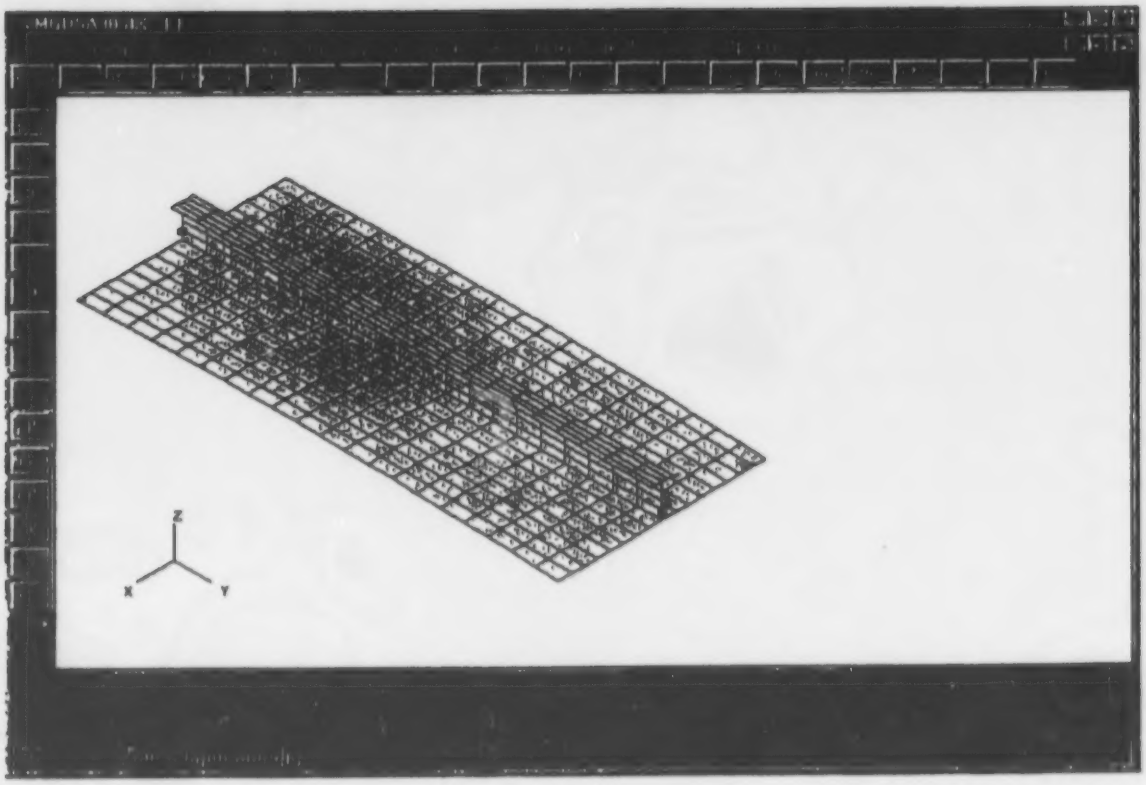

Figure 3.25: Finite Element Mesh of a Stiffened Panel Utilized to Compare Load-Shortening Curves Predicted by the VAST and FABSTRAN Programs

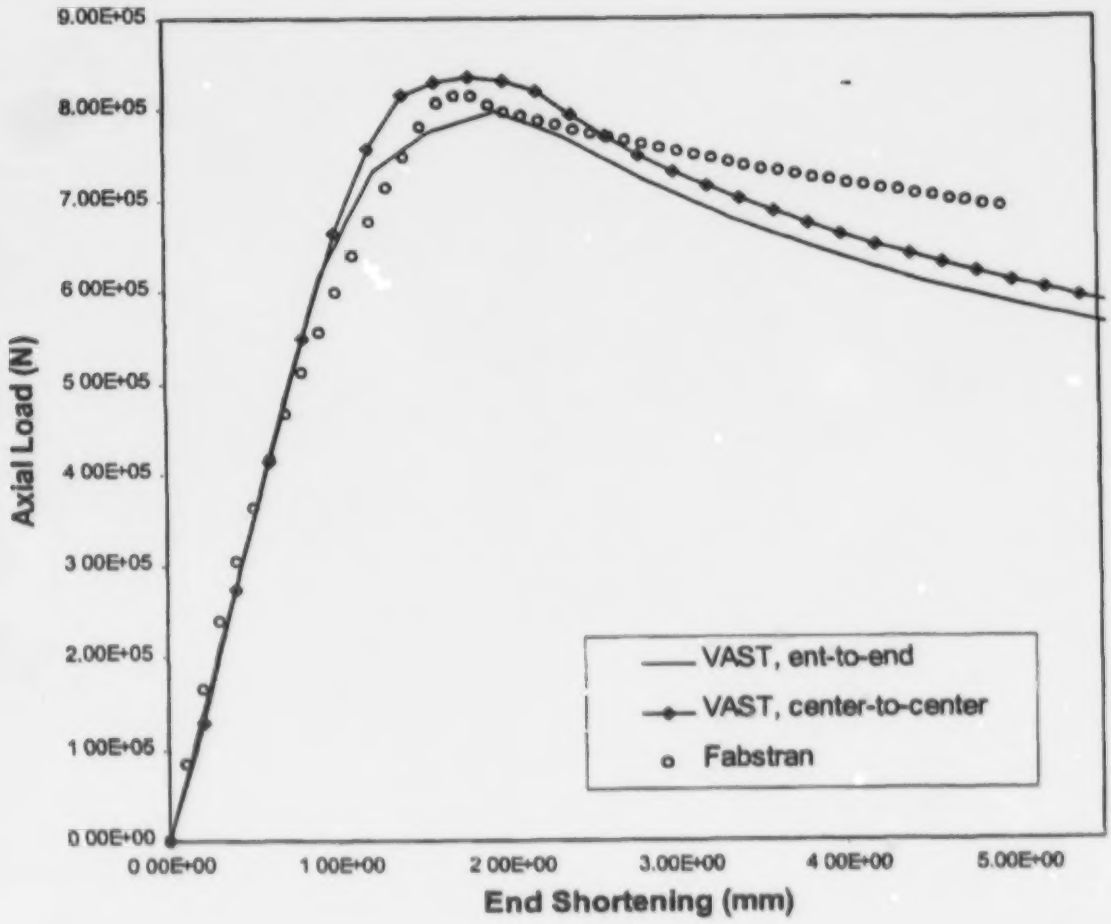

Figure 3.26: Comparison of Load-Shortening Curves Predicted by FABSTRAN and VAST with Different Boundary Conditions

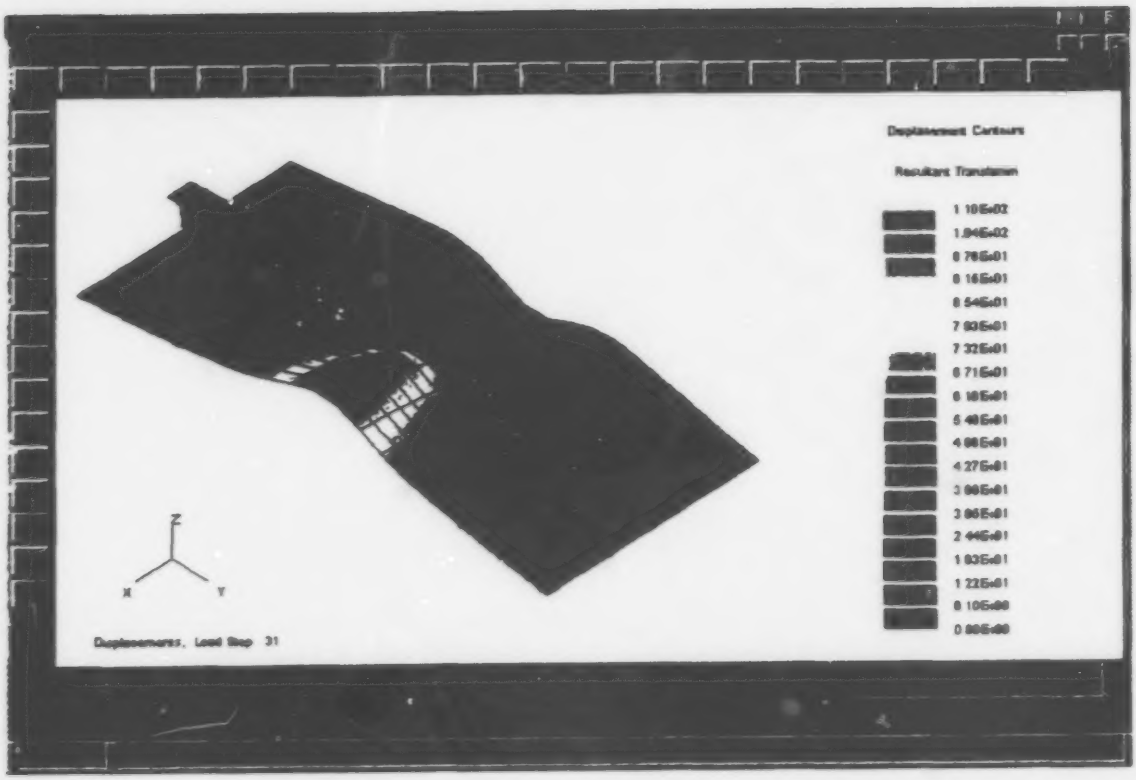

Figure 3.27: Final Deformed Configurations Predicted by VAST Using Different Boundary Conditions. (a) End-to-End Model

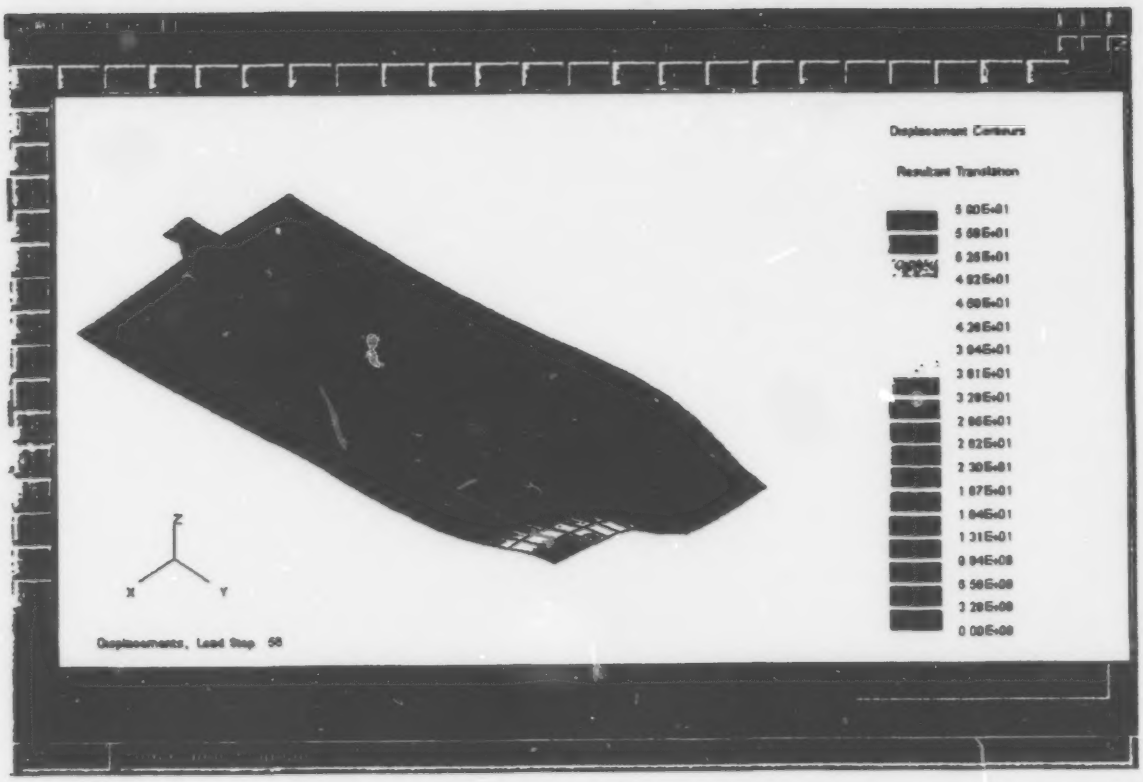

Figure 3.27(Continued): Final Deformed Configurations Predicted by VAST Using Different Boundary Conditions. (b) Center-to-Center Model

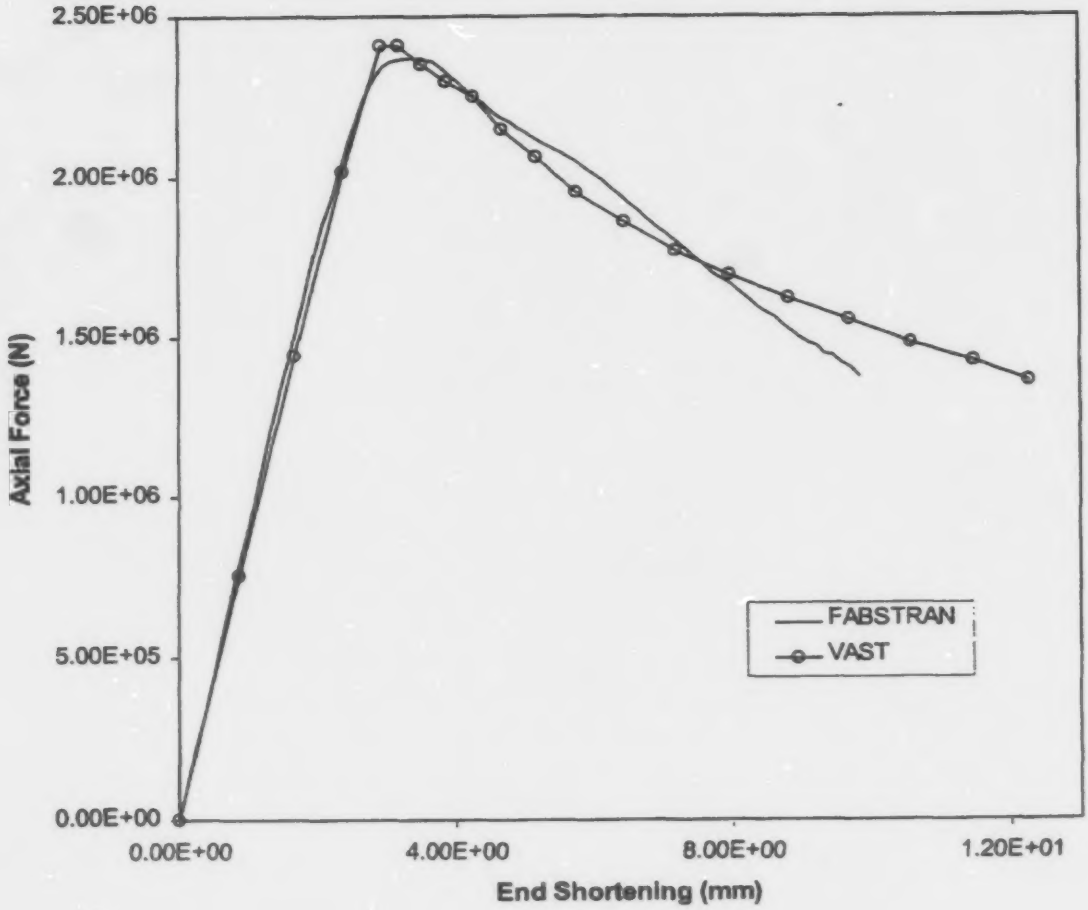

Figure 3.28: Comparison of Load-Shortening Curves Predicted by FABSTRAN and VAST for a Typical Stiffened Panel

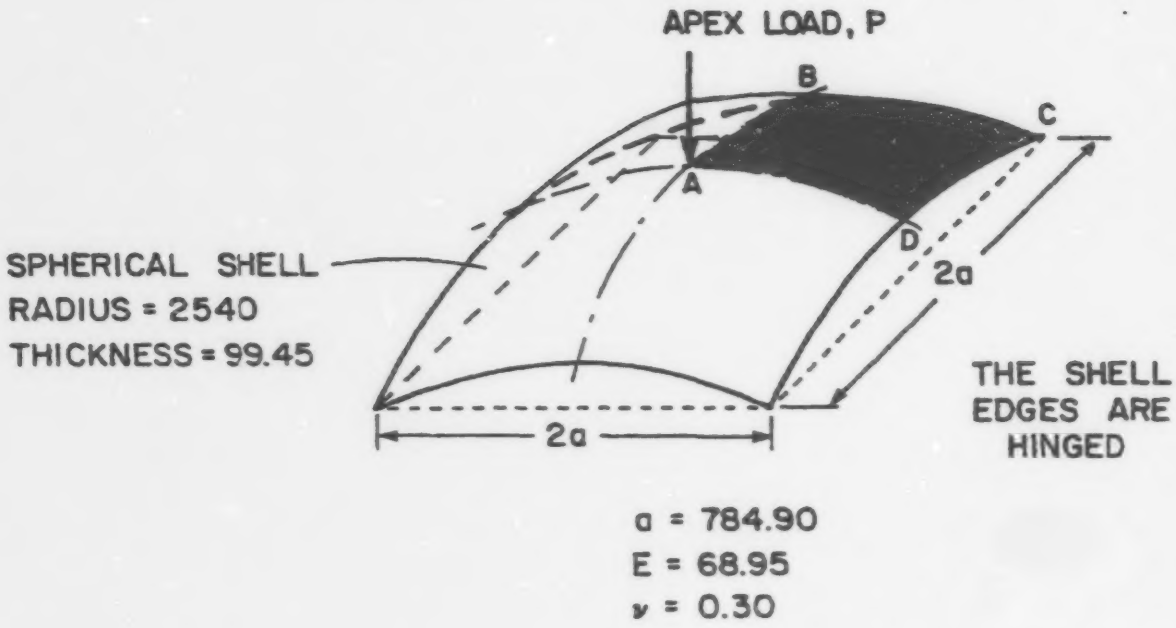

Figure 3.29: Problem Geometry and Material Properties for Geometrically Nonlinear Analysis of a Hinged Shallow Spherical Shell Subjected to a Center Point Load

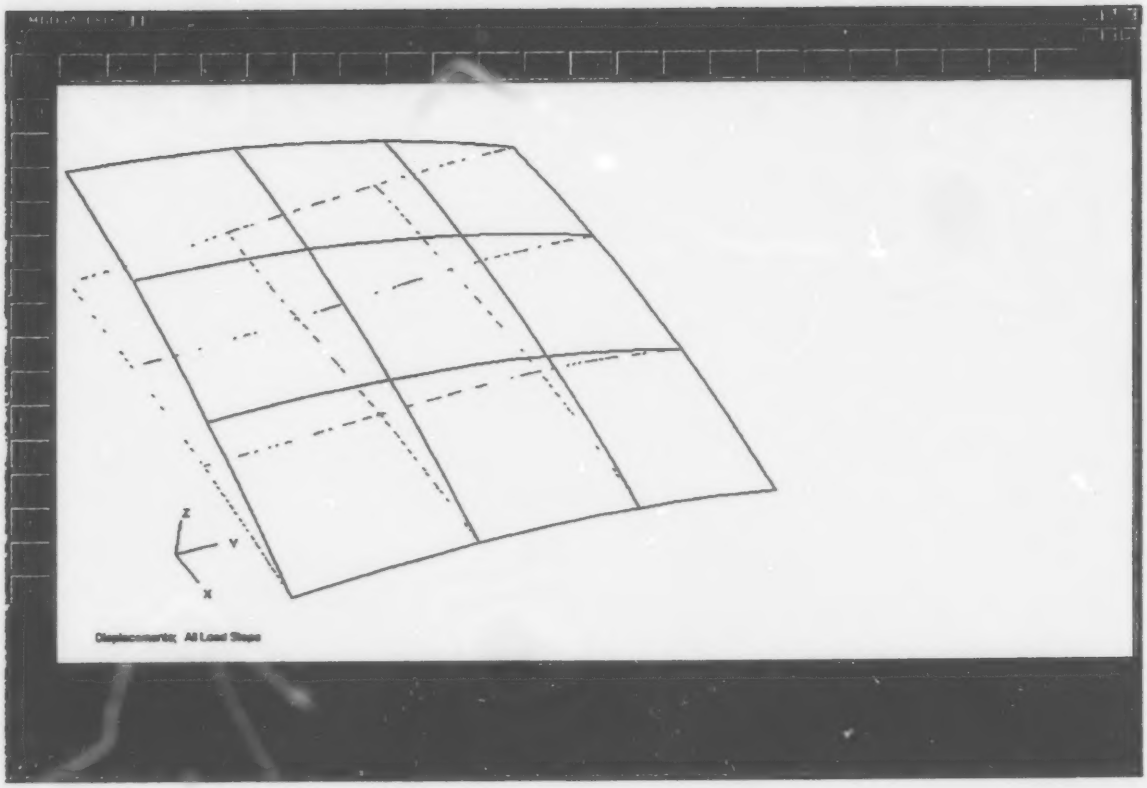

Figure 3.30: Initial Finite Element Mesh and Final Deformed Configuration of the Hinged Shallow Spherical Shell

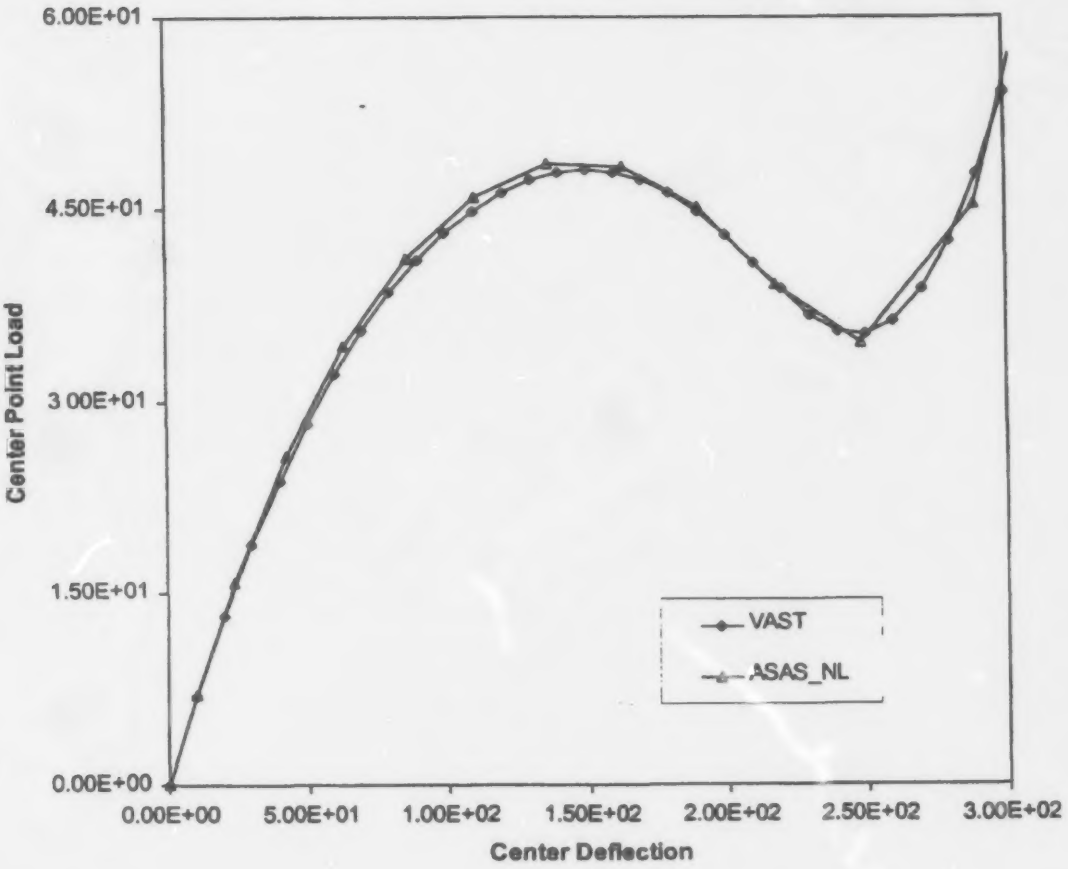

Figure 3.31: Load-Center Deflection Curves of the Hinged Shallow Spherical Shell Predicted by the VAST and ASAS-NL Programs

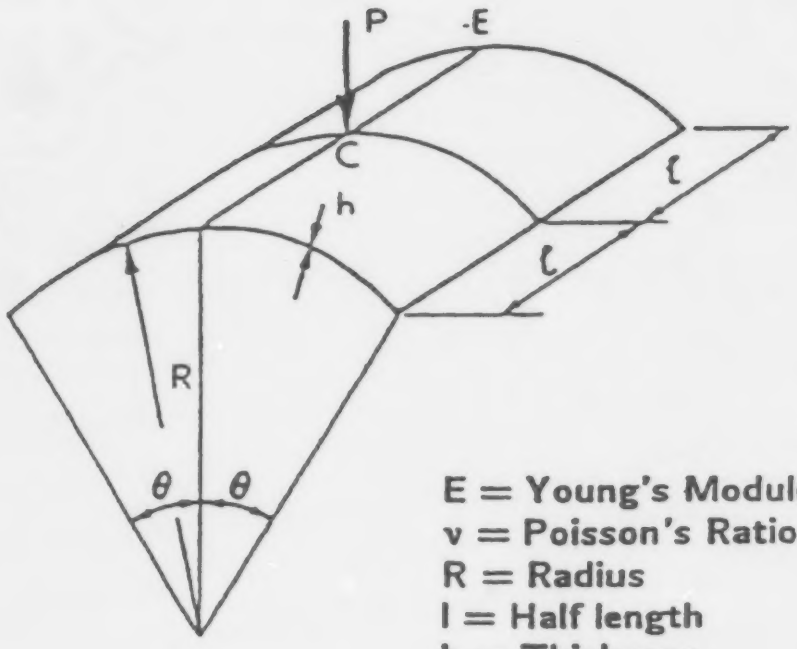

E = Young's Modulus = 310
ν = Poisson's Ratio = 0.3
R = Radius = 2540
l = Half length = 254
h = Thickness = 6.35
θ = Half angle = 0.1 rad.

Figure 3.32: Problem Geometry and Material Properties for Geometrically Nonlinear Analysis of a Hinged Cylindrical Shell Subjected to a Center Point Load

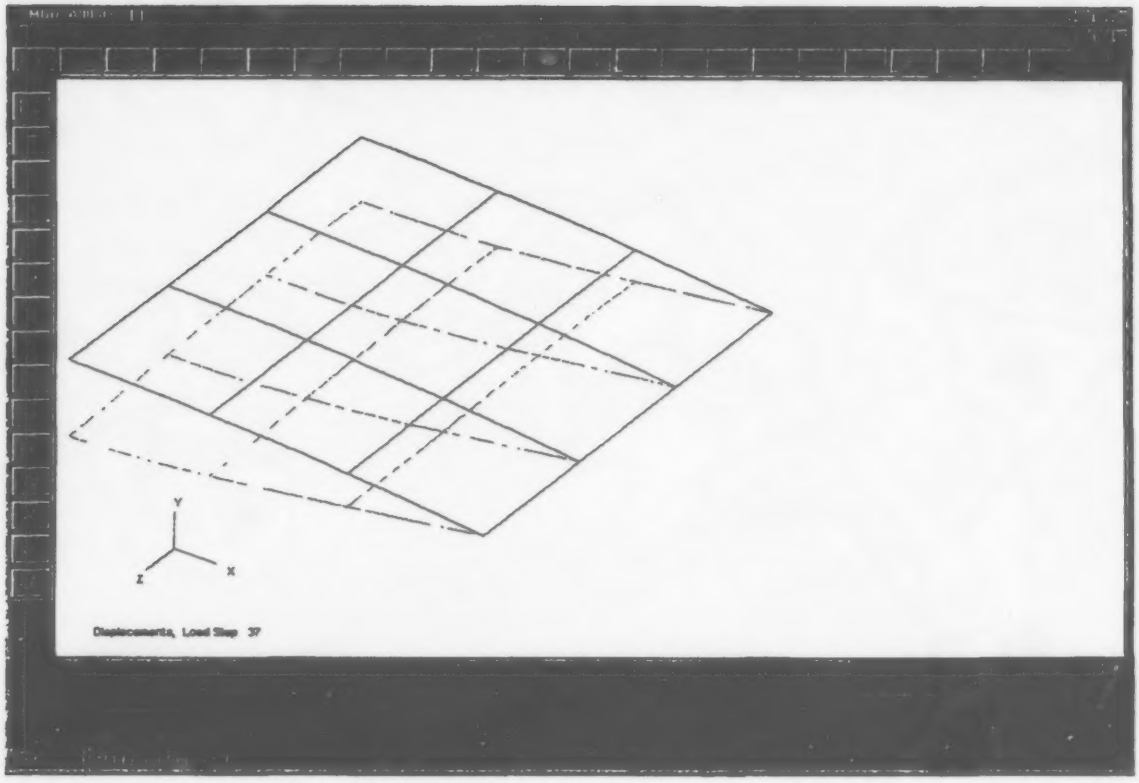

Figure 3.33: Initial Finite Element Mesh and Final Deformed Configuration of the Hinged Cylindrical Shell

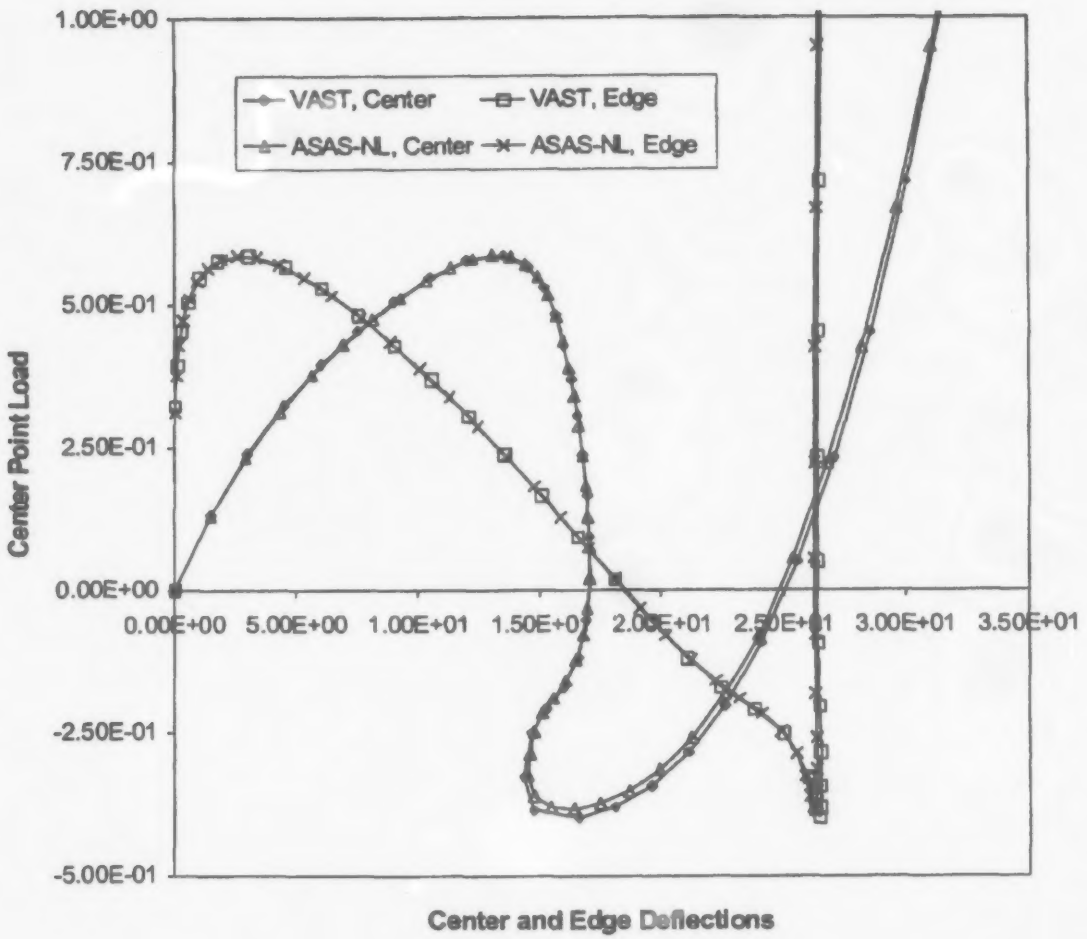

Figure 3.34: Load-Deflection Curves at Center and Edge Nodes of the Hinged Cylindrical Shell Predicted by the VAST and ASAS-NL Programs

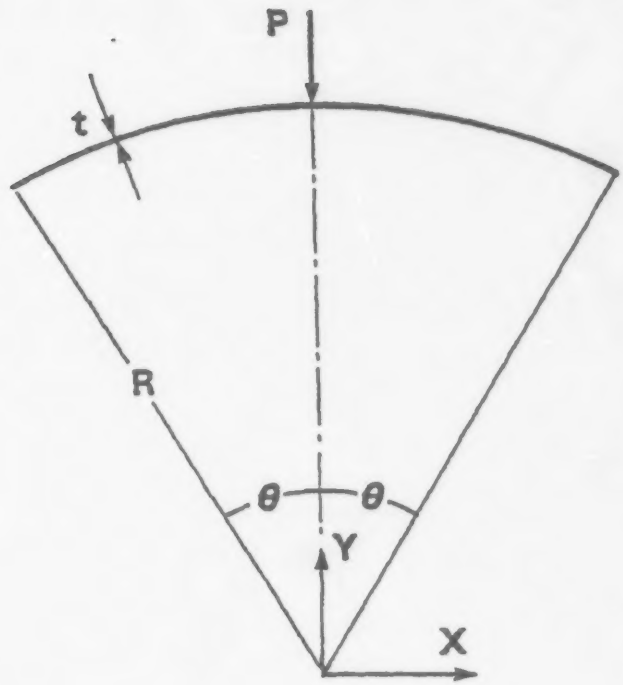

$E = 1.0 \times 10^7$ psi
$\nu = 0.3$
$\sigma_0 = 2.0 \times 10^4$ psi
$E_T = 1.0 \times 10^4$ psi
$R = 4.76$ in
$t = 0.01576$ in
$\theta = 10.9°$

Figure 3.35: Problem Geometry and Material Properties for Geometrically Nonlinear, Elastic-Plastic Analysis of a Hinged Spherical Shell Subjected to a Center Point Load

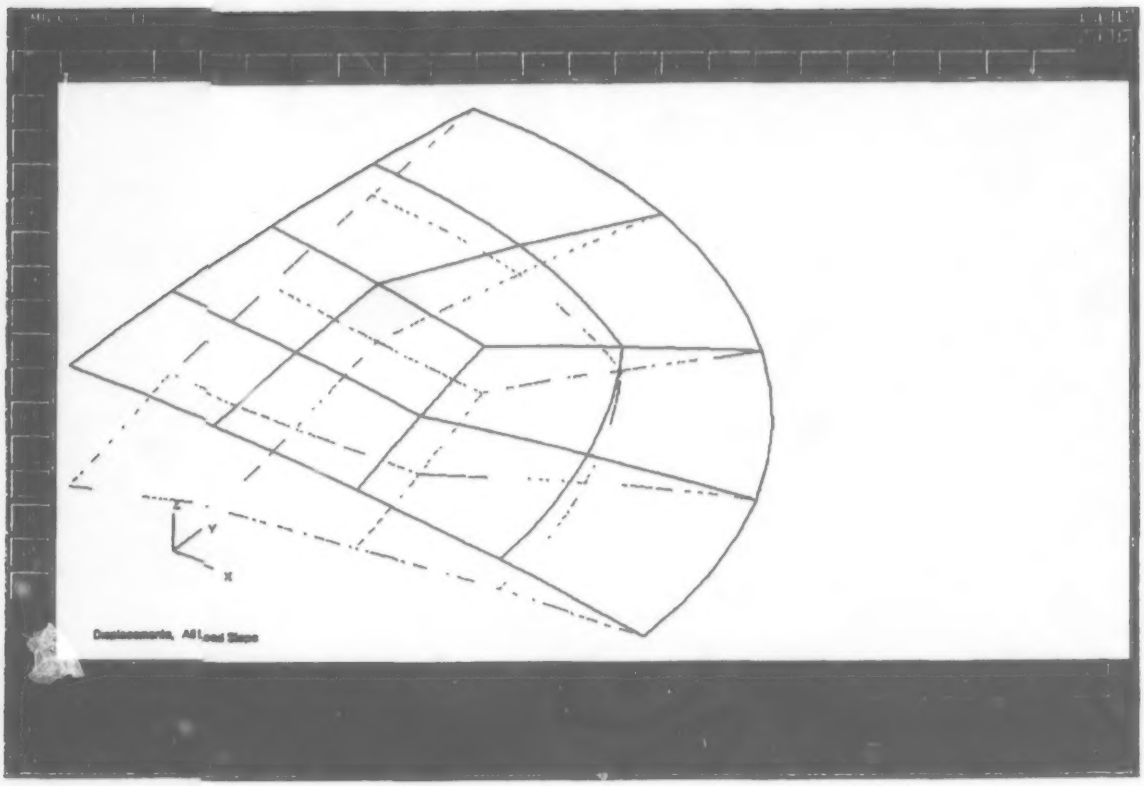

Figure 3.36: Initial Finite Element Mesh and Final Deformed Configuration of the Hinged Spherical Shell

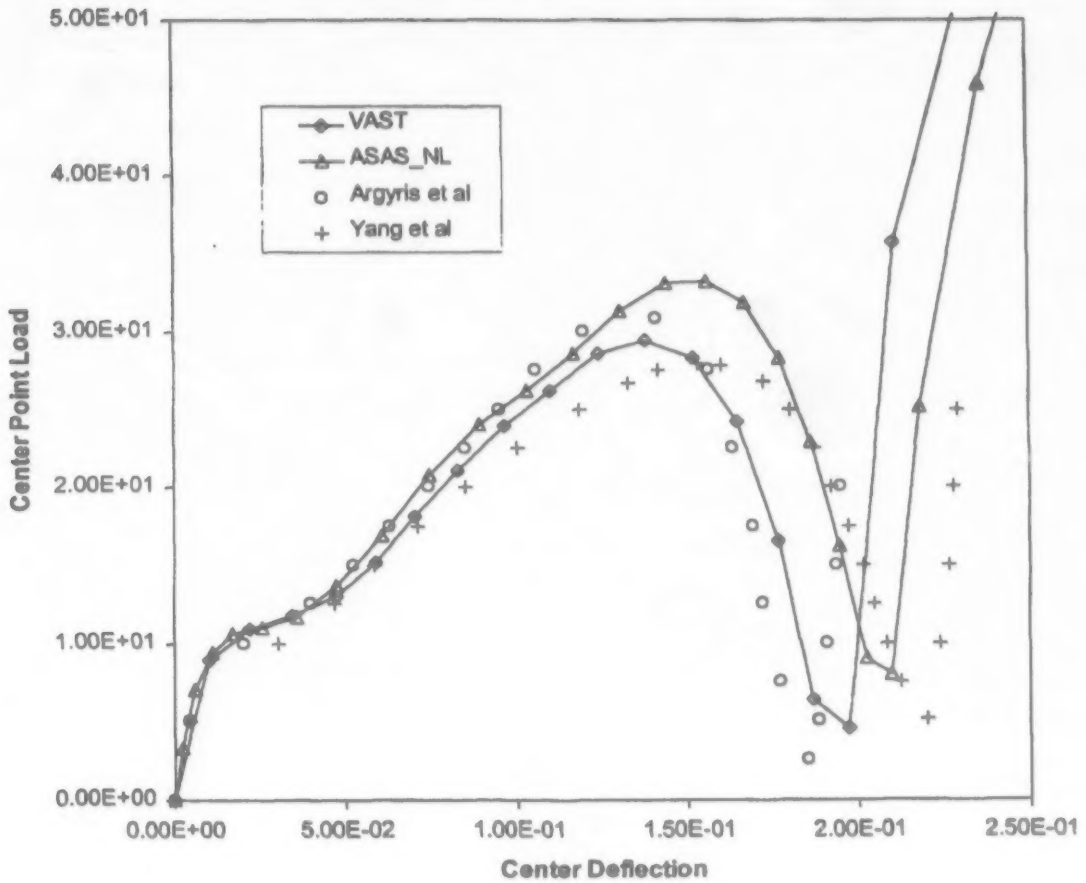

Figure 3.37: Load-Center Deflection Curves of the Hinged Spherical Shell Predicted by the VAST and ASAS-NL Programs

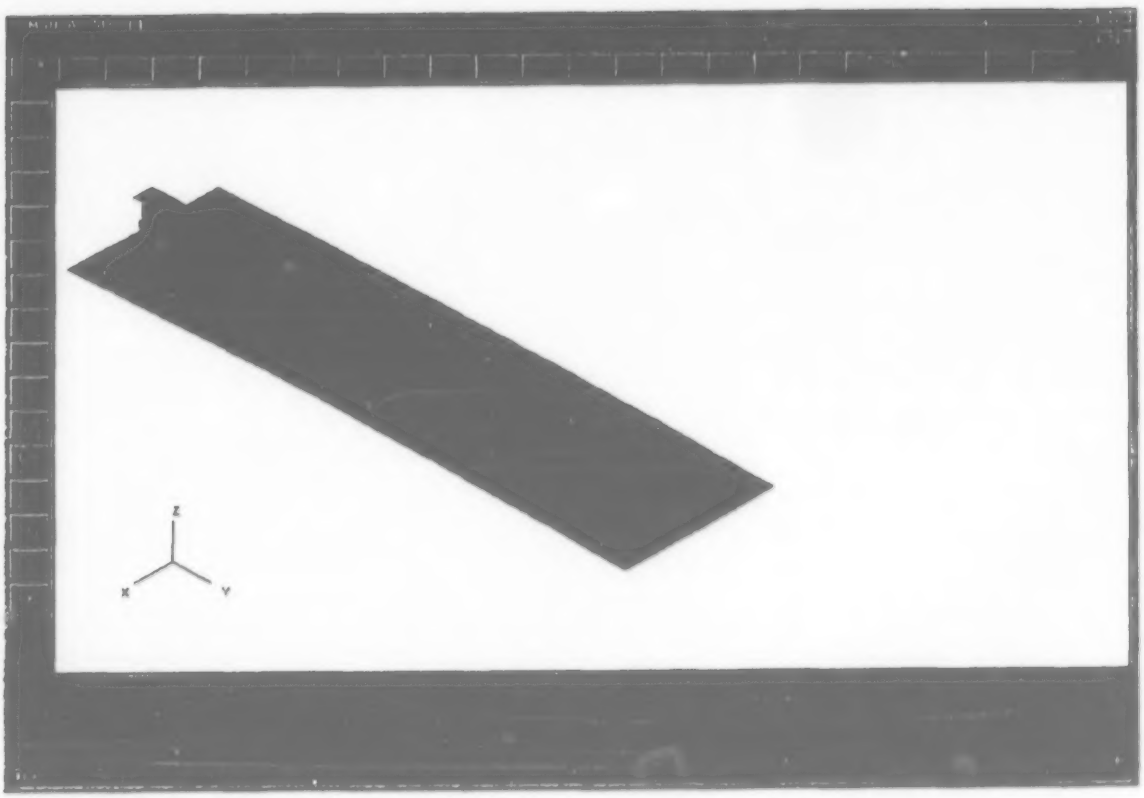

Figure 3.38: 8-Noded Shell Element Mesh of a Typical Stiffened Panel

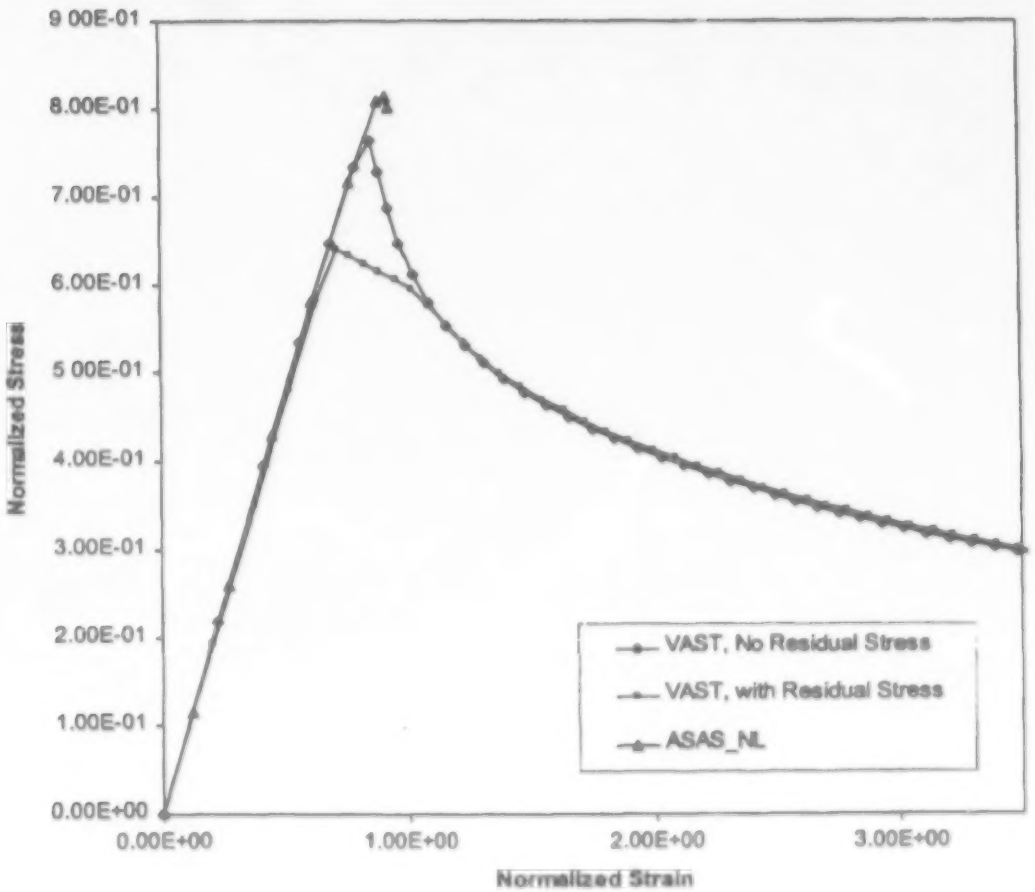

Figure 3.39: Comparison of Load-Shortening Curves Predicted by the VAST and ASAS-NL Program

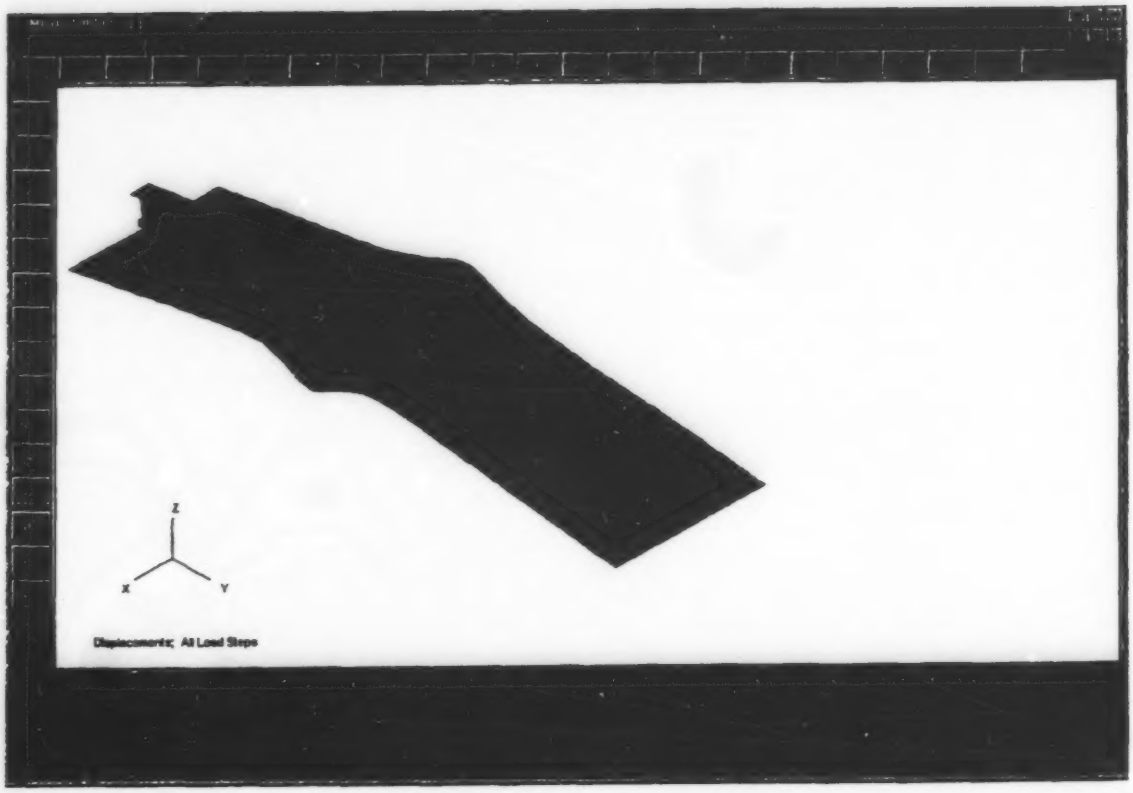

Figure 3.40: Final Deformed Configuration of the Stiffened Panel Predicted by VAST

4. STRUCTURAL COMPONENT STRENGTH ASSESSMENT BASED ON THE SSCP23 LIMIT STATES

4.1 Calculation of SSCP23 Limit States of Structural Components

In order to assess the strength of structural components against collapse under compression and yield under tension, the limiting average stresses that a structural component could take for different failure modes must be evaluated and compared with the component stresses caused by the external load. As described in the documentation of the Sea System Controllerate Publication No 23 (SSCP23), when assessing component strength on ship structures under compressive load, three successive modes of collapse must be considered [4.1]. These three collapse modes include buckling of plating between stiffeners, buckling of longitudinally stiffened panels between transverse stiffeners and overall buckling of the grillage between stiff supporters. In addition to the three failure modes discussed above, a failure mode known as "stiffener tripping" must also be considered. This mode involves the sideways collapse of the stiffener rotating about its toe with associated lateral bending of the web and can be initiated by both in-plane and lateral load.

At a meeting with the Scientific Authority of DREA, it was decided that under the present contract, four limit states would be incorporated into the ultimate strength shell program, including (1) buckling of plate between stiffeners, (2) buckling of longitudinally stiffened panels, (3) tripping of stiffeners and (4) overall yielding of structural components. The formulations required for calculating these SSCP23 limit states are presented in this section.

4.1.1 Buckling of Plating Between Stiffeners

The development of analytical method for evaluating the plastic buckling load of plate was initiated by Von Karman who presented a formulation for the "effective width" (b_e) of plate alongside each stiffener which could reach yield stress at failure. With the effective width, b_e , defined as:

$$b_e = b\frac{\sigma_{pa}}{\sigma_Y} \tag{4.1}$$

where σ_{pa}, σ_Y and b denote the average stress, yield stress and total width of the plate, respectively, Von Karman proposed [4.1]:

$$\frac{b_e}{b} = \frac{1.9}{\beta} \tag{4.2}$$

where β indicate the plate slenderness ratio of the plate defined as:

$$\beta = \left(\frac{b}{t}\right)\sqrt{\frac{\sigma_Y}{E}} \tag{4.3}$$

where t denotes the plate thickness; E, the Young's modulus and σ_Y, the yield stress. Although this formulation predicted collapse stresses reasonably well for slender steel and aluminum aircraft structures, it did not necessarily apply to heavier marine structures with lower β values. Von Karman's equation was later enhanced by Faulkner based on a broad survey of available experimental data, as

$$\frac{b_e}{b} = \frac{2}{\beta} - \frac{1}{\beta^2}. \tag{4.4}$$

Although a large number of analytical formulations have been proposed for evaluating collapse stresses of plates under compression, the most useful one was developed by Smith which involved nonlinear finite element analyses of a variety of plate configurations. One of the significant advantages of the nonlinear finite element analysis lies in its ability to take into account the effects of residual stresses and initial geometric imperfections, and other complicating factors. The nonlinear finite element solutions are normally presented in the form of normalized average stress-average strain curves known as

"load shortening curves". Three typical sets of load shortening curves, which were obtained for small, average and severe initial imperfections were given in reference [4.2]. Because it was recommended in SSCP23 that the average value curves be used in design, this set of curves was digitized in the present work, as shown in Figure 4.1, and incorporated into the ultimate strength shell program. The collapse stresses predicted by Von Karman, Faulkner and nonlinear finite element method are compared in Figure 4.2. It was very comforting to observe that the Von Karman's formula did not provide accurate results for plates with lower β values, however, the collapse stresses obtained using the Faulkner's equation and nonlinear FEA are in excellent agreement for all β values considered.

The calculation of the collapse stress of a given plate between stiffeners is performed in three steps: (1) calculate the plate slenderness ratio, β; (2) calculate the normalized collapse stress, σ_a/σ_y, by interpolating data generated by nonlinear FEA as shown in Figure 4.2; and (3) multiply this normalized stress by the yield stress to obtain the collapse average stress.

4.1.2 Buckling of Longitudinally Stiffened Panel

As for the prediction of collapse stress of plating, a large number of mathematical formulas have been proposed. As, these formulations do not take into account the residual stresses and initial imperfections, a large safety factor has to be applied. Faulkner reviewed various formulations for estimating the elastic-plastic buckling strength of beam-columns and proposed an iterative method for deriving the collapse average stress for a combination of stiffener and effective width of plating. However, this procedure is less soundly based than his plate effective width formula given in Equation (4.4), and needs to be used with caution and a safety factor of at least 1.5.

Thanks to the nonlinear finite element method, a much simpler procedure had been proposed by DERA for calculating the collapse stress of longitudinally stiffened panels [4.1].

In this method, the collapse strength of stiffened panel was presented in the form of curves of normalized collapse stress against column slenderness ratio for different values of β. The column slenderness ratio is defined as:

$$\lambda = \left(\frac{a}{\pi \kappa}\right)\sqrt{\frac{\sigma_y}{E}} \tag{4.5}$$

where κ denotes the radius of gyration computed using the original cross-sectional dimensions of the stiffened panel. Three sets of curves were presented in reference [4.2] for small, average and severe geometric imperfections. Because the average value curves were recommended for use in design, they were digitized in the present contract and implemented in the ultimate strength program. These curves are displayed in Figure 4.3.

Based on the above discussion, it is readily recognized that the evaluation of the collapse strength of a given stiffened panel requires three steps: (1) calculate both plate slenderness ratio, β, and the column slenderness ratio, λ; (2) obtain the stress ratio, σ_a/σ_y, corresponding to these particular values of β and λ through interpolation of the digitized curves shown in Figure 4.3; (3) multiply this stress ratio by the yield stress to obtain the collapse average stress.

4.1.3 Lateral Buckling of Stiffener (Tripping)

Stiffener tripping, or torsional buckling, is a difficult phenomenon to predict accurately because it depends strongly on, among other things, the rotational restraint at the toe of the web and the lateral bending stiffness of the web [4.1]. Faulkner derived a formulation for in-plane load case which made some allowance for rotational restraint at the toe. For practical Tee sectioned stiffened structures, it could be shown that the critical mode was in a single half sine wave of deflection, therefore an estimate of the critical elastic buckling stress can be derived as follows:

$$\sigma_w = (\sigma_S A_S + \sigma_P bt)/(A_S + bt) \tag{4.6}$$

where

$$\sigma_S = GJ/I_0 + \pi^2 E(I_z d^2 + \Gamma)/I_0 a^2 \tag{4.7}$$

$$\sigma_P = \frac{\pi^2 E t^2}{12(1-\nu^2)b^2}\left(\frac{a}{b}+\frac{b}{a}\right)^2 \tag{4.8}$$

indicate the stiffener and plate buckling stresses, respectively, and

E = Young's modulus;

G = Shear modulus;

ν = Poisson's ratio;

A_S = total stiffener area;

I_z = second moment about axis through web;

I_0 = polar second moment about toe;

J = torsion constant = $(t_W^3 d_W + t_F^3 d_F)/3$ for a Tee section;

Γ = warping constant = $A_W^3/36 + A_F^3/144$ for a Tee section;

d = distance from toe to shear centre (height of section for Tee);

a = stiffener length;

b = stiffener spacing;

t = plating thickness.

It should be noted that the polar second moment about toe, I_o, is defined as:

$$I_0 = \int (y^2 + z^2)dA = I_y + I_z \tag{4.9}$$

where I_y and I_z are moment of inertia about the principal axis through the toe.

4.1.4 Overall Yielding of Structural Components

For both plates and stiffened panels, this limit state can be conveniently defined as average stress over the cross-section of the structural component equals the yield stress:

$$\sigma_a = \sigma_y . \tag{4.10}$$

4.2 Calculation of Average Stresses in Structural Components Under Given Bending Moments in Horizontal and Vertical Planes

In order to provide a convenient tool for structural component strength assessment, a facility has been developed in the ultimate strength program to compute average axial stress in each structural component under given extreme bending moment values resulting from an extreme load analysis with MAESTRO and compare these component stresses against the various limit states from SSCP23.

As the first step of the present calculation, the coordinates of neutral axis were computed from the component geometric and elastic material properties over a ship hull cross-section, as:

$$Y_0 = \frac{\sum E_i A_i Y_i}{\sum E_i A_i}, \quad Z_0 = \frac{\sum E_i A_i Z_i}{\sum E_i A_i} \tag{4.11}$$

where $\{Y_i, Z_i\}$ denotes the horizontal and vertical coordinates of the center of gravity of i^{th} structural component, whereas E_i and A_i denote the Young's modulus and cross-sectional area, respectively. Making use of the coordinates of the neutral axis, the moments of inertia of the entire ship cross-section were readily obtained as:

$$E I_{Y0} = \sum E_i \left[I_{Yi} + A_i (Y_i - Y_0)^2 \right] \tag{4.12a}$$

$$EI_{Z0} = \sum E_i \left[I_{Z_i} + A_i (Z_i - Z_0)^2 \right] \tag{4.12b}$$

$$EI_{YZ0} = \sum E_i \left[I_{YZ_i} + A_i (Y_i - Y_0)(Z_i - Z_0) \right] \tag{4.12c}$$

where I_{Y_i}, I_{Z_i} and I_{YZ_i} denote the moments of inertia of the ith structural component with respect to the local center of gravity of the component $\{Y_i, Z_i\}$; and E indicates the average modulus of elasticity of the whole cross-section.

After the moments of inertia of the entire cross-section were computed, the curvature changes corresponding to the prescribed extreme bending moments were evaluated as:

$$\kappa_Y = \frac{(EI_{Y0})M_Y - (EI_{YZ0})M_Z}{(EI_{Y0})(EI_{Z0}) - (EI_{YZ0})^2}, \tag{4.13a}$$

and

$$\kappa_Z = \frac{(EI_{Z0})M_Z - (EI_{YZ0})M_Y}{(EI_{Y0})(EI_{Z0}) - (EI_{YZ0})^2}, \tag{4.13b}$$

Finally, the average axial stress was computed as:

$$\sigma_i = E_i \left[\kappa_Y (Y_i - Y_0) + \kappa_Z (Z_i - Z_0) \right]. \tag{4.14}$$

The structural component strength assessment was then carried out by comparing the average axial stress caused by the extreme bending moments with the limit state values from the SSCP23.

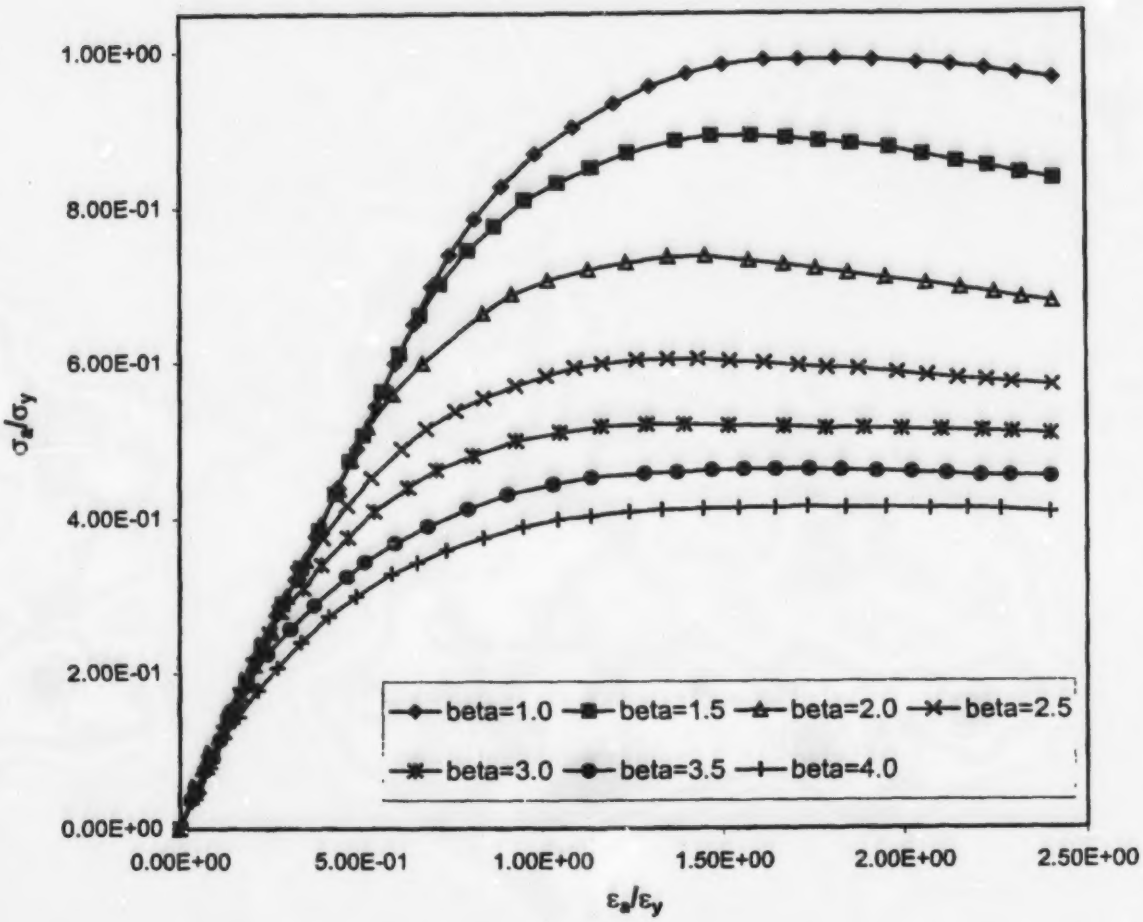

Figure 4.1: Digitized Load Shortening Curves for Buckling of Plate Between Stiffeners with Average Initial Imperfections

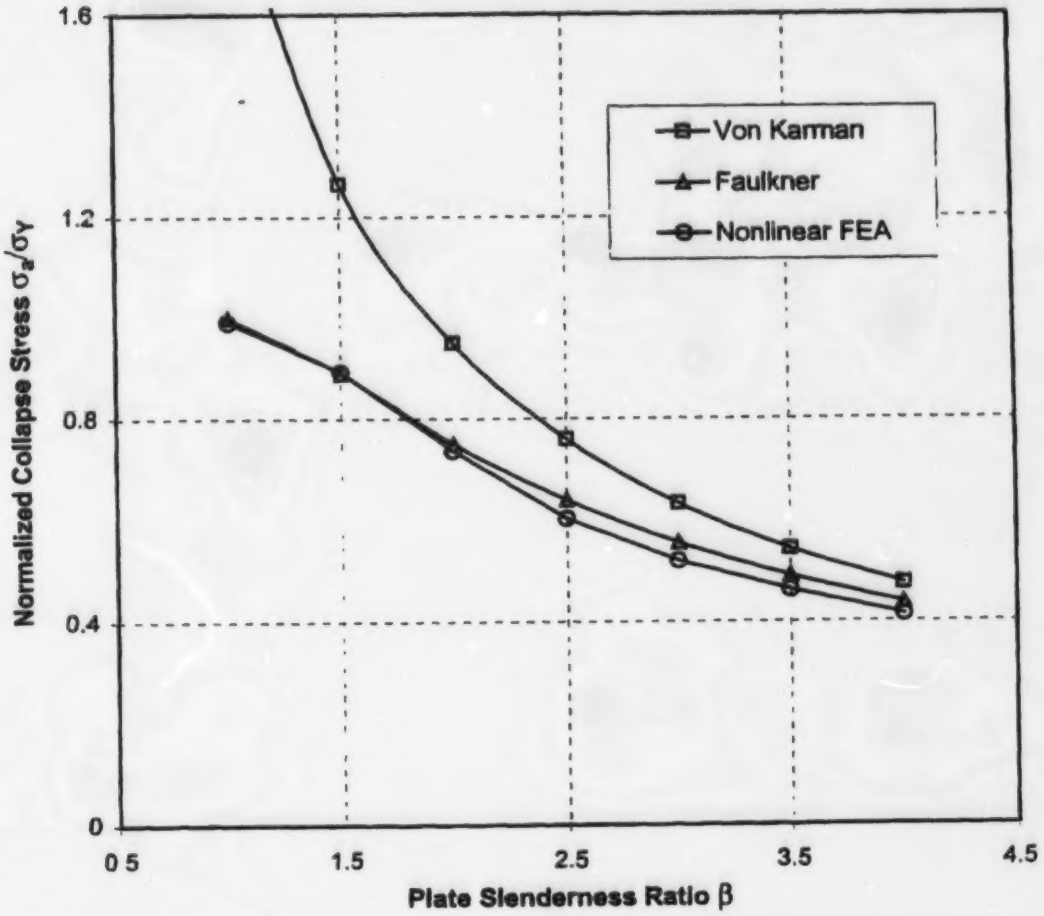

Figure 4.2: Comparison of Plate Collapse Stresses Predicted by the Analytical Formulations of Von Karman and Faulkner and the Nonlinear Finite Element Solutions

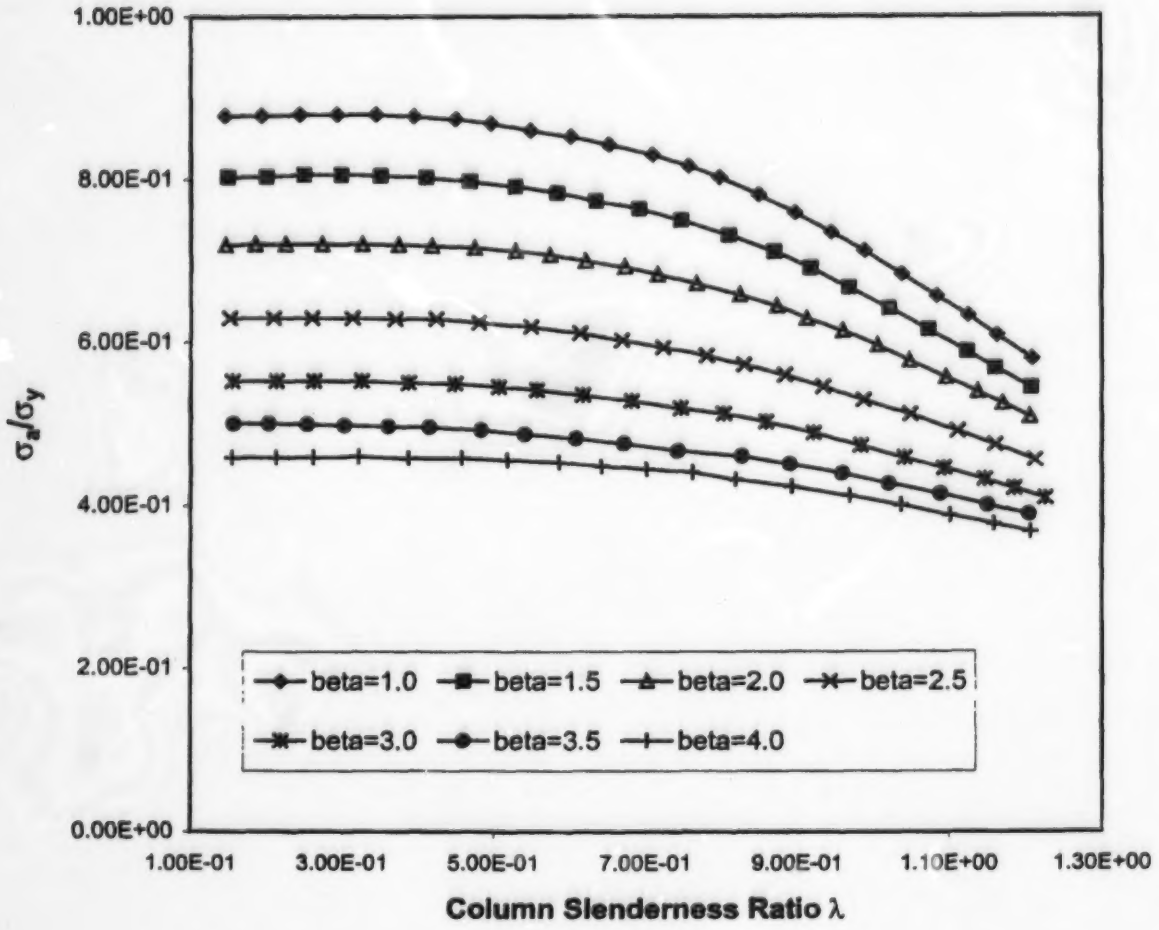

Figure 4.3: Digitized Column Strength Curves Obtained by Nonlinear Finite Element Analyses of Stiffened Panels with Average Initial Imperfection

5. CONCLUSIONS AND RECOMMENDATION FOR FURTHER WORK

This is the first part of a two-part final report concerning the recent incorporation of the ultimate strength analysis capability into the MGDSA program and the development of the ultimate strength shell program. In this part of the report, all the engineering work performed in this contract was presented in detail. This work included verification and modification of all four ultimate strength analysis programs; enhancement of the automatic mesh generator for stiffened panels, LSPANEL; development of input data translators for converting VAST input data to the FABSTRAN and ASAS-NL input data format; and calculation of the SSCP23 limit states and component forces under given extreme bending moments. For both ultimate strength analyses and nonlinear finite element analyses, numerical solutions produced by the different programs were compared and good agreement between the corresponding numerical solutions were always observed.

Using the ultimate strength application program developed in the present contract, both the moment-curvature curves and bi-axial interaction curves of a given ship cross-section can be obtained very conveniently. However, in order to increase the accuracy of the ultimate strength results, further improvements of the ultimate strength programs are still required. These improvements include the enhancement of the interpolation algorithm utilized by these ultimate strength codes to take account of other important factors, such as the stiffener area to total area ratio, level of plate and stiffener imperfection and level of residual stress. They should also include the allowance of special load-shortening curves in the ULTMAT program, and the expansion of the existing load-shortening curve database by adding curves for low plate and column slenderness ratios.

P515288.PDF [Page: 108 of 116]

6. REFERENCES

Chapter Two:

[2.1] T.S.Z. HU and D.C. HEATH, *EBMS – A Computer Program for Equivalent Beam Modeling of Ship Structures*, DREA Technical Memorandum.

[2.2] C.S. SMITH and R.S. DOW, *Ultimate Strength of a Ship's Hull Under Biaxial Bending (U)*, Admiralty Research Establishment, December, 1986.

[2.3] R.S. DOW, *NS94C/D Ultimate Strength Design Method for Ships*, Admiralty Research Establishment, 1997.

[2.4] R.S. DOW, *Testing and Analysis of a 1/3-Scale Welded Steel Frigate Model*, Admiralty Research Establishment.

Chapter Three:

[3.1] L. JIANG, J. WALLACE and M.W. CHERNUKA, *An Automatic Mesh Generator and Convergence Study for Calculating Load-Shortening Curves of Stiffened Plates for the Halifax Class Frigate*, Martec Technical Report TR-97-33, Martec Limited, October, 1997.

[3.2] M. SMITH, *Corrosion Modeling Data Input*, Facsimile, DREA, March 29, 1999.

[3.3] L. JIANG and M.W. CHERNUKA, *Improved Nonlinear Solution Techniques in the VAST Finite Element Program*, Martec Technical Report TR-99-32, Martec Limited, February, 2000.

[3.4] T.S.Z. HU, *Nonlinear Finite Element Simulation of the Test Procedure for Stiffened Panels Under Combined Lateral and In-Plane Loads*, DREA Technical Memorandum, March, 1997.

[3.5] L. JIANG and M.W. CHERNUKA, *Continued Development of a Normalized Effective Stress-Strain Curve Database of Stiffened Plates for the Halifax Class Frigate*, Martec Technical Report TR-98-08, Martec Limited, March 1998.

[3.6] F.W. WILLIAMS, "An Approach to the Nonlinear Behaviour of the Members of a Rigid Jointed Plane Framework with Finite Deformations". *Quarterly Journal of Mechanics and Applied Maths*, Vol.17, November, 1964.

[3.7] R.S. DOW and C.S. SMITH, *FABSTRAN: A Computer Program for Frame and Beam Static and Transient Response Analysis (Nonlinear) (U)*, Admiralty Research Establishment, December, 1986.

[3.8] *ASAS-NL User Manual*, Version 2.0, Update 4, WS Atkins Engineering Software, Surrey, England, October, 1998.

Chapter Four:

[4.1] A.C. SWIFT and R.S. DOW, *Implementation of SSCP23 Surface Ship Design Criteria in MAESTRO, A Structural Analysis & Optimization Program*, Defence Research Agency, UK, November, 1992.

[4.2] Chief Naval Architect, *Sea System Controllerate Publication No.23 (SSCP23) - Design of Surface Ship Structures*, Volumes 1&2, Ministry of Defence, UK, December, 1989.

APPENDIX A: LIST OF INPUT PARAMETERS FOR THE LSPANEL PROGRAM

CARD 1: (2I)
(global control parameters)

IETYPE = element type indicator.
= 4 for 4-noded quadrilateral shell element
= 8 for 8-noded quadrilateral shell element
IPROGRAM = program indicator.
= 1 for VAST
=2 for ASAS_NL
=3 for FABSTRAN

CARD 2: (3I, 7R)
(Boundary condition, elastic material properties and beam cross-section dimensions)

IMODEL = model type indicator.
= 1 for end-to-end model
= 2 for center-to-center model
ICASE = load case indicator.
= 1 for axial load
= 2 for prescribed axial displacement
IPARAM = plate dimension indicator.
= 1 if plate dimensions are defined by geometric parameters
= 2 if plate dimensions are defined by absolute values

E = Young's modulus
PR = Poisson's ratio
DEN = mass density

WD = height of web
WT = thickness of web
FD = width of flange
FT = thickness of flange

CARD 3: (3R, 2I, 3R)
(Plastic material properties and thermal properties and loads)

SIGY0 = initial yield stress
EIH = tangent modulus of isotropic hardening
EKH = tangent modulus of kinematic hardening
MINTEG = 2 for use of implicit integration of plastic constitutive equations
MTAN = 2 for use of consistent tangent operator

ALPHAT = coefficient of thermal expansion
TEMPP = temperature variation at plate-web junction
TEMPF = temperature variation at web-flange junction

CARD 4: (3R)
(Plate dimensions)

If IPARAM=1, provide the following parameters:
BETA = plate slenderness ratio
LAMBDA = column slenderness ratio
ARATIO = stiffener-to-total area ratio

If IPARAM=2, provide the following parameters:
T = plate thickness
A = stiffened panel length
B = plate width

CARD 5: (4I, 5R)
(Meshing parameters)

NEA3 = number of elements along the axial direction in the refined region
NEB = number of elements across the plate width
NEW = number of elements across the web
NEF = number of elements across the flange

A3 = length of the refined region

RA = ratio of element sizes in the coarse and the refined region
RA2 = element mesh aspect ratio along the length in the refined region
RB = element mesh aspect ratio across the plate width
RW = element mesh aspect ratio across the web

CARD 6: (6R, 2I)
(Initial geometric imperfection data)

SCALE-P = coefficient for plate imperfection
SCALE-S = coefficient for stiffener imperfection

IMP-F3 = coefficient for three half sine wave imperfection
IMP-F5 = coefficient for five half sine wave imperfection
IMP-F7 = coefficient for seven half sine wave imperfection
IMP-F9 = coefficient for nine half sine wave imperfection

NMODES = number of modes to be computed in buckling analysis (default=5)
IMODE = mode number to be included as extra imperfection in nonlinear analysis

CARD 7: (6R)
(Corrosion in plate ONE defined in percentage of reduction)

R01 = uniform reduction of thickness
RS1 = sinusoidal reduction of thickness
RA1 = maximum reduction of thickness along edge A
RB1 = maximum reduction of thickness along edge B
RC1 = maximum reduction of thickness along edge C
RD1 = maximum reduction of thickness along edge D

CARD 8: (6R)
(Corrosion in plate TWO defined in percentage of reduction)

R02 = uniform reduction of thickness
RS2 = sinusoidal reduction of thickness
RA2 = maximum reduction of thickness along edge A

RB2 = maximum reduction of thickness along edge B
RC2 = maximum reduction of thickness along edge C
RD2 = maximum reduction of thickness along edge D

CARD 9: (4R)
(Corrosion in the web defined in percentage of reduction)

R0W = uniform reduction of thickness
RSW = sinusoidal reduction of thickness
RP = maximum reduction of thickness along web-plate junction
RF = maximum reduction of thickness along web-flange junction

CARD 10: (5R)
(Corrosion in the web defined in percentage of reduction)

R0F = uniform reduction of thickness
RSF = sinusoidal reduction of thickness
RW = maximum reduction of thickness along web-plate junction
RFA = maximum reduction of thickness along flange edge A
RFB = maximum reduction of thickness along flange edge B

CARD 11: (I, C)

ICHAR = number of characters included in the PREFX
PREFX = character string containing the prefix of the generated data files

UNCLASSIFIED
SECURITY CLASSIFICATION OF FORM
(highest classification of Title, Abstract, Keywords)

DOCUMENT CONTROL DATA

(Security classification of title, body of abstract and indexing annotation must be entered when the overall document is classified)

1 ORIGINATOR (the name and address of the organization preparing the document. Organizations for whom the document was prepared, e.g. Establishment sponsoring a contractor's report, or tasking agency, are entered in section 8.)

Martec Ltd., Suite 400, 1888 Brunswick St., Halifax, NS, B3J 3J8

2. SECURITY CLASSIFICATION (overall security classification of the document including special warning terms if applicable).

UNCLASSIFIED

3. TITLE (the complete document title as indicated on the title page. Its classification should be indicated by the appropriate abbreviation (S,C,R or U) in parentheses after the title)

Incorporation of UK NS94 Ultimate Strength Analysis in MGDSA, Part I: Engineering Considerations

4. AUTHORS (Last name, first name, middle initial. If military, show rank, e.g. Doe, Maj. John E.)

Jiang, L., and Chernuka, M.W.

5. DATE OF PUBLICATION (month and year of publication of document)

March 2000

6a NO .OF PAGES (total containing information Include Annexes, Appendices, etc)

106 (approx.)

6b. NO. OF REFS (total cited in document)

14

7. DESCRIPTIVE NOTES (the category of the document, e.g. technical report, technical note or memorandum. If appropriate, enter the type of report, e g. interim, progress, summary, annual or final Give the inclusive dates when a specific reporting period is covered)

CONTRACTOR REPORT

8 SPONSORING ACTIVITY (the name of the department project office or laboratory sponsoring the research and development. Include address).

Defence Research Establishment Atlantic
PO Box 1012
Dartmouth, NS, Canada B2Y 3Z7

9a PROJECT OR GRANT NO. (if appropriate, the applicable research and development project or grant number under which the document was written Please specify whether project or grant)

1.g.c.15

9b CONTRACT NO. (if appropriate, the applicable number under which the document was written)

W8477-8-0004/001/SV

10a ORIGINATOR'S DOCUMENT NUMBER (the official document number by which the document is identified by the originating activity. This number must be unique to this document.)

TR-00-15

10b OTHER DOCUMENT NOs. (Any other numbers which may be assigned this document either by the originator or by the sponsor)

DREA CR 2000-112

11. DOCUMENT AVAILABILITY (any limitations on further dissemination of the document, other than those imposed by security classification)

(x) Unlimited distribution
( ) Defence departments and defence contractors; further distribution only as approved
( ) Defence departments and Canadian defence contractors; further distribution only as approved
( ) Government departments and agencies; further distribution only as approved
( ) Defence departments; further distribution only as approved
( ) Other (please specify):

12 DOCUMENT ANNOUNCEMENT (any limitation to the bibliographic announcement of this document. This will normally correspond to the Document Availability (11). However, where further distribution (beyond the audience specified in (11) is possible, a wider announcement audience may be selected)

UNCLASSIFIED
SECURITY CLASSIFICATION OF FORM

UNCLASSIFIED
SECURITY CLASSIFICATION OF FORM
(highest classification of Title, Abstract, Keywords)

13. ABSTRACT (a brief and factual summary of the document. It may also appear elsewhere in the body of the document itself. It is highly desirable that the abstract of classified documents be unclassified. Each paragraph of the abstract shall begin with an indication of the security classification of the information in the paragraph (unless the document itself is unclassified) represented as (S), (C), (R), or (U). It is not necessary to include here abstracts in both official languages unless the text is bilingual)

This report presents all the engineering work related to the incorporation of an ultimate strength analysis capability in MGDSA. The various ultimate strength analysis programs developed by DREA and DERA using the ISUM method were first verified on the PC platform. The ULTMAT program was modified to accept input data at the structural component level, and the accuracy and reliability of the NS94 suite of programs were improved. In order to generate load-shortening curves for damaged stiffened panel structures through nonlinear finite element analysis, the previously developed automatic mesh generator, LSPANEL, was enhanced to include the 8-noded shell element, a corrosion modeling capability, a more realistic residual stress pattern and higher sine functions for imperfection definition. The effects of damage and other important factors on load-shortening behavior of stiffened panels were investigated using the VAST program. Input data translators between VAST and other nonlinear FE programs, including FABSTRAN and ASAS-NL, were also developed and verified. The detailed mathematical formulations required for evaluating the SSCP23 limit states are presented and the method for calculating component stresses for given extreme bending moments is also included. The input data format for the updated LSPANEL program is summarized in Appendix A. The software development issues related to the present contract are dealt with in the second part of the final report.

14. KEYWORDS, DESCRIPTORS or IDENTIFIERS (technically meaningful terms or short phrases that characterize a document and could be helpful in cataloguing the document. They should be selected so that no security classification is required. Identifiers, such as equipment model designation, trade name, military project code name, geographic location may also be included. If possible keywords should be selected from a published thesaurus, e.g. Thesaurus of Engineering and Scientific Terms (TEST) and that thesaurus-identified. If it not possible to select indexing terms which are Unclassified, the classification of each should be indicated as with the title)

Ship structure
Ultimate strength
Hull girder strength
Longitudinal strength
Load shortening curve
Moment curvature
Stiffened panel

UNCLASSIFIED
SECURITY CLASSIFICATION OF FORM